SYNTHESIS AND CHARACTERIZATION OF NOVEL PERYLENE-3,4,9,10-TETRACARBOXYLIC ACID DERIVATIVES

A THESIS SUBMITTED TO
THE BOARD OF CAMPUS GRADUATE PROGRAMS
OF MIDDLE EAST TECHNICAL UNIVERSITY
NORTHERN CYPRUS CAMPUS

BY

OBAIDULLAH MOHIUDDIN

IN PARTIAL FULFILLMENT OF THE REQUIREMENTS
FOR
THE DEGREE OF MASTER OF SCIENCE
IN
SUSTAINABLE ENVIRONMENT AND ENERGY SYSTEMS

MAY 2017

Approval of the Board of Graduate Programs

_____
Prof. Dr. Oya Yerin Güneri
Chairperson

I certify that this thesis satisfies all the requirements as a thesis for the degree of Master of Science.

_____
Asst. Prof. Dr. Carter Mandrik
Program Coordinator

This is to certify that we have read this thesis and that in our opinion it is fully adequate, in scope and quality, as a thesis for the degree of Master of Science.

_____
Asst. Prof. Dr. Mustafa Erkut Özser
Supervisor

Examining Committee Members

Asst. Prof. Dr. Mustafa Erkut Özser	Chemistry Group. METU NCC	_____
Prof. Dr. Hüseyin İşçi	Chemistry Group. METU NCC	_____
Assoc. Prof. Dr. Volkan Esat	Mechanical Engineering Program. METU NCC	_____
Asst. Prof. Dr. Ertan Akün	Industrial Engineering Dept. CIU	_____
Asst. Prof. Dr. İme Akanyeti	Environmental Engineering Dept. CIU	_____

ETHICAL DECLARATION

I hereby declare that all information in this document has been obtained and presented in accordance with academic rules and ethical conduct. I also declare that, as required by these rules and conduct, I have fully cited and referenced all material and results that are not original to this work.

Name, Last name: Obaidullah, Mohiuddin

Signature:

ABSTRACT

SYNTHESIS AND CHARACTERIZATION OF NOVEL PERYLENE-3,4,9,10-TETRACARBOXYLIC ACID DERIVATIVES

Obaidullah Mohiuddin

M.S., Sustainable Environment, and Energy Systems Program

Supervisor: Asst. Prof. Dr. Mustafa Erkut Özser

May 2017, 104 pages

Increasing demand and high consumption of energy lead the researchers to think about the alternative renewable and sustainable source that could fulfil the energy requirement. For this purpose smooth transition to renewable technologies are necessary. There are several alternative technologies available, among them Dye Sensitized Solar Cell (DSSC) can be the promising one. DSSC has achieved around 12% power conversion efficiency, hence improvement is possible if new materials are synthesized. Our study aims to synthesize and characterization of novel isomerically pure perylene-3,4,9,10-tetracarboxylic acid derivatives that are promising family of organic dyes as light harvesting material (sensitizer). The study involves the synthesis of novel antisymmetric compounds and investigation of their structural, and photo-physical properties. This work demonstrates that perylene tetracarboxylic ester unit is a versatile building block for the synthesis of variety of light harvesting systems. The resulting compounds are soluble in variety of organic solvents, and show broad absorption bands extending up to near infrared region.

Keywords: Perylene, Dye sensitized solar cells, low-bandgap, Sensitizer.

ÖZ

Özgün Perilen-3,4,9,10-tetrakarboksilik Asit Türevlerinin Sentezi ve Karakterizasyonu

Obaidullah Mohiuddin

M.S Sürdürülebilir Çevre ve Enerji Sistemleri

Supervisor: Asst. Prof. Dr. Mustafa Erkut Özser

May 2017, 104 pages

Artan enerji talebi ve kullanımı araştırmacıları bu talebe karşılık verecek alternatif yenilenebilir ve sürdürülebilir enerji kaynakları üzerinde çalışmaya itmektedir. Bu amaçla yenilenebilir enerji teknolojilerine sorunsuz geçiş yapılabilmesi ihtiyacı bulunmaktadır.Mevcut alternatif teknolojiler arasında Boya Duyarlı Güneş Pilleri (DSSC) umut vaat eden teknoloji olarak öne çıkmaktadır. Mevcut DSSC verimlilikleri %12 dolaylarındadır, dolayısıyla yeni malzemelerin sentezlenmesi ile verimlilikleri arttırılabilir. Bu çalışmada izomerik saflıkta, ışık hasat edebilen, perilen-3,4,9,10-tetrakarboksilik asit türevlerinin sentezi ve karakterizasyonu amaçlanmaktadır. Çalışma özgün antisimetrik perilen türevlerinin sentezini, ve bu bileşiklerin fotokimyasal ve fotofiziksel özelliklerinin araştırılmasını hedeflemektedir

DEDICATION

To my Beloved Wife, Parents, in-laws, Siblings.

For their moral support, love, belief, and encouragement

ACKNOWLEDGEMENTS

First of all, I want to Thank Almighty ALLAH for blessing me this opportunity. I am very grateful to be the part of this research. It is my wish to acknowledge the contribution of others in this experimental work.

First and foremost, I would like to express my appreciation to my supervisor, Assist. Prof. Dr. Mustafa Erkut Özser for his limitless support and potential supervision during my graduate thesis. He was always more than a supervisor, and this research were not possible without his great support and feedbacks. There are not enough words to explain my appreciation to him.

I am also obliged to Dr. Erdal Onhuran for his social support, motivation, and encouragement throughout my studies and Assistantship in Department of Chemistry of Middle East Technical University Northern Cyprus Campus.

I acknowledge the technical support of METU-Ankara for NMR analysis and Dr Ertan Akün, from Cyprus International University (CIU) Nicosia- Engineering Faculty for the Fluorescence Spectroscopy. This project was funded by Middle East Technical University, Northern Cyprus Campus with Campus Research Fund, BAP-FEN-14-D-1.

I would also like to thanks my collogues Samuel Asumadu Sarkodie and Gözde Özesme for their immense support and contribution to this research, also the undergraduate students of chemical engineering program, Maryam Ghias, Bernard Oruche, Hafsa Butt and Sharmin Zzaman for their contribution to this research.

Finally I am thankful to ALLAH to bless me such a supportive, loveable wife Madina Obaidullah, my parents, Mr. and Mrs. Muhammad Mohiuddin, my siblings (Rabia Adnan, Abdus-Sammad Mohiuddin, Abdullah Mohiuddin, and Abdul-Haq Mohiuddin).

TABLE OF CONTENTS

LIST OF TABLES

LIST OF FIGURES

NOMENCLATURE

e^-	Electron
AM	Air mass
$CHCl_3$	Chloroform
DMF	Dimethylformamide
DSSC	Dye-sensitized solar cell
eV	Electron-volt
GW	Gigawatt
IPCC	Intergovernmental Panel on Climate Change
NIR	Near-Infrared
NMP	N-Methylpyrrolidone
NMR	Nuclear Magnetic Resonance
PDI	Perylene Diimide

CHAPTER 1

INTRODUCTION

1.1 Motivation

Fulfilling the energy demand without degrading the environment is one of the top concerns of this century [1]. Till now the demand is continuously being met by conventional fossil fuels, such as oil, coal, and gas but the continuous and massive consumption resulting in depletion of fossil fuels. One of the main reasons for searching an alternative and clean sources of energy is the emission of greenhouse gasses, which contributes to global warming [2]. Energy demand must be fulfilled by the renewable resources to protect the environment. Worldwide investments in renewable energy resources are continuously increasing for better efficiency. Renewable and green energy resources including solar wind and geothermal are abundantly available as compared to other resources. These resources are not evenly available. The most available resource is the solar energy and it is expected to play a significant role in the future energy supply [3], [4]. Earth receives approximately 3×10^{24} joules/year which is 10^4 times more than the world's current energy consumption [5], [6]. As solar resources are widely available but we are still unable to convert solar energy into electrical energy efficiently and cost effectively. Currently, researchers are focusing on improving the conversion efficiency and storage [3]. Converting solar energy into electrical energy efficiently is still the challenge. There is a dramatic development in these technologies but a lot of effort is still required to accomplish the challenge which is; low cost, high efficiency, long-term stability and usage of material that are widely available.

1.2 Generation of Solar Cells

Three generations have been categorized based on the material, cost effectiveness, and performance. In 1893, Edmond Becquerel discovered the photovoltaic effect and the fundamental working principle of first two generations, relies on the photovoltaic effect [4]. The first generation crystalline silicon solar cells are the most dominant as compared to others because of their relatively high efficiency but still required a high capital cost and have a high payback

period. [3]. Regarding the availability, silicon is the second most abundant element in earth's crust and is available in the form of silica dioxide, but for photovoltaic applications, pure silica is required. The production of pure silica requires an enormous amount of energy. Crystalline silicon cells are of two types, mono-crystalline, and multi-crystalline. Concerning efficiency, mono-crystalline is much better than multi-crystalline. Up till now, 25% efficiency has been achieved with crystalline solar cells. The second generation solar cells are a thin film which includes CdS, CdTe, $CuInSe_2$ (CIS), amorphous Si, and $CuInGaSe_2$ (CIGS). The working principle of the thin film is the same as the crystalline solar cells, but thickness has reduced from millimeter to just a few microns. The fabrication process is simple and cheaper to produce but has lower efficiency as compared to crystalline solar cells, so far thin film have achieved 20% efficiency [4]. In 2001, the cost per watt dropped to $0.73 [7].

The major drawback reported in the literature is that the first and second generation for single p-n junction solar cells are limited to Shockley Queisser theoretical limit of ~30% [8]. The third generation solar cells are those which are unique (involving different mechanism) and not restrained by Shockley Queisser limit. Most of the third generation solar cells have not reached in the commercial phase, although the research showed dramatic improvement. Efficiencies of all the solar cells technologies are indicated in the Figure 1.1. In third generation solar cells the most dominant ones are polymer solar cells, organic tandem solar cells and dye-sensitized solar cells.

1.3 Polymer Solar Cells

Polymer solar cells are usually made by dissolving polymers in an organic solvent and transferring to the substrate via printing or coating methods. The layer formation for solar cells is known as solar cell stack. Here the light harvesting material is referred to as active layers, between the hole transport layer (HTL) and electron transport layer (ETL). The two electrodes are negative ETL and positive HTL. One of the electrodes must be transparent to allow the sunlight (photons) to reach to active layer for electron injection process.

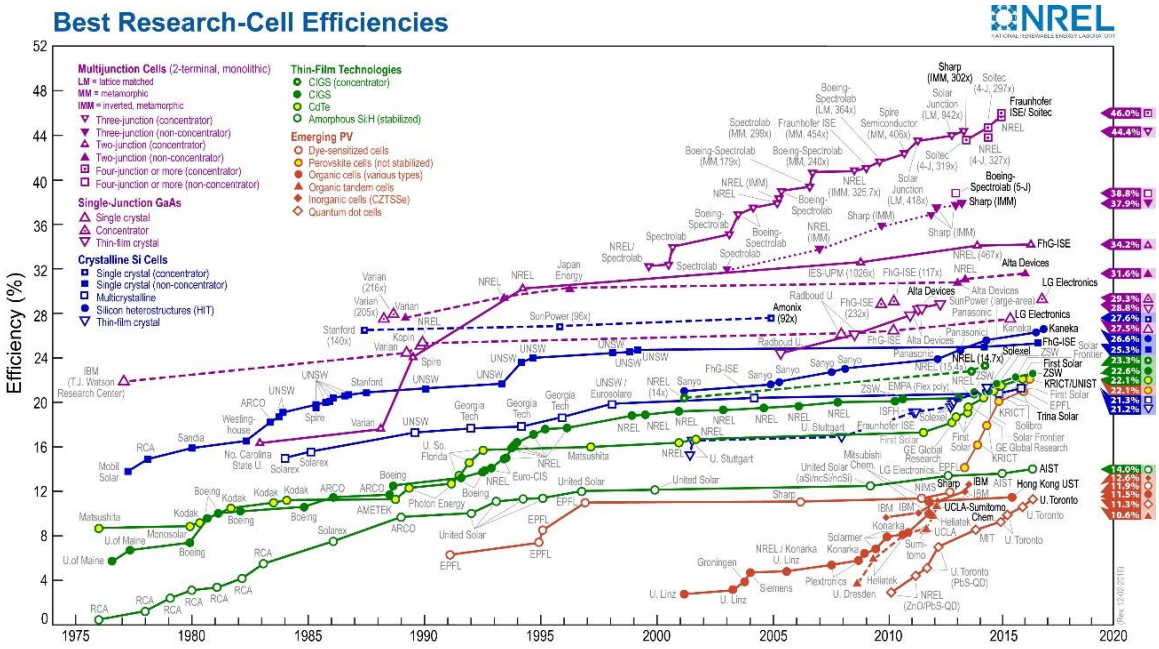

Figure 1.1. Efficiency of all the solar cell technologies [9].

1.3.1 Transport layer

The transport layer is the material that allows the electron or hole to pass due to an appropriate position of the energy level. Commonly used electron transport layer (ETL) are calcium (Ca), Zinc oxide (ZnO), titanium dioxide (TiO_2) and Lithium fluoride (LiF). For HTL the most common materials are polystyrene sulfonate (PEDOT:PSS) and molybdenum oxide.

1.3.2 Electrode

The most common electrode used in the polymer solar cell is indium tin oxide (ITO). It has low resistance to high optical transmission making it suitable for polymer solar cells. Usually, the resistance is less than 10 Ohm/sq and transmission is greater than 85% on glass. There are two main criteria for selecting an electrode: (I) It should have a suitable energy level, and (II) one of the electrodes should be transparent to allow the light to transmit and reach to active layer for electron excitation process.

1.3.3 Substrate

For the support of solar cell stock, the substrate which is used in polymer solar cells, can either be glass or plastics. Floating glass substrate have been used with transparent ITO electrode for lab productions, while for large scale, PET foil used.

1.3.4 Chemistry of polymer solar cell

The active layer of polymer solar cells is organic semiconductors which are characterized by the bandgap (E_g). This gap is the energy difference between the valence electron and nearest free electron state. In other words, it can be defined as the energy difference between the highest occupied molecular orbital (HOMO) and lowest unoccupied molecular orbital (LUMO).

$$E_g = E_{LUMO} - E_{HOMO} \quad \textbf{(1.1)}$$

If at room temperature, the band gap energy of any material is greater than the thermal energy and the thermal activation has no effects on excitation to the conduction state of a valence electron, the material will be classified as the semiconductor. If absorbed photon energy is greater than bandgap energy, excitation of the electron will occur from HOMO to LUMO.

$$E_{photon} = \frac{c.h}{\lambda_{Photon}} \geq E_g \quad \textbf{(1.2)}$$

Here c is the speed of light, h is the Planck's constant and λ_{Photon} is the wavelength of light. If the absorbed energy is less than the band gap energy, the electron will still excite from HOMO but will not be able to reach to the LUMO and will come back to its original state after losing the energy. If the absorbed energy is greater than the band gap energy, the electron will excite from HOMO and will go above the LUMO level. This state is unstable and thus, electron needs to release some energy in the form of heat to reach the LUMO state. In other words, the energy greater than the bandgap energy will be released as heat.

$$E_{thermal\ loss} = E_{Photon} - E_g \quad \textbf{(1.3)}$$

The electron needs to be removed from the LUMO state to generate electricity. For this purpose, secondary semiconductor (acceptor) is used in the active layer. The LUMO level of the secondary semiconductor is lower lying so that the electron transfer from the LUMO of primary semiconductor (donor) to the LUMO of the acceptor. To make the electron transfer more favorable. The LUMO level of donor must be greater than the LUMO level of acceptor as describe in the equation

$$E_{LUMO}^{Donor} - E_{LUMO}^{Acceptor} \geq E_{exe-b} \quad \textbf{(1.4)}$$

The Donor in polymer solar cells is conjugated polymer while the acceptor is a derivative of C60 fullerene. Most of the excitation occurs in the donor molecule, and then excited electrons are transferred to the acceptor. Whereas there is also excitation in the acceptor molecules due to the absorption of photons, and the holes then transferred to the donor. For this transfer and excitation processes, following condition must be met.

$$E_{HOMO}^{Donor} - E_{HOMO}^{Acceptor} \geq E_{exe-b} \quad \textbf{(1.5)}$$

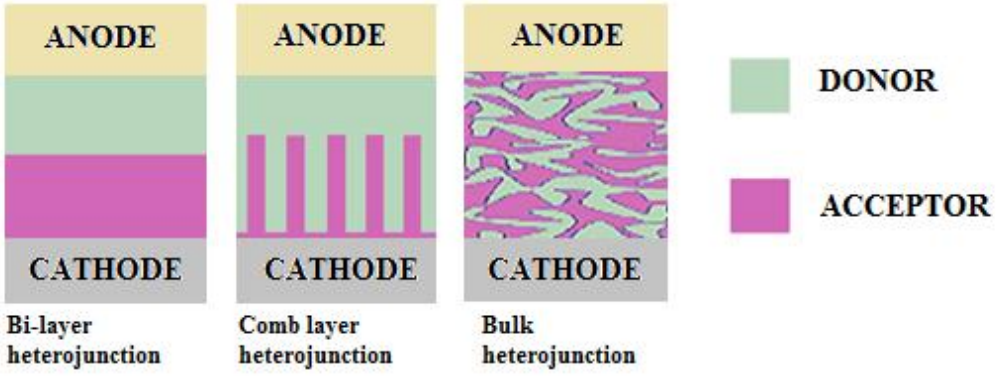

Figure 1.2: Various structure of donor and acceptor in organic solar cells.

The layer of donor and acceptor molecules have a significant effect on the efficiency of polymer solar cell. So far, three structures have been proposed for the combination of donor and acceptor. The first one is the bi-layer heterojunction. It is not the optimal structure as there is only small area that can generate electricity while the absorption occurs in the larger area. The second

structure is the comb layer; it can be made by imprint lithography. The third one involves most optimal structure known as a bulk heterojunction (BHJ). It can be obtained by dissolving donor and acceptor in an organic solvent together and upon solvent evaporation, forms a bulk heterojunction layer as shown in the Figure 1.2.

1.4 Tandem Solar Cells

In polymer solar cells, the organic semiconductor in an active layer have a narrow absorption band for solar radiation making it less efficient. In Figure 1.3 shows the arrangement of the layers of tandem solar cells.

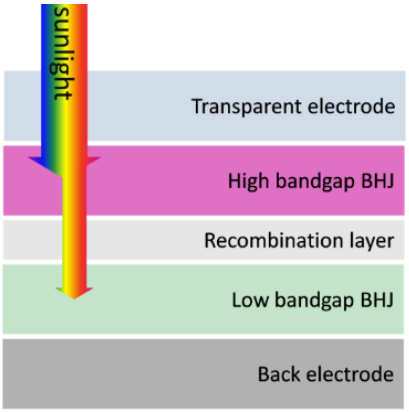

Figure 1.3: Structure of Tendem solar cells

The tandem solar cell idea came after this comparison by combining numerous junctions in one solar cell that will increase the absorption window spectrum. The general structure of a tandem solar cell has shown in Figure 1.3, where recombination layer is in between the high band BHJ and Low band BHJ. This combination not only increases the solar absorption spectrum but also increase the possible achievable efficiency through reducing the thermal relaxation loss (thermalisation).

1.5 Dye Sensitized Solar Cells

1.5.1 History

The first attempt for 'artificial photosynthesis' has been made in 1972 for the generation of electrical energy from a dye sensitizer semiconductor, consisted of ZnO and Chlorophylls [10], although the concept had developed in the 1960s. The idea of dye-sensitized solar cells (DSSC) is introduced in 1988 [11]. After the development of DSSC in 1991 by Gratzel and O'Regan [12], it was proved that DSSC could be the efficient alternative as renewable energy technology.

1.5.2 Advantages

In terms of efficiency, the DSSC is still behind as compared to first and second generation solar cells although it has several edges over these technologies at some point. In cloudy condition, the DSSC work much better than the Si polycrystalline solar cell. Efficiency is not highly dependent on the direct incident of solar radiation so the cost of tracking mechanism can be saved. The efficiency of DSSC is nearly independent of temperature and can operate well in the temperature range of 25-65 $^{\circ}$C unlike Si polycrystalline solar cell. [13]. DSSC is still in research phase and commercial production is not started yet, but expected that the cost would have the advantage over conventional solar cells. The materials available for DSSC is biocompatible and available abundantly so mass production of DSSC will not be difficult and can be easily extended up to terawatt scale. One of the key parameters for solar cells is the long-term stability. It has been confirmed by various researchers that the commercial DSSC can have stability up to 20 plus years. In the fast growing solar energy technologies, DSSC has the advantages over all the technologies to make it feasible and potential candidate for large-scale production.

1.5.3 Mechanism of DSSC

DSSC inspired by the natural photo-chemical process occurs in plants that convert solar energy into the biological material known as photosynthesis. The efficiency of photosynthesis in plants are around 0.02-0.05% [14]. The core component of DSSC is, a dye as a sensitizer, two electrode in which one is anode (TiO_2) sensitized with dye and the other electrode is known as the counter

electrode. Between two electrodes the electrolyte contains redox mediator as shown in the Figure 1.4. The operating steps are discussed below in detail.

1.5.4 Sensitizer

In DSSC the sensitizer is the light harvesting component and absorbs solar radiation (photons). Electron excitation take place from HOMO (S) to LUMO(S*) as shown in the Figure 1.5. Excitation takes place in the order of nanoseconds.

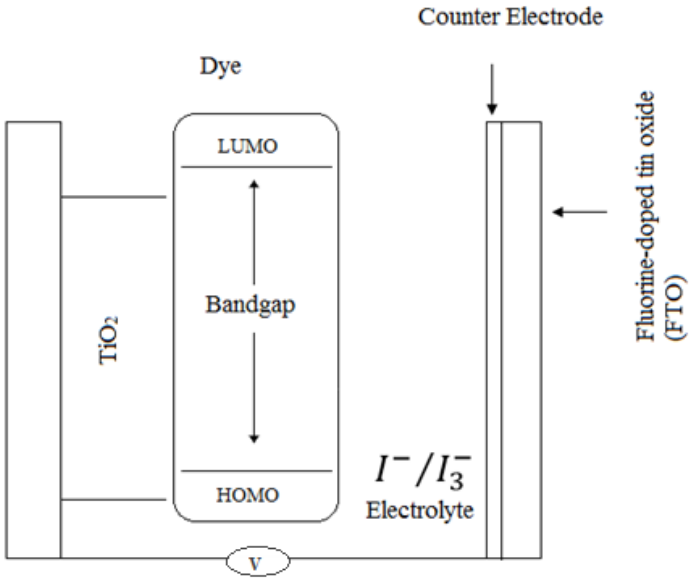

Figure 1.4: Strucuture of Dye sensitzied solar cell

1.5.5 Semiconductor

The most common semiconductor used in the DSSC is TiO_2 and the sensitizer is adsorbed on the surface of the semiconductor. After the excitation, the nanosized semiconductor extract the electron from the dye (LUMO) and dye becomes oxidized (S^+). The TiO_2 conduction band must be below in energy than the LUMO of dye for efficient electron transfer. The electron transfer

from dye to semi-conductor also known as injection of electron, and takes place between 100 fs to 100 ps where feasibility of the process dependent on several factors. [15].

1.5.6 Redox Mediator

To regenerate the dye, a redox mediator, usually iodide/triiodide couple is used. The time scale of dye regeneration is in μs scale [16].

$$2I^- \longrightarrow I_2 + 2e^- \quad \textbf{(1.6)}$$

An electron from conduction band produces the voltage and travel to the FTO electrode and recombine with the electrolyte.

$$I_3^- + 2e^- \longrightarrow 3I^- \quad \textbf{(1.7)}$$

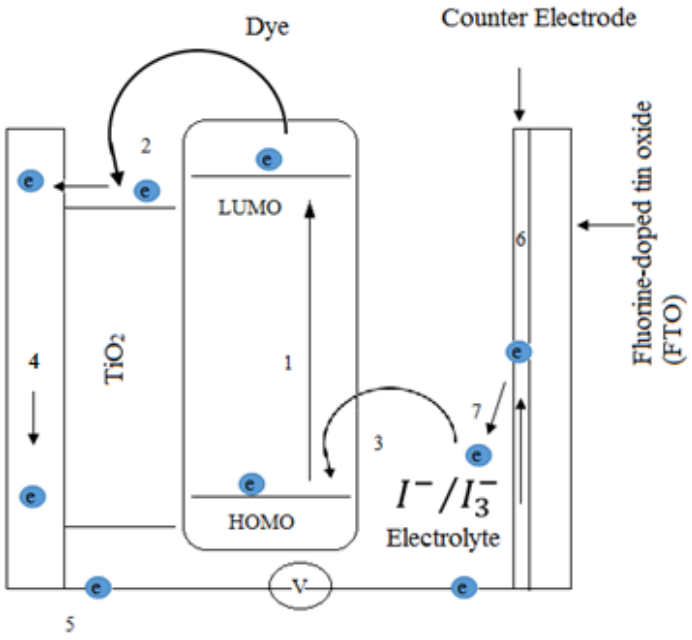

Figure 1.5: Mechanism of Dye sensitized solar cells.

1.5.7 Time Scale

In DSSC every step have a separate timeframe, as shown in the Figure 1.6. Dye regeneration is faster than the recombination of photoelectrons injected into the conduction band of TiO_2 [4].

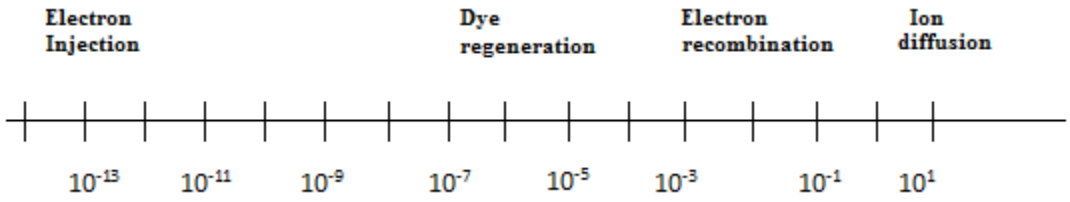

Figure 1.6: Time scale of each step for dye sensitized solar cells.

CHAPTER 2

LITERATURE REVIEW

In the past few years, a lot of work has been published on dye-sensitized solar cells and is increasing exponentially as shown in the Figure 2.1. As in DSSC, the light harvesting and charge carrier transport are two separates functions, this offer the researcher to work on the specific function for system optimizations.

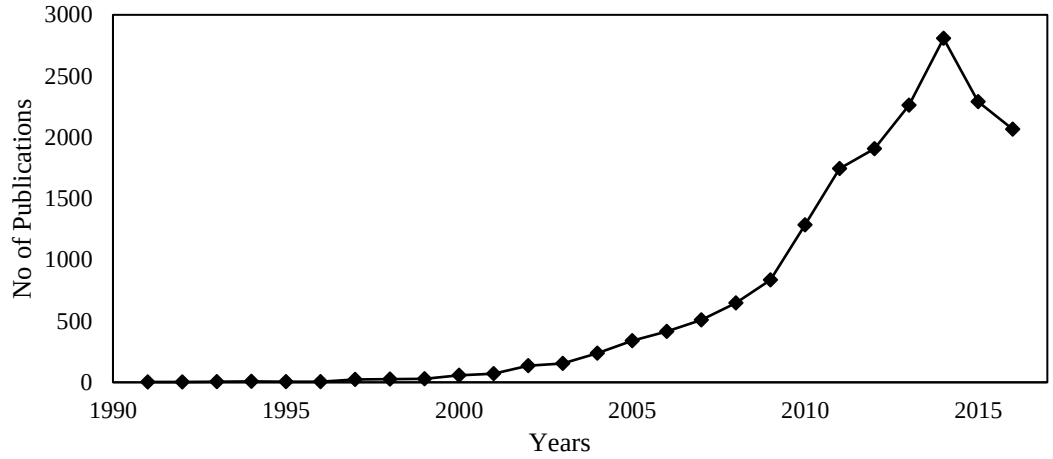

Figure 2.1: Annual no. of publications of dye sensitized solar cells [17].

2.1 Nanostructured Semiconductor Layer

Thin films of transparent and highly porous nanoparticles that absorb the dye on the surface are proven to be essential as semiconducting material [18]. The application of Mesoporous TiO_2 layer consisting of 20nm-sized nanoparticles is the actual source for the uprising the DSSC [12]. Usually, the thickness of the film is 6-8 μm with the porosity of ~60-70%.[18]. Among all the wide bandgap oxide semiconductors, TiO_2 found out to be a promising material. It is abundant in nature, chemically stable, environment friendly and its HOMO and LUMO energies are suitable for dye and electrolyte in DSSC [3]. The electronic excitation energy of rutile and anatase phases are 3 eV and 3.2 eV, respectively[19].

ZnO has also been employed in DSSC as a semiconductor due to similar bandgap and position of conduction and valence band that of TiO_2. Both nanotube[20] and nanoparticled [21] structure of ZnO have been used in DSSC. For flexible substrate such as polymers, ZnO is supportive as it does not require annealing process at high temperature [3]. ZnO was the part of the founding research on DSSC [22]. ZnO is found to be more supportive with electron transportation due to its higher electron mobility as compared to TiO_2 but has an issue with stability. It has been noticed that the anchoring groups in a dye causes dissolution and form Zn^{2+} ions, which can react with the ruthenium-based dyes such as N3 and N719 and formed insoluble complexes. Due to the formation of insoluble complexes charge transportation is disturbed, resulting a decrease in efficiency. [23]. Research has been done with employing alternative semiconductor such as In_2O_3, Y_2O_3, SnO_2, Nb_2O_5 [24]–[27] and found that they are not so efficient but can be a potential candidate in future.

2.2 Sensitizer (Dye)

In 1971 photosensitization of a Chlorophylls was investigated on ZnO (semi-conductor) with a very low efficiency but quantum efficiencies of 0.125 electrons per absorbed photon were achieved [28]. In 1993 natural porphyrins and numerous derivatives of chlorophylls were investigated by Kay and Gratzel on 12 μm mesoporous TiO_2 and reached the conversion efficiency of 2.6%. Chemically improved chlorophyll-containing carboxylic group as an anchoring group with the common iodide based redox-mediator achieved 3.1% conversion efficiency. If bacterial carotenoids are used, efficiency can be improved to 4% [29]. Chlorophyll derivatives with anchoring group such as carboxylic, could improve the efficiency to 6.5% [30], [31].

A natural dye such as anthocyanin that can be extracted from Blackberries have also been investigated with the efficiency of 1%[32]. Several other natural dyes have been tested, and highest efficiency achieved up to date with a natural dye is 1.7% [33].

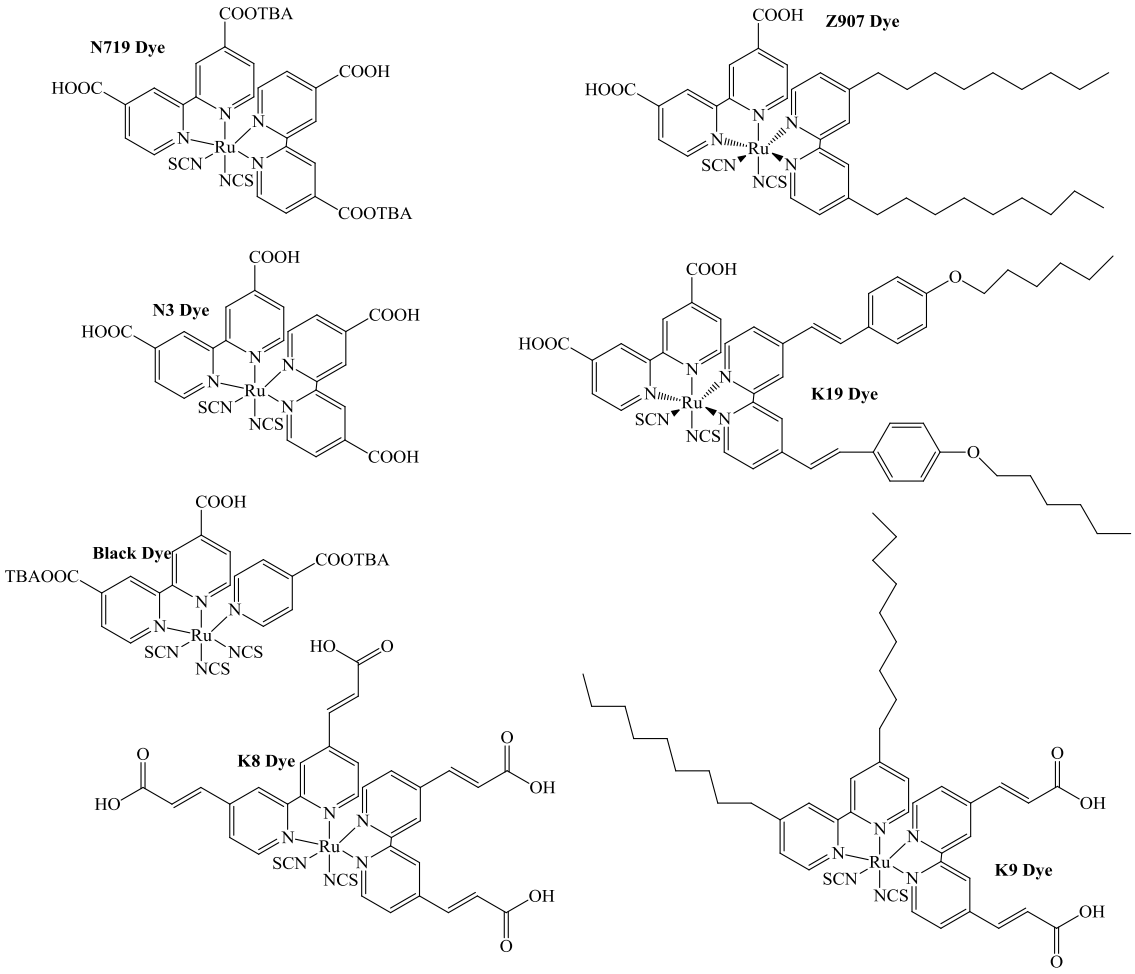

Figure 2.2: Structure of various sensitizers

Many sensitizers have been synthesized for dye-sensitized solar cells. In 1993 ruthenium-based dye known as (N3) has been synthesized by Gratzel and coworkers, showing 10% efficiency and high stability. The chemical name of N3 is cis-di(thiocyanato)bis(2,2' –bipyridyl-4-4'-dicarboxylate)ruthenium(II). Due to its properties, N3 was found to be the most outstanding dye and has grabbed the attraction of many researchers. The IPCE (incident Power Conversion Efficiency) was found to be 80% between the wavelengths of 480 to 600 nm and near 100% between 510 to 570 nm . The quantum yield of electron injection from semiconductor found to be 100%. No significant decomposition was observed before 10^7 turnovers [19]. Despite several

benefits, it also has some weaknesses such as comparatively low molar extinction coefficient and insignificant absorption in red region of spectrum [34].

Some other ruthinium derivatives as shown in Figure 2.2, are were also synthesized. In 2001 Gratzel group synthesized Black dye based on ruthenium, that is consider as the best dye so far with IPEC 80% within the visible region to near infra-red up to 920 nm with the overall efficiency up to 10.4%[4], [34], [35].

2.2.1 Perylene diimides in DSSC

Perylene derivatives has been introduced as a sensitizer in DSSC due to its outstanding photo-physical, photochemical, electrochemical and thermal characteristics, as well as ability to form derivatives with anchoring group such as carboxylic acid that can help the sensitizer to attach with the semiconductor surface.

2.2.2 Synthesis of Perylene Dimides Derivatives.

For the synthesis of perylene dimide derivatives, perylene-3,4,9,10-tetracarboxylic dianhydride (PTCDA) is standard starting material. Condensation reaction between perylene-3,4,9,10-tetracarboxylic dianhydride and aniline/alkly amines produces PDI derivatives with high yield. The synthesis of PTCDA is shown in Reaction-scheme 2-1. [36].

Derivatives of PDI dye can be obtained by derivatizations at the imide position. For synthesizing symmetrical PDI derivatives, the common procedure is the condensation reaction of PTTCDA with primary amines and aromatic aniline, in a high boiling point solvent such as (quinolone/imidazole), using zinc acetate as catalyst [37]. Another approach to synthesize symmetrical perylene diimide is treating the PTCDA with reactive amine in hot alcohol, like n-butanol, a carboxylic acid, like acetic acid or by using water and alcohol as mixed-solvent system. The condensation reaction of PTCDA and o-phenylenediamine derivatives produces perylene benzoimidazole derivatives. However, this reaction produce two regioisomers. Purification of regioisomeric mixture can be achieved by recrystallization and/or column chromatography, as shown in Reaction-scheme 2-1.

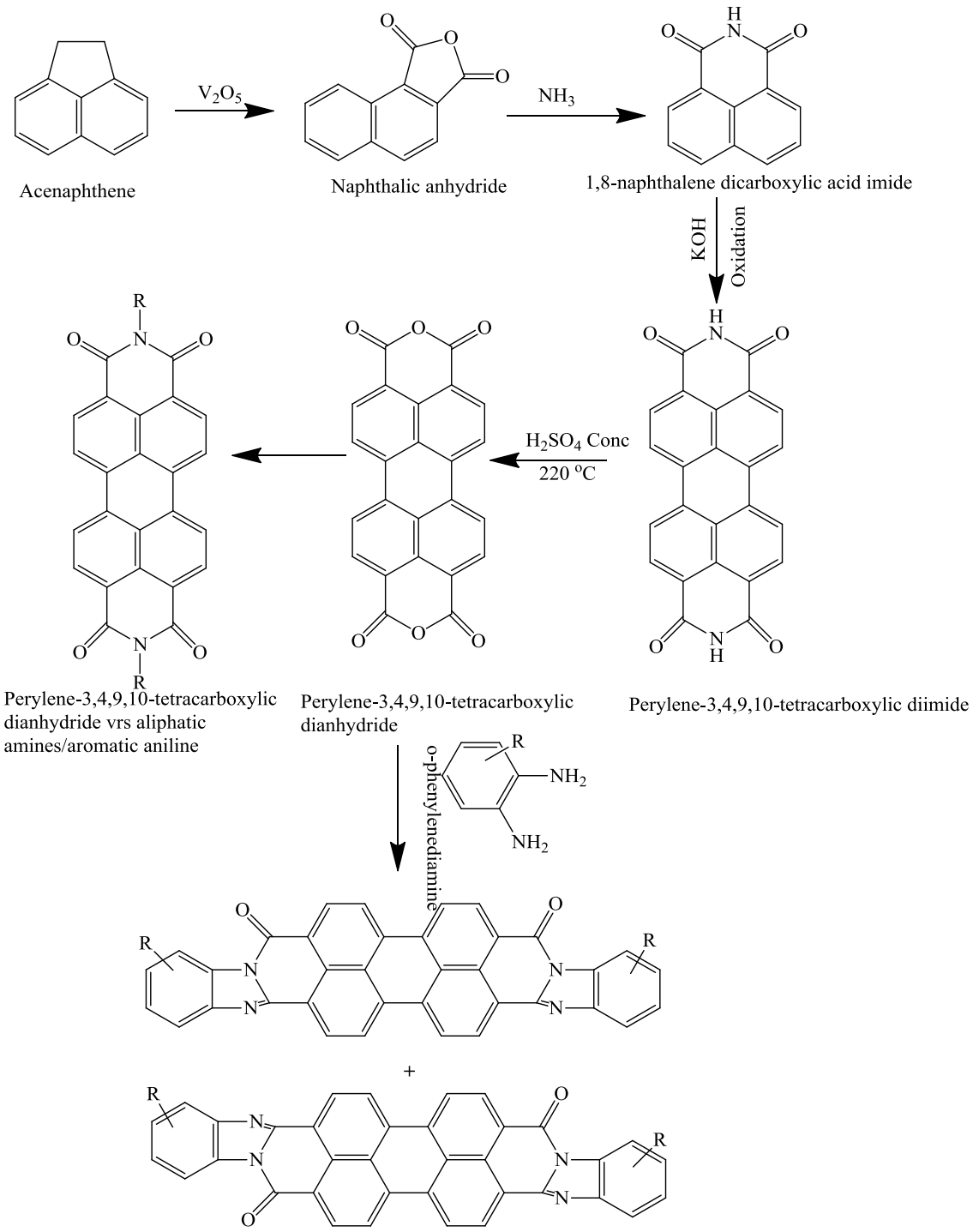

Reaction-scheme 2-1: Imide substituent positions of PDI preparations.

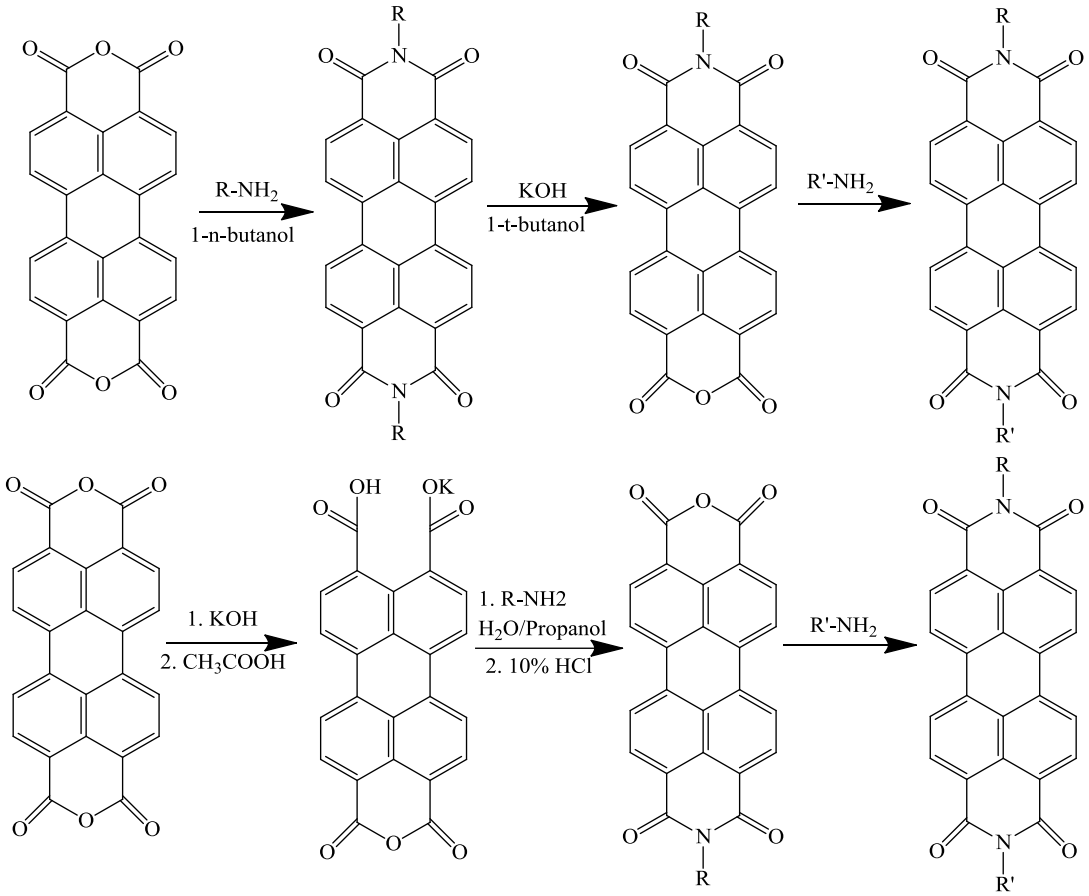

Reaction-scheme 2-2: Imide substituent positions of asymmetric PDI preparations

Reaction-scheme 2-2 shows the preparation of asymmetric PDI derivatives with substituent at imide positions. Mainly two approaches has been applied in synthesis of assymetric PDI derivatives [38]. First step essentially begins from synthesis of respective symmetrical PDI derivatives. Further hydrolysis produces perylene monoimide monoanhydride compound. Imidization of perylene monoimide monoanhydride derivatives with a second amine can produce desired asymmetrical PDI. Notably, it has been found that symmetrical PDI are dominant products even when only one equivalent or less of the primary amine is added to the reaction mixture. Another method for synthesis of asymmetrical PDI derivatives involves the hydrolysis of PTCDA with KOH to lead to mono anhydride mono potassium salt, followed by imidizations as shown in the scheme 2-2.

2.2.3 Bay-Substituted Derivatives

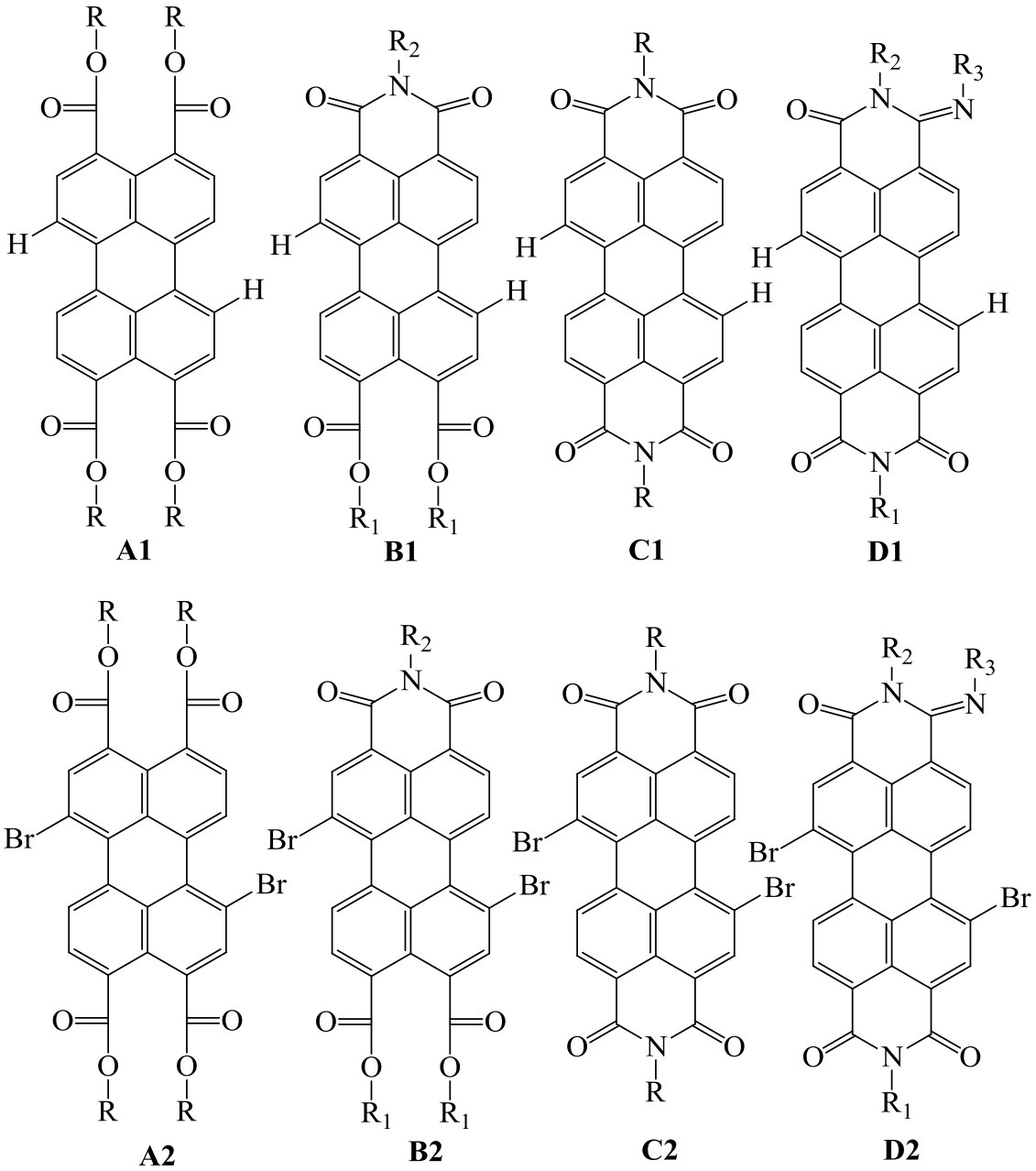

Figure 2.3: Perylene tetracarboxylic acid derivatives.

The substitution at bay region normally consist of two or four substituent, with a prior halogenation of perylene-3,4,9,10-tetracarboxylic bisanhydride to yield 1,7-dibromorperylene-3,4,9,10-tetracarboxylic bisanhydride [39] or 1,6,7,12-tetrachloroperylene-3,4,9,10-tetracarboxylic bisanhydride[40]. 1,7- substitution produces the isomeric mixture of 1,6 and 1,7-di-substituted perylene bisimides as well as some 1,6,7-trisubstituted isomers.. It has been shown that 1,6 and 1,7 isomers may show distincly different properties.

The synthesis of isomerically impure 1,7-dibromoperylene-3,4,9,10-tetracarboxylic tetraesters have been described in literature recently [41].

The synthesis starts with the commercially available perylene-3,4,9,10-tetracarboxylic bisanhydride (E1) which is converted into perylene-3,4,9,10-tetrabutylester (E2), followed by bromination at bay region in dichloromethane at room temperature, giving isomers of 1,7 (2) and 1,6 (2a) –dibromoperylene-3,4,9,10-tetracarboxylic tetrabutylester. From the regioisomerically impure mixture pure 1,7-dibromoperylene-3,4,9,10-tetracarboxy tetrabutylester (2) can be isolated by crystallization, as shown in Reaction-scheme 2-3. By utilizing the solubility difference of mono and bisanhydride in solution, mono or bisanhydride synthons can be synthesized by careful adjustment of reaction conditions and solvent. E4 and E5 can be imidized with amines in NMP and acetic acid to form respective compounds (E6 and E7). E6 can be further treated with p-TsOH.H_2O in excess toluene at 100 °C to produces E8 as shown in the Reaction-scheme 2-4.

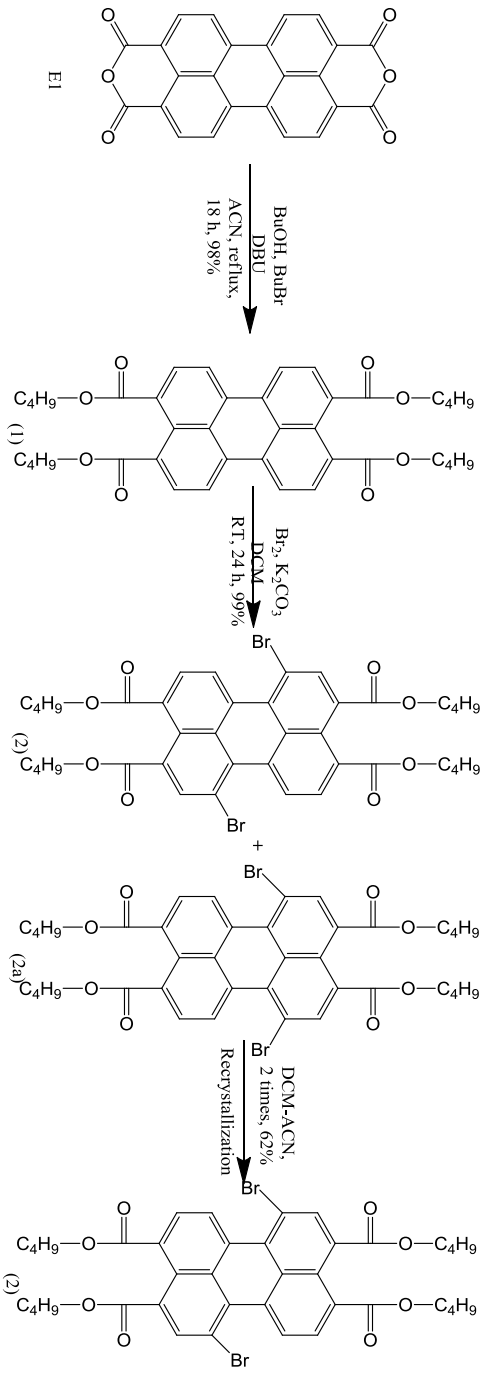

Reaction-scheme 2-3: Synthesis and purification of 1,7-dibromoperylene-3,4,9,10-tetracarboxy tetrabutylester (2) from PBA(E1).

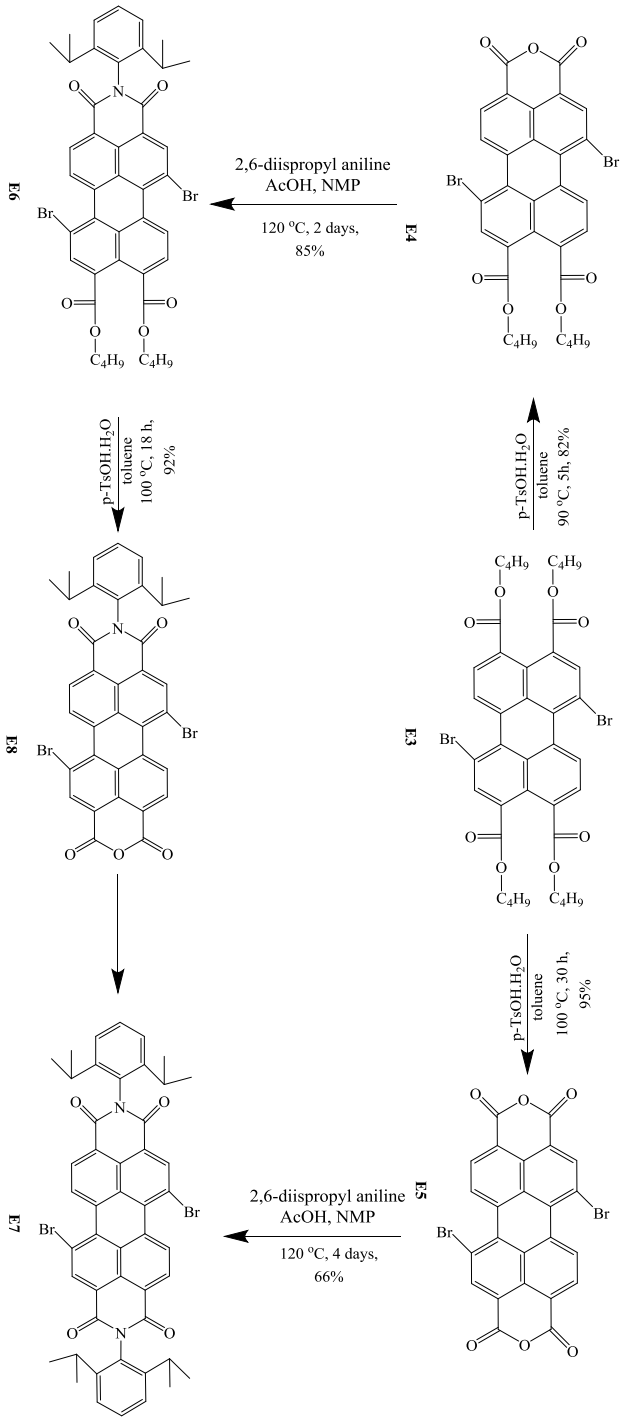

Reaction-scheme 2-4: Synthesis of 1,7-drbromo substituted derivatives.

2.2.4 Perylene Derivatives for DSSC

Some perylene derivatives that are used as sensitizers in DSSC fabrication are shown in Figure 2.4. Compounds (a) and (b) in Figure 2-4, having carboxylic as an anchor group was among the first perylene derivatives used as DSSC component, achieving 30%IPCE between 458-488 nm, with the overall efficiency of 0.89%.[42]. After that several other derivatives have been synthesized [43], [44],[45], [46], [47],[48].

Due to good light harvesting ability, PDI derivatives have shown good potential for DSSC. PMIMA have taken too much attention where anhydrides are acting as an anchoring group. It has been found that the electron withdrawing groups such as imide or anhydride on both sides of molecule considerably reduce the favorable charge transfer of an excited electron from molecule towards the conduction band of metal oxide. It could be the reason of perylene diimide derivatives not to compete with ruthenium complex dye and so far have achieved 3.08%, which is quite less than ruthenium complex dye [49].

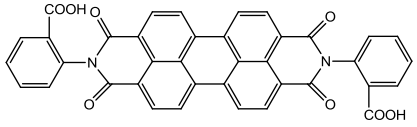

(a)

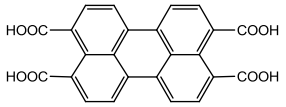

(b)

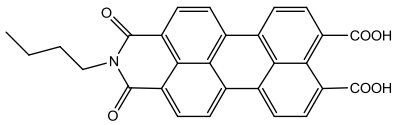

(c)

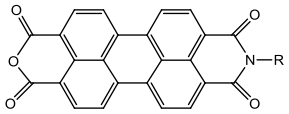

d1: R=1-Pentyl-hexyl
d2: R=1-Isobutyl-3-methyl-butyl
d3: R=2-Ethyl-hexyl
d4=2,6-Diisopropyl-phenyl
d5=Cyclohexyl

(d)

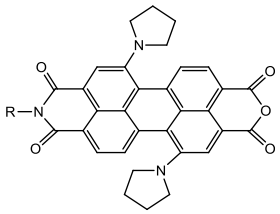

(e): R=2,6-diisopropylphenyl
(f): R=cyclohexyl

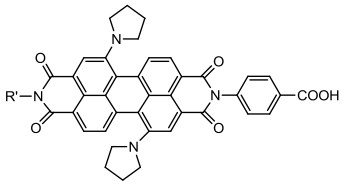

(g): R'=2,6-diisopropylphenyl
(h): R'=cyclohexyl

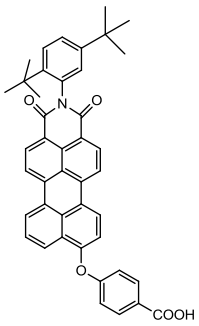

(i)

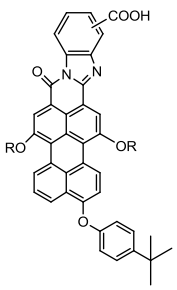

(j)

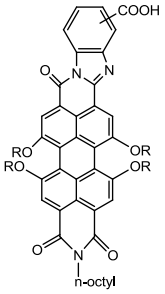

(k)

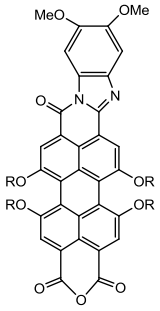

(l)

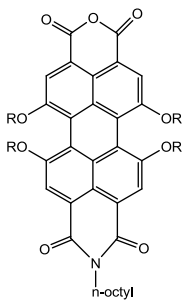

(m)

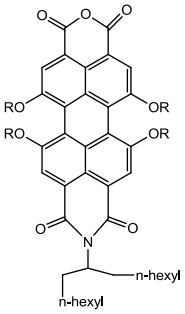

(n)

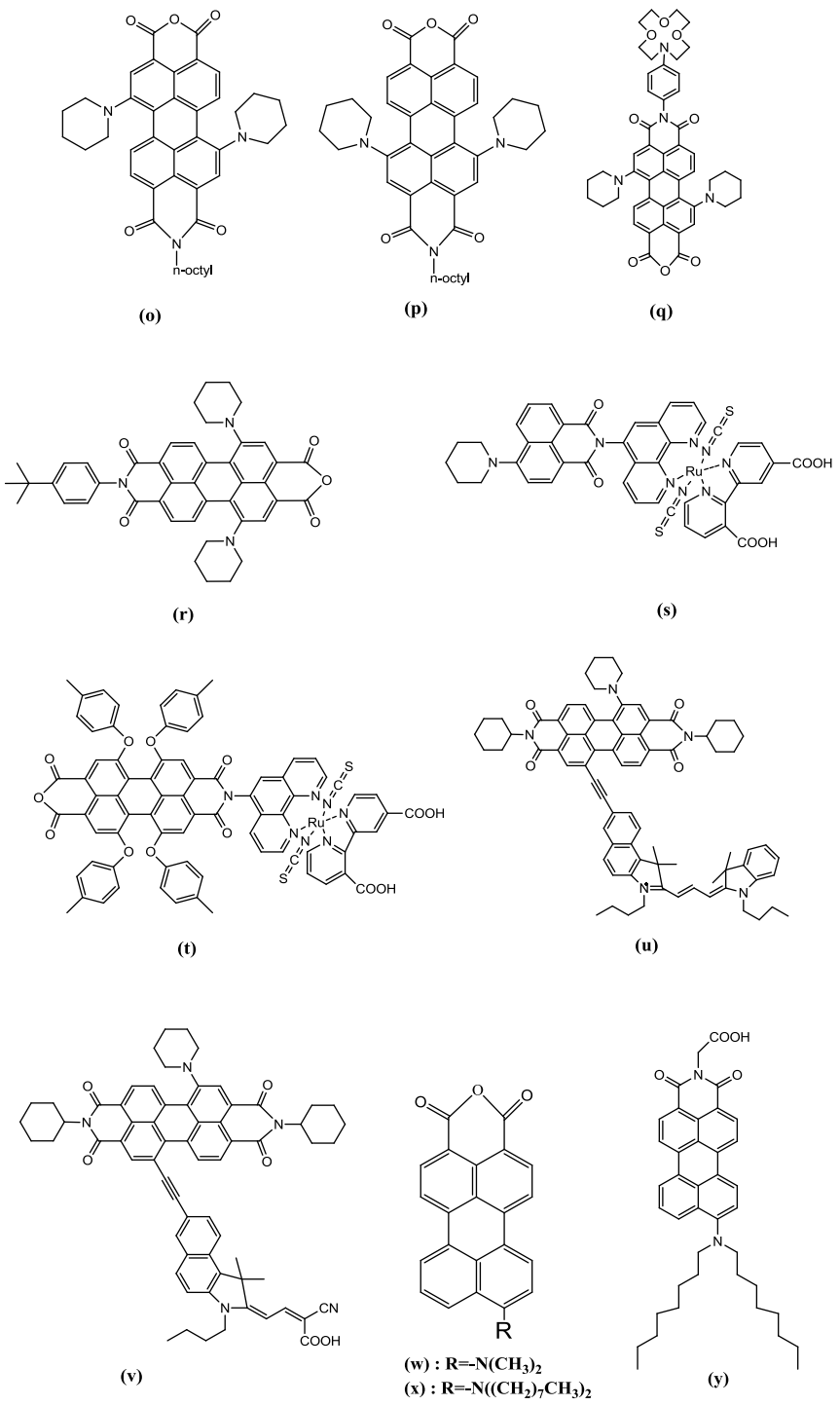

Figure 2.4: Structure of derivatives of perylene di-imides

2.2.5 Sensitizer selection

In DSSC, the dye act as a sensitizer (light harvesting molecule) and is considered as the heart of DSSC. The choice of dye as a sensitizer is countless but for effective photo-generation, some criteria need to be fulfilled.

Absorption: The absorption spectrum should be broad to harvest sun light efficiently.

Solubility: The dye must be soluble in the suitable solvent so that it can be easily transferred to TiO_2 surface (Semiconductor) [18].

Anchoring group: The dye must have a functional group that helps the dye molecule to spontaneously assemble to the surface of the semiconductor. The most common ones are carboxylate, hydroxamate or phosphonate. It has been found that carboxylate groups perform better than phosphonate groups. For carboxylate group, ATR-FTIR measurements show that it binds on the surface of the semiconductor by bidentate chelation [50].

Band gap: For efficient electron transfer from dye to semiconductor the LUMO level of dye should be above the LUMO level of semiconductor and for efficient recombination, the HOMO level of dye should lie below the redox potential of redox couple in the electrolyte.

Non-aggregation: For reducing the surface aggregation additives such as cheno are added into the sensitizer [51]. Macrocyclic organic dyes have aggregation issue and this can be solved by adding bulky molecule (mostly chenodeoxycholic acid) during the synthesis of sensitizer [52].

Stability: The dye should have the lifetime of around 20 years (10^8 redox/oxidation reaction cycle) to compete with the conventional solar cells [18].

2.3 Electrolyte

During the conversion of light into electricity, electrolyte plays a vital role as it acts as the electron transfer mediator (transfer electrons to regenerate the dye from the oxidized state). There are some criteria that must be fulfilled by the electrolyte to be selected in the DSSC which are listed below.

- For preventing the degradation of dye, it should have a long-term optical, thermal, chemical and electrochemical stability.
- Electrolyte must also be able to transport the carriers between the working electrode and the back electrode.
- It is essential for the liquid electrolyte to prevent the loss of solution by evaporation or leakage. It should also have a good contact with the counter electrode and the porous nano-crystalline oxide layer.
- There should not be a substantial absorption in the visible region.

Till now three types of electrolyte categories have been introduced such as liquid, quasi-solid and solid, depending upon their viscosity. The most common electrolyte used in DSSC is the liquid electrolyte. They are usually prepared by the redox couple dissolved in high dielectric constant organic solvent. It has also been reported that additives can be added to increase the performance. [23], [53].

The most common and highly employed redox-couple is I^-/I_3^- iodide/triiodide, principally due to slow recombination reaction. These type of electrolytes are simply synthesized by dissolving iodide salts in the solvent with cations such as Mg^{2+}, Na^+, Li^+. Due to the corrosive properties of iodine, alternatives redox-couple such as Br^-/Br^{-3} [54], $SCN^-/(SCN)^{-3}$ [55], and $SeCN^-/(SeCN)^{-3}$ [56] have also been investigated. All of them show encouraging electrochemical and non-corrosive properties but struggle in maintaining chemical stability. Some of the coordination compounds such as cobalt and copper complexes have been used as a mediator [57], [58]. Presently Co complexes are considered as the most efficient and promising redox-couple because they are non-volatile, non-corrosive and comparatively transparent in the visible light region. Furthermore, redox based electrolyte (Co(II)/(III)tris(bipyridyl) has achieved efficiency up to 12% [59].

Alternative methods and techniques have been proposed and are currently under investigation to improve the efficiency. Some of the special considerations are room temperature ionic liquids, quasi-solid electrolytes and the solid electrolytes.

The room temperature ionic liquids (RTIL) are characterized by high ionic conductivity, good chemical and thermal stability and less volatility. For DSSC the most widely used RTILs are alkylpyridinium salt, trialkyl methylsufonium salt and alkyl imidazolium salt. The only problem they have is high viscosity, resulting in slow diffusion of charge carriers [60].

Quasi solid electrolyte can be synthesized from organic solvent-based or ionic liquid electrolyte that can be gelled, polymerized, or dispersed in polymeric matrix or in which nanoparticles are dispersed [23].

Solid state electrolytes are characterized by conductive polymers, hole conducting molecular solids or organic p-type conductors, such as 2,2′,7,7′-tetrakis(N,N-dimethoxyphenylamine)-9,9′-spirobifluorene (spiro-MeOTAD) [61], polyaniline (PANI) [62], polypyrrole [63], poly(3,4-ethylenedioxythiophene) (PEDOT) [64] and poly-3-hexylthiophene (P3HT) [65].

2.4 Counter Electrode

The counter electrode is made-up from glass covered with the film of conductive oxide. Catalyst coating is essential to ensure satisfactorily fast reduction kinetics at the TCO-coated cathode [23].

The catalysts which are widely used in DSSC are carbon-based materials and platinum (Pt). The employment of platinum increases the magnitude of current and voltage and has been characterized by low counter electrode resistance [66]. There are several approaches of platinum coating such as electrochemical [67], [68], spin coating [69], vapor deposition [70] and sputtering [19].

2.5 Sealing

Sealing can enhance the long-term stability of the DSSC if done properly, that is the reason it is one of the technological challenges. There are some criteria that the sealing material should fulfil such as

- Should be completely chemically inert towards all the components of the DSSC including the electrolyte.

- Good adherence to the glass substrate and the TCO coating.
- High Resistance to both ambient oxygen and water vapor.

Till now various sealing materials have been employed such as water glass (sodium silicate) and epoxy glue, aluminum foil laminated with polymer foil [71], vacuum sealent Torr Sear®, an ionomer resin Surlyn® (grade 1702) from Du Pont or the combination of these. When selecting the sealing material, the tolerance of sealing material is checked for iodide and triiodide [53].

2.6 Main Parameters of Solar cells

Using photovoltaic effect, photovoltaic device convert incident sunlight to electrical energy. The production of electrical energy under light is achieved by the capability of photovoltaic device to produce current and voltage over external load at the same time.

The typical current-voltage (I-V) characteristic of basic solar cells along with some important parameters such as open circuit voltage V_{oc}, short circuit current, I_{sc}, and maximum power point, P_{max}, is shown in the Figure 2.5.

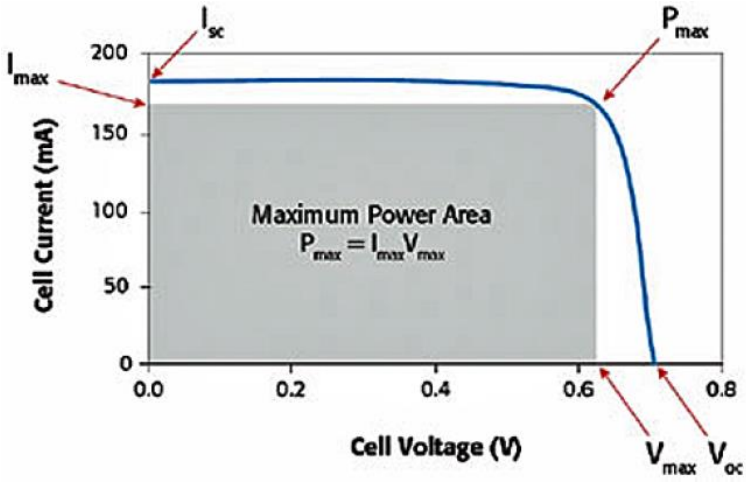

Figure 2.5: Current-Voltage curve for dye sensitized solar cells

When the solar device is connected with an infinite resistance (no current flow) the maximum voltage generated is called as open circuit voltage (V_{oc}) and it is defined as the difference between the potential of the conduction band of TiO_2 and the redox potential of the electrolyte.

When the electrodes are short circuited, the maximum current is called short circuit current I_{SC}. Whereas when the product of current and voltage is maximum the power is considered as maximum power (P_{max}).

The current flow is highly dependent on the area of device irradiated by the solar energy, so it is better to denote maximum current density I_{max} and short circuit current density I_{sc} instead of short circuit current and maximum current, by only dividing these values with the area of the cell which is illuminated by the sun.

With the IV characteristic an important parameter is obtained known as fill factor (FF). It is defined as the ratio of theoretical maximum power ($I_{max}\ V_{max}$) and the measured power ($I_{sc}\ V_{oc}$).

$$FF = \frac{I_{max}V_{max}}{I_{sc}V_{oc}} \quad \textbf{(2.1)}$$

Power conversion efficiency (PCE) is also derived from I-V characteristics and it is defined as the ratio of maximum power generated by the cell and the power density of incoming solar radiation.

$$PCE = \frac{P_{max}}{P_{inc}} = \frac{I_{sc}V_{oc}FF}{W_{inc}} \quad \textbf{(2.2)}$$

2.6.1 Light Intensity and temperature

The number of photons is directly related to the light intensity; higher the light intensity, higher will be the number of photons. Short circuit current shows linear increase when light intensity increases. Open circuit voltage also increases slightly with increase in light intensity. Decrement has been noticed in fill factors because of ohmic losses in the conducting glass electrodes [72]. V_{oc} decreases and current rises significantly when the temperature increases. The effect on fill factor is dependent on solvent used for electrolyte. Fill factor in high viscosity solvents such as propylene carbonate, increases with temperature. Voltage decreases due to increment of dark current, which causes an increases in the rate constant of triiodide reduction. Within the temperature range the quantum efficiency values are not affected. It has been found that the

sensitized charge injection rate is independent of temperature, which implies a quantum mechanical tunneling process. One of the advantage of DSSC is that the effect of temperature on the cell efficiency is trivial because of different compensating factors.

CHAPTER 3

MATERIALS AND INSTRUMENTS

Solvents and chemicals employed in this research were purchased either from Sigma-Aldrich or Merck Millipore, as reagent grade purity. All the chemicals were used without any further purification unless otherwise reported. Air sensitive reactions were carried out under dry nitrogen (N_2) atmosphere. Solvent used for chromatographic separation were purified according to the standard purification methods [73]. Pore size of 60 Å, 70-230 mesh, 63-200 µm silica gel were used for column chromatography. Thin layer chromatography (TLC) was done using, silica gel coated with fluorescent indicator F254 on aluminum plate. Nuclear magnetic resonance (NMR) spectra were recorded on a Bruker Avance 400 MHz spectrometer. Fourier transform infrared spectra (FTIR) were recorded with a Varian-660 IR spectrometer in the spectral range of 4000-400 cm^{-1} in the transmittance mode. Solid samples were recorded as KBr pellets. UV-visible measurements were recorded on a PG-Instruments T80+ spectrophotometer. Shimadzu RF-5301 PC spectrofluorophotometer were used to measure the fluorescence emission spectra and the spectral data were processed into graphical representation in Microsoft Excel^{Tm}; the data were analyzed through linear regression analysis in OriginLab® software. All the solvents employed for spectral measurements were spectroscopic grade.

3.1 Synthetic Procedures

3.1.1 Synthesis of perylene-tetracarboxylic tetrabutyl ester (Compound 1)

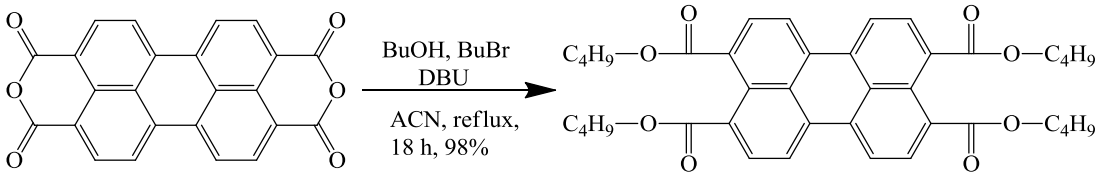

PDA (Compound 1)

Reaction-scheme 3-1: Syntheisis of perylene-tetracarboxylic tetrabutyl ester (Compound **1**)

A mixture of PDA (MW=392.32 g/mol) (0.980 g, 1 equivalent), 1,8-Diazabicyclo[5.4.0] underc-7-ene (DBU) (4 equivalent), n-butanol (1.50 g, 8 equivalent) in 500 ml of Dimethylformamide (DMF) was stired at 60 °C for 0.5 hour. 1-Bromobutane (2.74 g, 8 equivalent) was added to the mixture and a subsequent addition of another 9 ml of DMF, and further stirred for 3 hours. After cooling the resulting mixture to room temperature, the solvent was poured into water (100 ml) and stirred for 15 minutes, after which it was filtered. The crude residue collected, was subjected to column chromatography on silica gel, eluting with dichloromethane (CH_2Cl_2), to give compound **1** as golden-orange solid (yield 1.54 g).

IR (KBr): 3247, 2964, 2330, 1730, 1587, 1447, 1304, 1034, 810, 737, 606 cm-[1].

UV-vis: $\lambda_{max}CHCl_3$ = 472 nm (ε = 30000, R^2=0.98) and 443 nm (ε = 23800, R^2 = 0.98); λ_{max} DMF = 469 nm (ε = 46100, R^2 = 1.00) and 441nm (ε = 38600, R^2 = 1.00).

^{1}H NMR ($CDCl_3$, 400MHz): 1.04 (t, 12H), 1.55 (m, 8H), 1.83 (m, 8H), 4.37 (t, 8H), 7.80 (d, 4H), 7.85 ppm (d, 4H).

^{13}C NMR ($CDCl_3$,100 MHz): 13.8, 19.3, 30.7, 65.3, 121.1, 128.3, 128.5, 130.1, 132.4, 168.5 ppm.

3.1.2 Synthesis of 1,7-dibromoperylene-3,4,9,10-tetracarboxyl tetrabutylester (Compound 2)

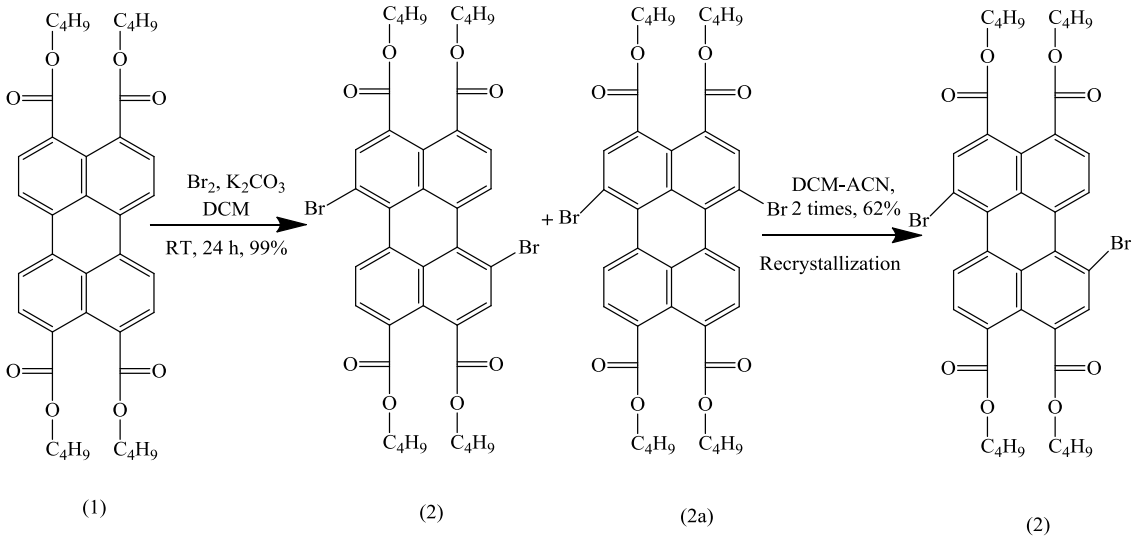

Reaction-scheme 3-2: Synthesis of 1,7-dibromoperylene-3,4,9,10-tetracarboxyl tetrabutylester (Compound **2**)

In a 50 ml round-bottom flask, a mixture of perylene tetrabutylester (0.500 g, 0.766 mmol) and K_2CO_3 (0.250 g, 1.81 mmol) were taken and mixed in CH_2Cl_2 (10 ml). Drop wise, bromine (0.5 ml, 9.70 mmol) was added to the resulting mixture and stirred for 24 hours at room temperature. Afterwards, an aqueous solution of sodium metabisulphite ($Na_2S_2O_5$) was added drop wise to the reaction mixture while stirring. The organic layer of the reaction mixture was washed with several portion of water and dried over sodium sulphate (Na_2SO_4). The solvent was then removed by rotary evaporation giving crude product (0.597 g) consisting of a mixture of 1,7-and 1,6-dibromo isomers. The reaction scheme is shown in Reaction-scheme **3-2**. The isolation of the regioisomerically pure 1,7-dibromo was accomplished by a double crystallization from dichloromethane/acetonitrile mixture [76].

IR (KBr): 3577, 3328, 2952, 2870, 2511, 2331, 2086, 1944, 1731, 1589, 1454, 1385, 1303, 1168, 1051, 951, 816, 740, 603 cm^{-1}.

UV-vis: $\lambda_{max}CHCl_3$ = 468 nm (ε = 32400, R^2 = 1.00) and 443 nm (ε = 28700, R^2 = 1.00); λ_{max}DMF = 466 nm (ε = 31500, R^2 = 1.00) and 441 nm (ε = 28200, R^2 = 1.00).

^{1}H NMR ($CDCl_3$, 400 MHz): 1.00 (t, 12H), 1.60-1.46 (m, 8H), 1.81-1.77 (m, 8H), 4.34 (t, 8H), 8.08 (d, 2H), 8.28 (s, 2H), 8.91 ppm (d, 2H).

^{13}C NMR ($CDCl_3$,100 MHz): 13.8, 19.3, 30.6, 65.6, 65.8, 118.7, 126.5, 127.6, 129.0, 130.4, 131.1, 131.7, 136.7, 167.1, 168.0 ppm.

3.1.3 Synthesis of 1,7-Dibromoperylene-3,4,9,10-tetracarboxy monoanhydride Dibutylester (Compound 3)

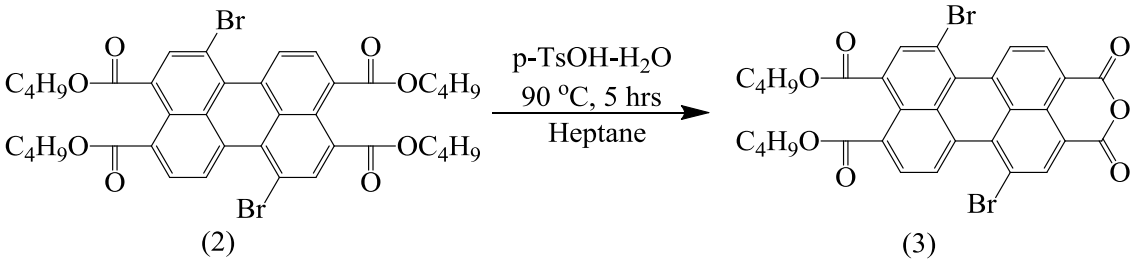

Reaction-scheme 3-3: Synthesis of 1,7-Dibromoperylene-3,4,9,10-tetracarboxy monoanhydride Dibutylester (Compound **3**)

Regioisomerically pure compound-2 (1.00 g, 1.23 mmol) and p-toluenesulfonic acid monohydrate (p-TsOH-H_2O) (305 mg, 1.60 mmol) were taken in 3 mL of n-heptane. The reaction was stirred at 90 °C for 5 hours, and the product (compound **3**) began to precipitate from the reaction mixture. The reaction was cooled to room temperature after 5 hours and the product was filtered off and washed with few portion of methanol, and water. The dried orange precipitate was subsequently taken into methanol (200 ml) and refluxed for 2 hours. Resulting mixturewas cooled to room temperature and filtered to remove the unreacted starting compound. The residue was monoanhydride compound **3**. Finally the dried residue was dissolved in a little amount of

dichloromethane and filtered to remove the insoluble bisanhydride. The solvent was then evaporated to produce a crude product (32 % yield) [76].

IR (KBr): 3454, 3058, 2943, 2871, 2727, 2510, 2364, 1782, 1706, 1602, 1458, 1379, 1271, 1168, 1019, 806, 695 cm^{-1}.

$\lambda_{max}CHCl_3$ = 505 nm (ε = 41200, R^2 = 1.00) and 484 nm (ε = 34100, R^2 = 1.00); $\lambda_{max}DMF$= 497 nm (ε = 32000, R^2 = 1.00) and 469 nm (ε = 26800, R^2 = 1.00).

Melting point: 205 °C (literature 202 °C).

^1H NMR ($CDCl_3$, 400 MHz): δ = 9.27 (d, J=8.0 Hz, 1H), 9.24 (d, J-8.1 Hz, 1H) , 8.89 (s,1H), 8.68 (d, J=8.0 Hz,1H), 8.34 (s,1H), 8.15 (d, J=8.0 Hz, 1H), 4.39-4.33 (m, 4H) , 1.85-1.78 (m,4H), 1.54-1.48 (m,4H), 1.04-1.00 ppm (m, 6H).

3.1.4 Synthesis of N-[2-(diethylamino)ethyl]-1,7-dibromoperylene-3,4,9,10-tetracarboxy monoimide dibutylester (Compound 4).

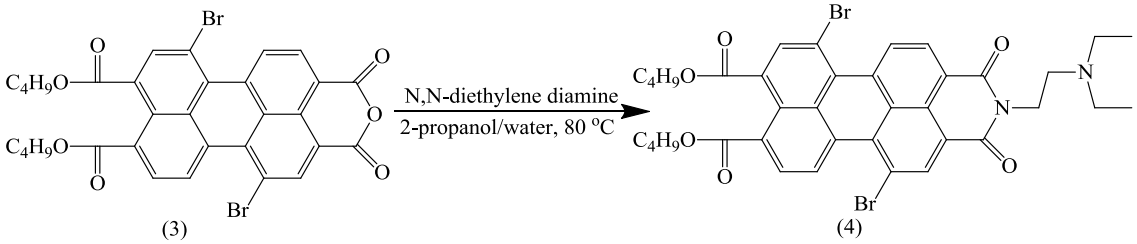

Reaction-scheme 3-4: Synthesis of N-[2-(diethylamino)ethyl]-1,7-dibromoperylene-3,4,9,10-tetracarboxy monoimide dibutylester (Compound **4**).

0.200 g of compound **3** (0.294 mmol, 1 equivalent), N,N-diethylene diamine (0.588 mmol, 2 equivalent, 0.0826 ml) and acetic acid (5 equivalent, 1.47 mmol, 0.083 ml) in 6 ml of water and 2-propanol mixture (2:1) was stirred at 80°C under N_2 for 4 days, during which time followed by TLC for the disappearance of starting material (compound **3**). After cooling down to RT, solvent

was removed under reduced pressure giving 0.31 g of orange solid. Crude product was subjected to column chromatography on silica gel, eluting with dichloromethane/methanol (10/1), to give compound **4** in pure form. Yield, 78% (R_f=0.39).

IR (KBr): 2962, 2929, 2892, 1699, 1658, 1589, 1504, 1456, 1404, 1381, 1348, 1300 cm^{-1}.

UV-vis: $\lambda_{max}CHCl_3$ = 504 nm (ε = 34100, R^2 = 1.00) and 474 nm (ε = 27500, R^2 = 1.00); λ_{max}DMF = 499 nm (ε = 23800, R^2 = 1.00) and 470 nm (ε = 19400, R^2 = 1.00).

^{1}H NMR (400 MHz, CDCl3): δ = 9.20 (d, J = 8.0 Hz, 2H), 9.16, (d, J = 8.0 Hz, 2H), 8.85 (s, 1H), 8.63 (d, J = 8.0 Hz, 1H), 8.33 (s, 1H), 8.12 (d, J = 8.0 Hz, 1H), 4.36 (m, 6H), 2.85 (t, J = 7.3 Hz, 2H), 2.72 (q, J=7.0 Hz, 4H), 1.80 (m, 4H), 1.12 (t, J=7.0 Hz, 6H), 1.01 ppm (t, J = 7.3 Hz, 6H)

^{13}C NMR (100 MHz, CDCl3): δ = 167.7, 166.9, 163.1, 162.6, 137.8, 136.8, 133.9, 133.5, 131.9, 131.8, 131.5, 130.8, 130.5, 129.9, 129.0, 128.1, 128.0, 126.9, 126.7, 122.1, 121.9, 120.2, 119.3, 66.0, 65.8, 49.6, 47.4, 38.0, 30.6, 30.5, 19.3, 19.2, 13.8, 11.9 ppm.

HRMS (ESI-TOF): Calculated for $C_{38}H_{39}N_2O_6Br_2$ $[M + H]^+$: 777.1175, found: 777.1146.

3.1.5 Synthesis of N-[2-(diethylamino)ethyl]-1,7-di(4-tert-butylphenoxy)perylene-3,4,9,10-tetracarboxy monoimide dibutylester. (Compound 5)

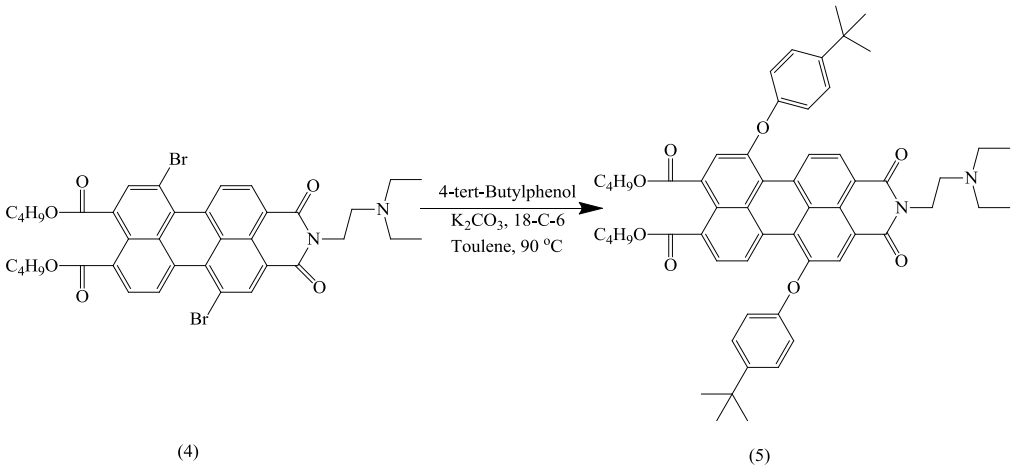

(4) (5)

Reaction-scheme 3-5: Synthesis of N-[2-(diethylamino)ethyl]-1,7-di(4-tert-butylphenoxy)perylene-3,4,9,10-tetracarboxy monoimide dibutylester. (Compound **5**)

A mixture of 4-(tert-butyl) phenol (3 equivalent, 44 mg), K_2CO_3 (6 equivalent, 44 mg) and 18-crown-6 in dry toluene (20 ml) was stirred for 45 minutes at room temperature under N_2. Subsequently, 76 mg of compound **4** was added. Resulting reaction mixture was stirred for 4 hours at 90°C under N_2. After cooling to room temperature, solvent was removed under vacuum. The crude product obtained, was introduced to the column chromatography on silica gel, eluting with 70% ethyl acetate in hexane. 80 mg product was isolated with the yield of 89% (R_f=0.30).

IR (KBr): 2962, 2924, 2868, 1718, 1697, 1649, 1591, 1506, 1409, 1349, 1263, 1219, 1193 cm^{-1}.

UV-vis: $\lambda_{max}CHCl_3$ = 518 nm (ε = 38700, R^2 = 1.00) and 485 nm (ε = 30000, R^2 = 1.00); $\lambda_{max}DMF$= 513 nm (ε = 37200, R^2 = 1.00) and 480 nm (ε = 29000, R^2 = 1.00)

^{1}H NMR (400 MHz, CDCl3): δ = 9.38-9.35 (m, 2H), 8.53 (d, J = 8.5 Hz, 1H), 8.33 (s, 1H), 8.03 (d, J = 8.3 Hz), 7.75 (s, 1H), 7.45-7.41 (m, 4H), 7.09-7.03 (m, 4H), 4.33-4.25 (m, 6H), 2.81-2.77

(m, 2H), 2.70-2.65 (m, 4H), 1.78-1.66 (m, 4H), 1.51-1.44 (m, 4H), 1.36 (s, 18H), 1.09 (t, J = 14.3 Hz, 6H), 0.95 (t, J = 14.8 Hz, 3H), 0.90 ppm (t, J = 14.3 Hz, 3H).

HRMS (ESI-TOF): Calculated for $C_{58}H_{65}N_2O_8$ $[M + H]^+$: 917.4741, found: 917.4717.

3.1.6 Synthesis of N-[2-(diethylamino)ethyl]-1,7-di(pyrrolidinyl)perylene-3,4,9,10-tetracarboxy monoimide dibutylester. (Compound 6)

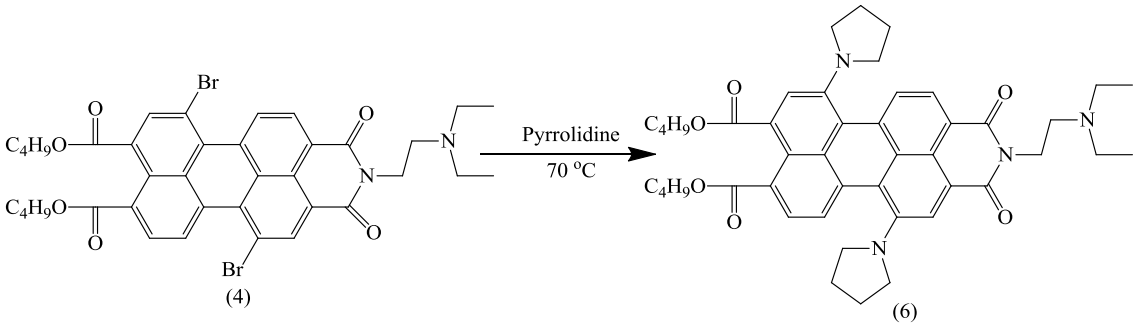

Reaction-scheme 3-6: Synthesis N-[2-(diethylamino)ethyl]-1,7-di(pyrrolidinyl)perylene-3,4,9,10-tetracarboxy monoimide dibutylester. (Compound **6**)

Compound **4** (100 mg, 1 eq) was dissolved in 7 ml of pyrrolidine and stirred for 24 hrs at 70 °C. After cooling to room temperature, the solvent was removed under reduced pressure. The resulting crude product was bluish green. The crude product was subjected to column chromatography with DCM/MeOH=10/0.5 as eluent. 50 mg product was isolated with the yield of 51.4 % (R_f = 0.14).

IR (KBr): 2962, 2924, 2850, 1714, 1685, 1647, 1585, 1552, 1508, 1446, 1409, 1375, 1344, 1288, 1257, 1222 cm^{-1}.

UV-vis: $\lambda_{max}CHCl_3$ = 653 nm (ε = 41500, R^2 = 1.00) and 610 nm (ε = 32000, R^2 = 1.00); $\lambda_{max}DMF$= 650 nm (ε = 40800, R^2 = 1.00) and 605 nm (ε = 30700, R^2 = 1.00).

^{1}H NMR (400 MHz, CDCl3): δ = 8.45 (s, 1H), 8.37 (d, J = 8.0 Hz, 1H), 7.97 (d, J = 8.0 Hz, 1H), 7.93 (s, 1H), 7.83 (d, J = 8.0 Hz, 1H), 7.39 (d, J = 8.3 Hz, 1H), 4.37-4.30 (m, 6H), 2.89-2.84 (m, 2H), 2.77-2.72 (m, 4H), 1.84-1.71 (m, 4H), 1.56-1.42 (m, 4H), 1.17 (t, J = 14.31, Hz, 6H), 1.03-0.95 ppm (m, 6H).

HRMS (ESI-TOF): Calculated for $C_{46}H_{55}N_4O_6$ $[M + H]^+$: 759.4122, found: 759.4100

3.2 Experimental Findings and Calculations

3.2.1 Maximum extinction coefficient (ε_{max})

At a particular wavelength, the strength of light absorbed by a solution is known as the maximum extinction coefficient. The relationship between absorbance and concentration is known as ***Beer Lambert's law***.

$$\varepsilon_{max} = \frac{A}{cL} \quad \textbf{(3.1)}$$

ε_{max} is the maximum extinction coefficient at a certain wavelength (L.mol^{-1} cm^{-1}), c is the concentration (mol. L^{-1}), **A** is the absorbance and ***L*** is the path length of sample (cm).

3.2.2 Absorption and Emission properties.

The molar absorptivity coefficient can be determined by plotting absorbance against concentration at the selected wavelength. For this purpose, different concentrations were prepared and absorbances were measured with UV-vis spectrophotometer in two different solvents $CHCl_3$ and DMF. The wavelengths corresponding to the two highest peaks were recorded and absorbance values of each of the concentration were plotted against concentration on separate graph to determine the molar absorptivity coefficient from slope, as shown in the Figure A.13 to Figure A.60 in appendix.

3.2.3 Singlet Excitation Energies (Es)

The energy required for an electron to get excited from ground state to the first singlet excited state is known as singlet excitation energy. Mathematically, it is given as

$$E_s = \frac{2.86\times10^5}{\lambda_{max}} \quad \textbf{(3.2)}$$

Where λ_{max} is the maximum absorption wavelength (in Å), **Es** is singlet energy (in kcal.mol^{-1}). Calculated singlet energies of title compounds 1-6 are tabulated in Table 3-1. The results shows

that the substitution of electron donor group at bay region significantly decreases the singlet excitation energies. Results of compound **5** and **6** suggests that stronger the electron donor attached at bay region, may results in a decrease in the singlet excitation energies.

Table 3-1: Singlet excitation energies for the compounds **1-6**

Analysis	Compounds					
	1	**2**	**3**	**4**	**5**	**6**
			Solvent: $CHCl_3$			
λ_{max} (Å)	4720	4680	5050	5040	5180	6530
Es (kcal.mol^{-1})	60.59	61.11	56.63	56.75	55.21	43.80
			Solvent: DMF			
λ_{max} (Å)	4690	4660	4970	4990	5130	6500
Es (kcal.mol^{-1})	60.98	61.37	57.55	57.31	55.75	44.00

3.2.4 Oscillator strength (f)

In an atomic or molecular system, the electronic transition strength is measured by oscillator strength which is given as,

$$f = 4.32 \times 10^{-9} \Delta\bar{\upsilon}_{1/2} \varepsilon_{max} \quad \textbf{(3.3)}$$

In equation 3.2, ***f*** is the oscillator strength, ε_{max} is the maximum extinction coefficient at the maximum absorption wavelength (L.mol^{-1} cm^{-1}). $\Delta\bar{\upsilon}_{1/2}$ is the half-width of an absorption (cm^{-1}). The half-width of an absorption $(\Delta\bar{\upsilon}_{1/2})$ represents the full or half-width of the maximum intensity curve, which is calculated as:

$$\Delta\bar{\upsilon}_{1/2} = \bar{\upsilon}_1 - \bar{\upsilon}_{11} \quad \textbf{(3.4)}$$

Using equation 3.3 half-widths of compounds 1-6 were estimated, and tabulated in the Table 3-2.

Table 3-2: Half-width estimation for the compounds **1**-**6**

Compound	λ_{max} (nm)	$\lambda_{\perp}$ (nm)	$\lambda_{\parallel}$ (nm)	$\bar{\upsilon}_{\perp}$ (cm^{-1})	$\bar{\upsilon}_{\parallel}$ (cm^{-1})	$\Delta\bar{\upsilon}_{1/2}$ (cm^{-1})
			Solvent: $CHCl_3$			
1	472	455	486	21959	20559	1400
2	468	452	485	22133	20634	1499
3	505	486	524	20573	19071	1502
4	504	437	470	22883	21277	1607
5	518	466	541	21459	18484	2975
6	653	580	685	17241	14599	2643
			Solvent: DMF			
1	469	453	483	22075	20687	1388
2	466	452	482	22143	20747	1397
3	497	481	520	20807	19242	1565
4	499	482	517	20747	19342	1405
5	513	460	534	21739	18727	3013
6	650	575	685	17391	14599	2793

3.2.5 Theoretical Radiative lifetimes (τ_0)

Theoretical lifetime **(τ_0)** of an excited molecule can be expressed as;

$$\boldsymbol{\tau_0} = \frac{3.5\times10^8}{\bar{\upsilon}_{max}^2\times\varepsilon_{max}\times\Delta\bar{\upsilon}_{1/2}} \qquad \textbf{(3.5)}$$

Where ε_{max} is the maximum extinction coefficient at the maximum absorption wavelength (L. mol^{-1}. cm^{-1}), $\bar{\upsilon}_{max}$ is the mean frequency of the maximum absorption band (cm^{-1}), and $\Delta\bar{\upsilon}_{1/2}$ is the half width of an absorption band (cm^{-1}).

Using above equation, the calculated theoretical radiative lifetime of the compounds are tabulated in Table 3-3

Table 3-3: Theoretical radiative lifetime of compounds

Compounds	1	2	3	4	5	6
	Solvent: $CHCl_3$					
$\bar{\upsilon}^2_{max}$ (cm^{-2})	4.49×10^8	4.57×10^8	3.92×10^8	3.94×10^8	3.73×10^8	2.35×10^8
$\Delta\bar{\upsilon}_{1/2}$ (cm^{-1})	1400	1499	1502	1607	2975	2643
ε_{max} ($M^{-1}\,cm^{-1}$)	29100	32400	41200	34100	38700	41500
τ_0 (ns)	18.6	15.8	14.4	16.2	8.17	13.6
	Solvent: DMF					
$\bar{\upsilon}^2_{max}$ (cm^{-2})	4.55×10^8	4.60×10^8	4.05×10^8	4.02×10^8	3.80×10^8	2.37×10^8
$\Delta\bar{\upsilon}_{1/2}$ (cm^{-1})	1388	1397	1565	1405	3013	2793
ε_{max} ($M^{-1}\,cm^{-1}$)	23800	31500	32000	23800	37200	40800
τ_0 (ns)	23.3	17.3	17.2	26.1	8.23	12.9

3.2.6 Optical Band Gap Energy

The optical band gap estimations of compounds 1-6 using maximum absorption wavelength of the lowest energy band are tabulated in the Table 3-4.

Table 3-4: Optical band gap at maximum absorbance wavelength

Compounds	**1**	**2**	**3**	**4**	**5**	**6**
			Solvent: CHCL3			
$\lambda_{0\rightarrow0}$ (nm)	472	468	505	504	518	653
E_g eV	2.63	2.65	2.46	2.46	2.39	1.90
			Solvent: DMF			
$\lambda_{0\rightarrow0}$ (nm)	469	466	497	499	513	650
E_g eV	2.64	2.66	2.49	2.48	2.42	1.91

3.2.7 Fluorescence Quantum Yield

Figure 3.1 shows all the typical process that can occur when a fluorophore excited. In general, after excitation, the process may involve are deactivation via emission of photons, internal conversion and vibrational relaxation (loss of heat to the surrounding, non-radioactively) and the intersystem crossing to the triplet manifold and subsequent non-radiative deactivation [74].

Fluorescence quantum yield (ϕ_F) is the ratio of photons emitted via fluorescence to the photons absorbed.

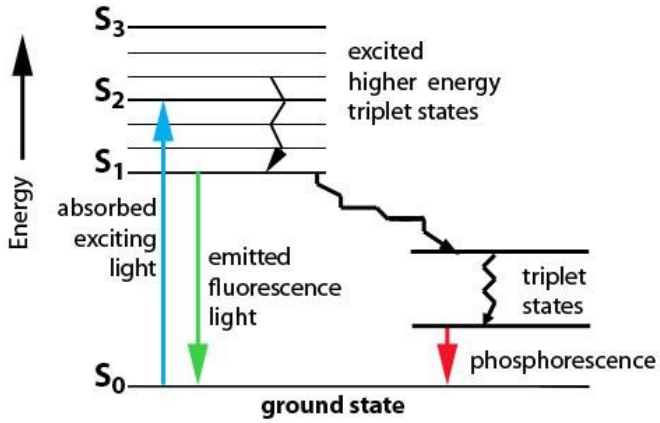

Figure 3.1: Typical Jablonski Diagram

For quantum yield determination, Winfield [75] method were employed which is one of the most reliable methods for determining quantum yield. The method involves the use of a standard sample with known quantum yield.

$$\phi_F = \phi_{st}\left(\frac{Gradiant_u}{Gradiant_{st}}\right)\left(\frac{\eta_u^2}{\eta_{st}^2}\right) \quad \textbf{(3.6)}$$

In Eq (3.5) ϕ_F and ϕ_{st} are the fluorescence quantum yield of unknown and standard sample respectively. $Gradiant_u$ and $Gradiant_{st}$ are the slope of integrated fluorescence intensity versus absorbance of unknown and standard sample respectively. η_u and $\eta_{st}$are the reflective index of the solvent and standard solution respectively. For compounds 4-6, fluorescence quantum yields are determined in DMF, and data is tabulated in Table 3-5.

3.2.8 Theoretical Fluorescence Lifetime (τ_F)

Theoretical fluorescence lifetime of a molecule is the theoretical time that a fluorophore stays at excited state before emitting photons (fluorescence) and can be calculate as:

$$\tau_F = \tau_0 \times \Phi_F \quad \textbf{(3.7)}$$

In Eq (3.6) τ_0 is the theoretical radiative lifetime and τ_F is the fluorescence lifetime in ns respectively and Φ_F is the quantum yield.

3.2.9 Fluorescence Rate constant (k_F) and Rate constant of radiation-less Deactivation (K_d)

The reciprocal of theoretical radiative lifetime (in s^{-1}) is known as the fluorescence rate constant.

$$k_F = \frac{1}{\tau_0} \quad \textbf{(3.8)}$$

τ_0 is the theoretical radiative lifetime in ns. Rate constant of radiationless deactivation, k_d, can be calculated as

$$k_d = \left(\frac{k_F}{\tau_0}\right) - k_F \quad \textbf{(3.9)}$$

Calculated values for τ_0 (ns), τ_F (ns), k_F (s^{-1}), and k_d (s^{-1}) are tabulated in Table 3-5.

Table 3-5: Calculated photophysical data for compounds **4-6** in DMF

	Φ_F	τ_0 (ns)	τ_F (ns)	k_F (s^{-1})	k_d (s^{-1})
Compound 4	0.027	26.12	0.704	3.83×10^{07}	1.38×10^{09}
Compound 5	0.040	8.23	0.331675	1.22×10^{08}	2.89×10^{09}
Compound 6	0.001	12.97	0.012426	7.71×10^{07}	8.04×10^{10}

CHAPTER 4

RESULTS AND DISCUSSION

In this study, we carried out the synthesis and characterization of regioisomerically pure antisymetric 1,7-disubstituted-perylene-3,4,9,10-tetracarboxylic acid derivatives to understand and compare their photophysical properties with that of symmetric perylene bisimides bearing same substituents. To accomplish this task electron donating groups were successfully substituted at bay region of perylene unit as shown in Figure 4.1.

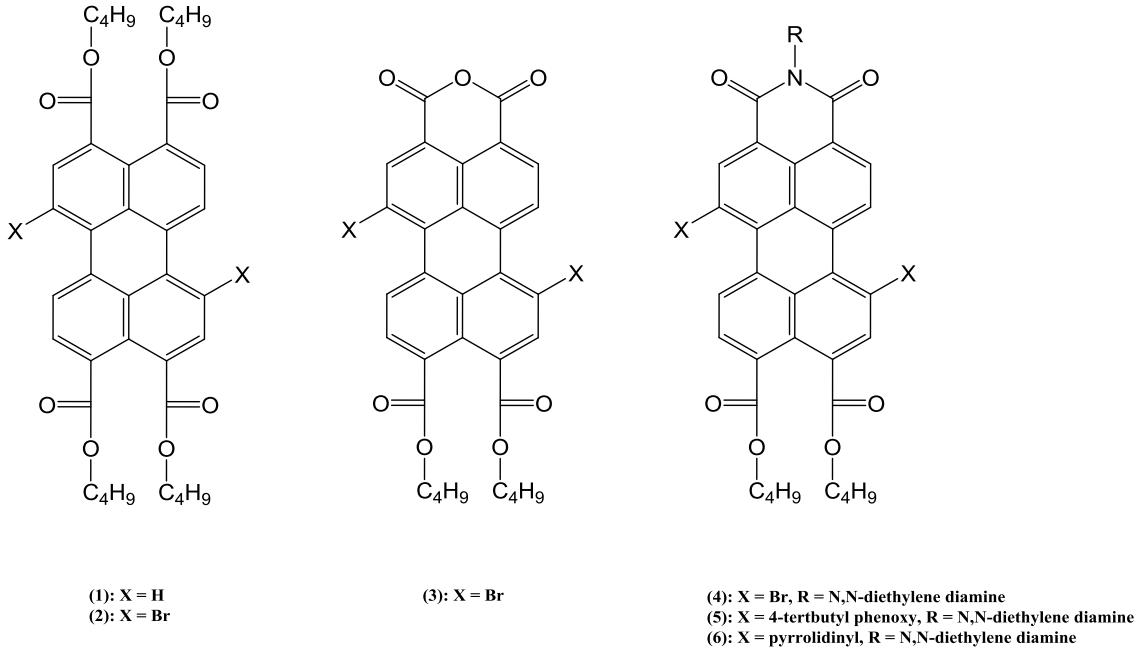

Figure 4.1: Targeted Structure

4.1 Chemical Synthesis

The key intermediates for the synthesis of the Novel antisymetric 1,7-perylene-3,4,9,10-tetracarboxylic acid derivatives, perylene-3,4,9,10-tetrabarboxylic tetraesters (**1**), 1,7-Dibromoperylene-3,4,9,10-tetracarboxylic tetraesters (**2**) and 1,7-Dibromoperylene-3,4-9,10-

tetracarboxylic tetraesters-monoanhydride (**3**) were synthesized according to the previously published procedures [76], as shown in Reaction-scheme 4-1 and Reaction-scheme 4-2. The dibromination of PDA can be done at room temperature with good yield. The resulting bromination mixture consist of (1,7/1,6)-dibromoro regioisomers with (4/1) ratio, as proven by ^{1}H NMR, and is separated via repetitive crystallization from acetonitrile and dichloromethane solvent mixture [76].

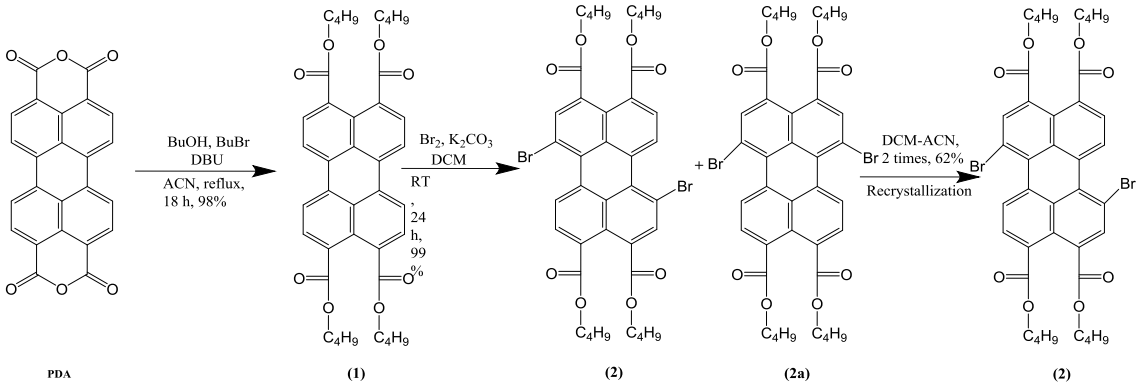

Reaction-scheme 4-1: Synthesis of Pure 1,7 dibromoperylene-3,4,9,10-tetracarboxy tetrabutylester

Compound 2 is a very versatile synthon, in a way that, it can be selectively converted into either 1,7-dibromo bisanhydride, or to 1,7-dibromo monoanhydride dibutylester, where the dianhydride compound can be further utilized in the synthesis of regioisomerically pure 1,7-disubsituted perylene diimides. Reaction-scheme 4-2 shows the synthesis of regioisomerically pure monoanhydride-dibutylester compound **3** from compound **2**. In order to suppress the dianhydride formation, which reduces the yield of formation of **3**, a solvent that dissolves compound **2** but hardly dissolves compound **3** is used at the reaction temperature.

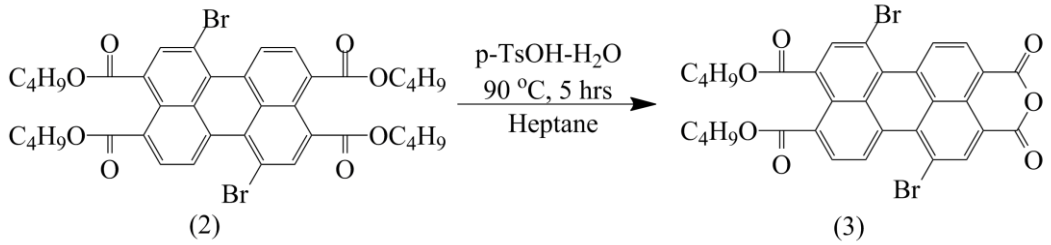

Reaction-scheme 4-2: Synthesis of 1,7-dibromoperylene-3,4,9,10-tetracarboxylic monoanhydride

Imidization of isomerically pure 1,7-dibromo perylene monoanhydride (**3**) with N,N-diethylenediamine was successfully achieved in 2-propanol/water mixture as solvent and using acetic acid as catalyst, as shown in Reaction-scheme 4-3. Compound **4** is a key compound in the further derivatization of regioisomerically pure perylene monoimide(PMI), that the substitution of bromines at the 1,7-positions would give bay substituted PMI derivatives.

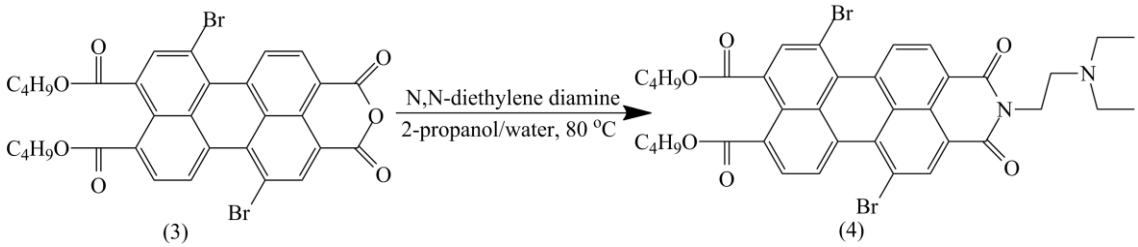

Reaction-scheme 4-3: Synthesis of N-[2-(diethylamino)ethyl]-1,7-dibromoperylene-3,4,9,10-tetracarboxy monoimide dibutylester

In order to attach the phenoxy groups, nucleophilic substituting reactions that involve double aromatic substitution were applied. The reaction was carried out in dry toluene as solvent at 90 °C with a mild base K_2CO_3 and crown-ether (18-crown-6) as phase transfer catalyst as shown in

Reaction-scheme 4-4. The desired novel perylene imide product was obtained in pure form after column chromatographic separation with a yield of 78%.

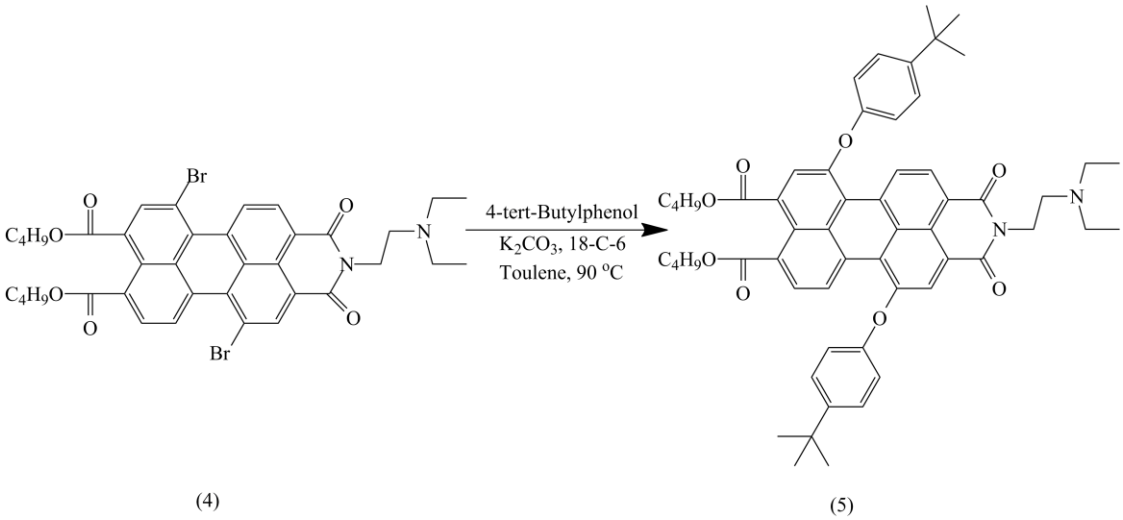

(4) (5)

Reaction-scheme 4-4: Synthesis of regioisomerically pure N-[2-(diethylamino)ethyl]-1,7-di(4-tert-butylphenoxy)perylene-3,4,9,10-tetracarboxy monoimide dibutylester.

Secondary cyclic amines like pyrrolidine are known to be good electron-donating substituents. The synthesis of compound **6** was achieved by reacting compound **4** with pyrrolidine at 70 °C as shown in Reaction-scheme 4-5. After the column chromatographic separation, the bluish-green perylene monoimide was obtained with a yield of 55%.

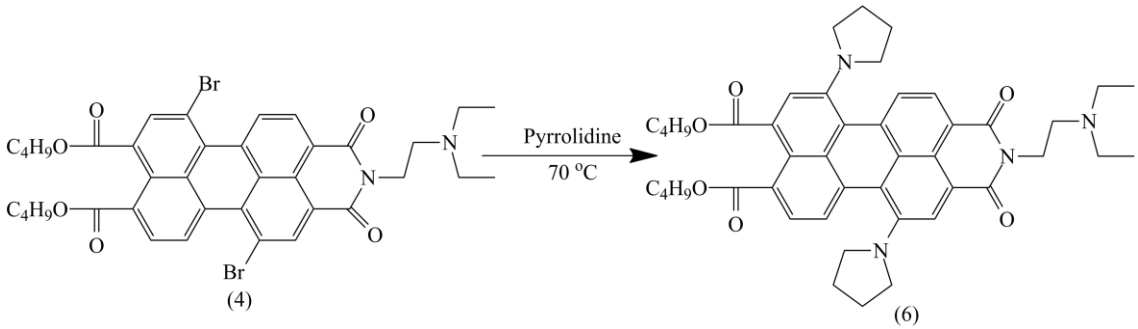

Reaction-scheme 4-5: Synthesis of regioisomerically pure N-[2-(diethylamino)ethyl]-1,7-di(pyrrolidinyl)perylene-3,4,9,10-tetracarboxy monoimide dibutylester.

The structures of all synthesized compounds were identified by IR, NMR spectral analysis and with high resolution mass spectrometry (HRMS) analysis.

4.2 Physical Properties

Figure 4.2 to Figure 4.5 shows the picture of compounds **1**-**6** in chloroform under daylight and under UV light (254, 302, and 365) nm respectively. While compounds 1-3 are fluorescent, 4-6 are weakly fluorescent.

Figure 4.2: Picture of compound **1-6**, under daylight

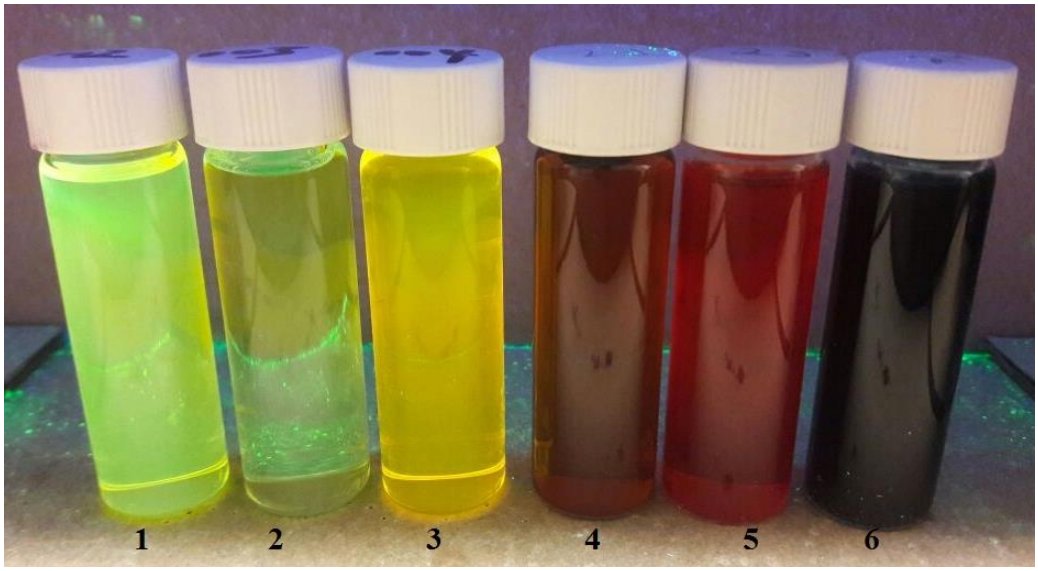

Figure 4.3. Picture of compound **1 -6**, under 254nm

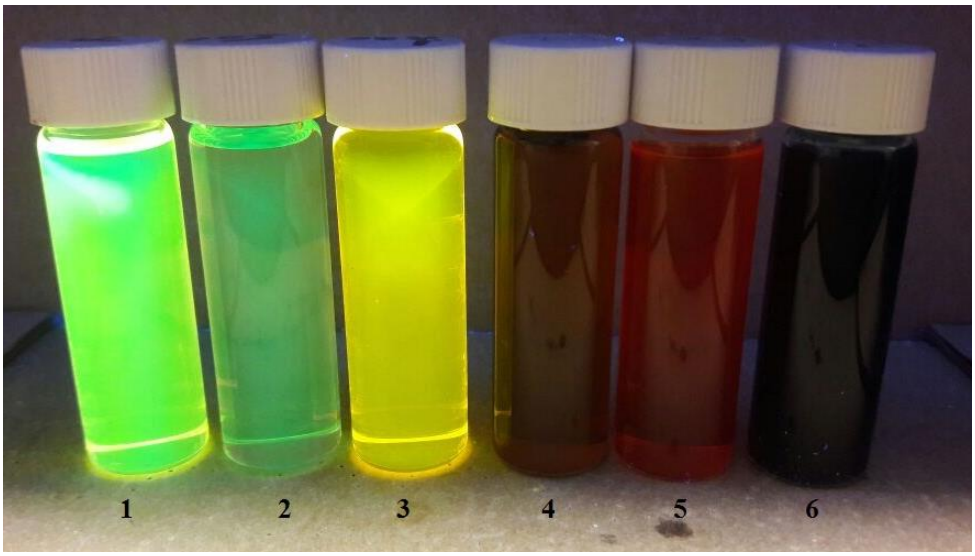

Figure 4.4. Picture of compound **1 - 6**, under 302

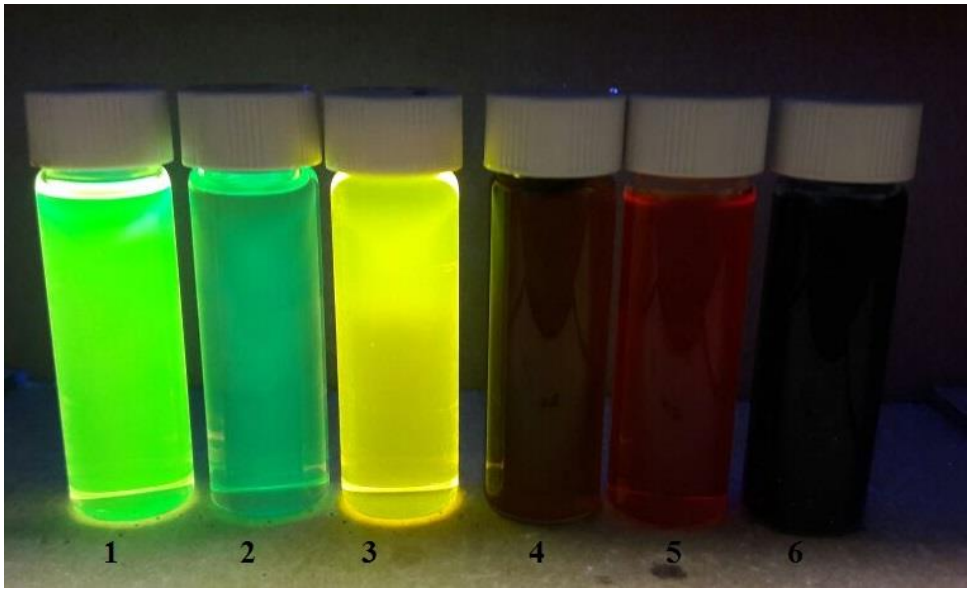

Figure 4.5. Picture of compound **1 - 6**, under 365

4.3 Solubility Properties

The solubility properties has been analyzed in various solvents, and data is presented in Table 4-1. Solubilities are determined at a concentration of 10 mg mL^{-1} in solvents at 25 °C (RT) and 60 °C (Hot).The solvents used for solubility test are chloroform (non-polar), ethanol (polar protic), dimethylformamide and acetonitrile (polar aprotic).

Table 4-1: Solubility test for compound **1** to **6**

Solvent	Compounds											
	1		**2**		**3**		**4**		**5**		**6**	
	RT	**Hot**	**RT**	**Hot**	**RT**	**Hot**	**RT**	**Hot**	**RT**	**Hot**	**RT**	**Hot**
$CHCl_3$	+	+	+	+	+	+	+	+	+	+	+	+
	Yellowish green color		Dark yellow color		Dark yellow color		Dark red		Dark pink		Dark blue	
EtOH	+-	+	-	+	+-	+	+-	+	-	+	-	+
	Yellowish green color		Dark yellow color		Dark yellow color		Pale yellow		Reddish orange		Dark blue	
DMF	+	+	+-	+	+	+	+-	+	-	+	-	+
	Yellowish green color		Dark yellow color		Dark yellow color		Pale red color		Pale pink color		Dark blue	
MeCN	-	+	-	+	+-	+	-	+-	-	+	-	+
	Yellowish green color		Dark yellow color		Dark yellow color		Pale yellow		light pink		Dark blue	

(+): Soluble, (+ -) partially soluble (3-7 mg mL^{-1}), and (-) insoluble. RT (Room Temperature), and Hot (60 °C)

The best solubility are observed in $CHCl_3$, where all the compounds are soluble at RT and 60 °C (hot). The compound **1** and **3** are completely soluble in DMF at RT and at hot conditions. However, compound **2**,**4**,**5**,**6** are partially soluble at RT and fully soluble under hot conditions. Compound **1**,**3**,**5**,**6** are partially soluble in EtOH at RT but fully soluble in hot conditions. None of the compounds are fully soluble at RT in MeCN but compounds 1, 2, 3, and 6 are fully soluble

in hot conditions. Core-unsubstituted perylene bisimide compounds usually show poor solubility and strong aggregate formation tendencies, especially in higher polarity solvents due to the strong π-π interactions between the aromatic perylene cores. The introduction of bay substituents distorts the perylene core, leading to twisting of the core ring plane, which reduces the degree of π-π interactions and aggregate formations, resulting in significantly increase solubility.

4.4 Optical Properties

4.4.1 Steady-State Absorption

It is shown that substitution at the peri positions do not alter the absorption properties for PDI compounds (owing to the available node on the imide nitrogen HOMO and LUMO), however, considerably affect aggregation and solubility properties. On the other hand, substitution at bay region alter the solubility, optical and electronic properties significantly.

Figure 4.6 and

Figure 4.7 shows the absorption spectra of compounds 1- 6 in $CHCl_3$ and DMF respectively.

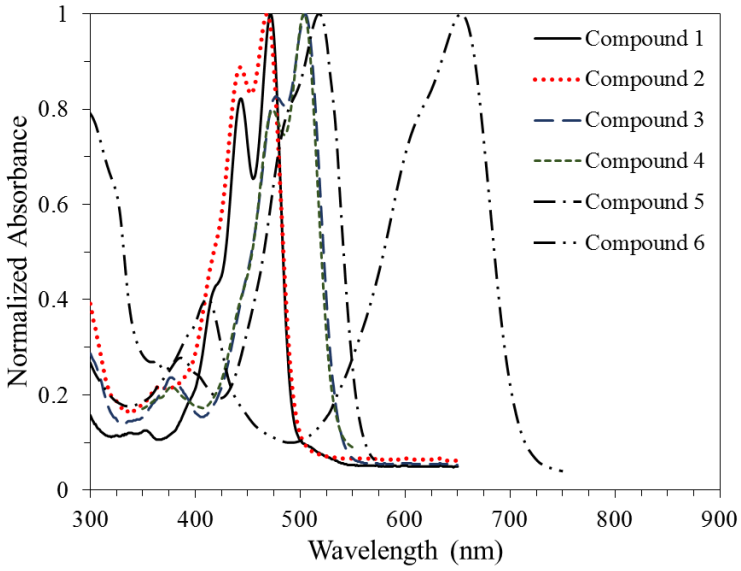

Figure 4.6: Absorption Spectra of compound **1** to **6** in Chloroform ($CHCl_3$)

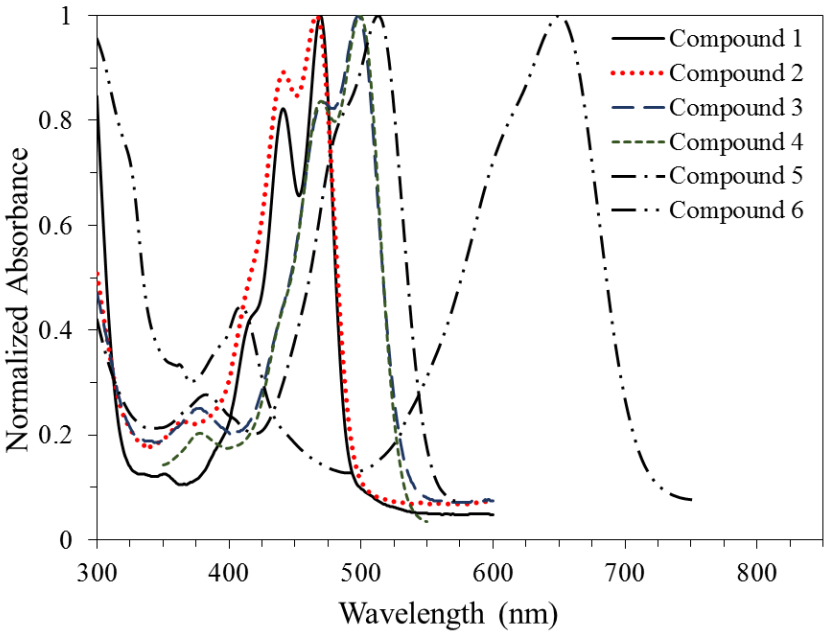

Figure 4.7: Absorption Spectra of compound **1** to **6** in Dimethylformamide (DMF)

There is evidence that 1,6- and 1,7 di-substituted perylene imides may show considerably altered photophysical and electrochemical properties [77]. Hence, the isomerically pure 1,7-di-substituted compounds (4 to 6) are significant compounds for investigating the structure property relation of this class of compounds.

Perylene diimide compounds are usually characterized with three well-defined sharp absorption bands, which are vibronic in nature ($S_0 \rightarrow S_1$ transitions). Among the compounds **1-6**, taking 1,7-dibromo perylene tetracarboxylic monoanhydride dibutylester (**3**) as parent compound (λ_{abs} = 505nm, λ_{abs} = 484 nm *in* $CHCl_3$), large hypsochromic shifts were observed with perylene tetracarboxylic tetraesters (**1**) (λ_{abs} = 472 nm and λ_{abs} = 443 nm *in* $CHCl_3$), and (**2**) (λ_{abs} = 468 nm and λ_{abs} = 443 nm *in* $CHCl_3$), as 33 nm and 41 nm (in the case of (**1**)), and 37 nm and 41 nm (in the case of (**2**)) respectively. Attachment of two electron donating tert-butyl-phenoxy groups at the 1,7-positions in compound **5** resulted in 13 nm red shift of $S_0 \rightarrow S_1$ transitions with λ_{max} moving from 505 nm to 518 nm, in $CHCl_3$. Observed shift in absorption maxima is the result of

electronic coupling between the electron-rich tert-butyl-phenoxy substituents and electron-deficient perylene core.

The steady state UV-visible absorption spectra of compound **6** shows a broader absorption band within 350-700 nm band. Absorption maxima of lowest energy transition now shift to 653 nm, in $CHCl_3$ and, 650 nm in DMF. In addition to the characteristic of $S_0 \rightarrow S_1$ transition band locating λ_{max} at 653 nm, a second peak is located at 411 nm, in $CHCl_3$ and at 409 nm, in DMF. This second peak is presumably the result of $S_0 \rightarrow S_2$ transitions.

In both compounds 5 and 6, substitution at the bay positions resulted in bathochromic shifts of the absorption maxima, and a broadening of the absorption bands leading to the loss of three characteristic sharp absorption bands observed in core-unsubstituted perylene bisimides. Observed band broadening would be the result of increased conjugation between the bay-substituents and perylene ring and/or bay-substituents induced twisting of the perylene core.

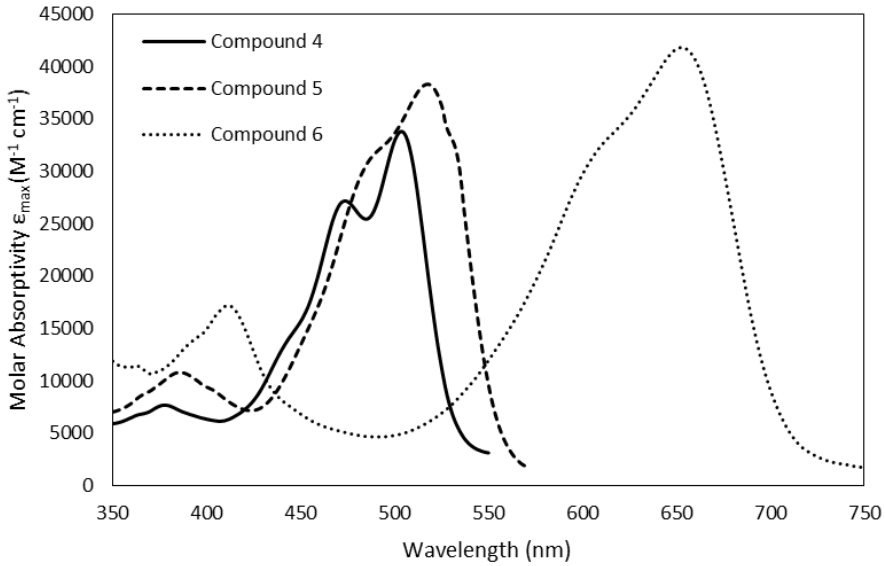

Figure 4.8: The UV-vis absorption spectra, plotted as molar absorptivity (M^{-1} cm^{-1}) versus wavelength (nm) of compounds **4**-**6** in $CHCl_3$

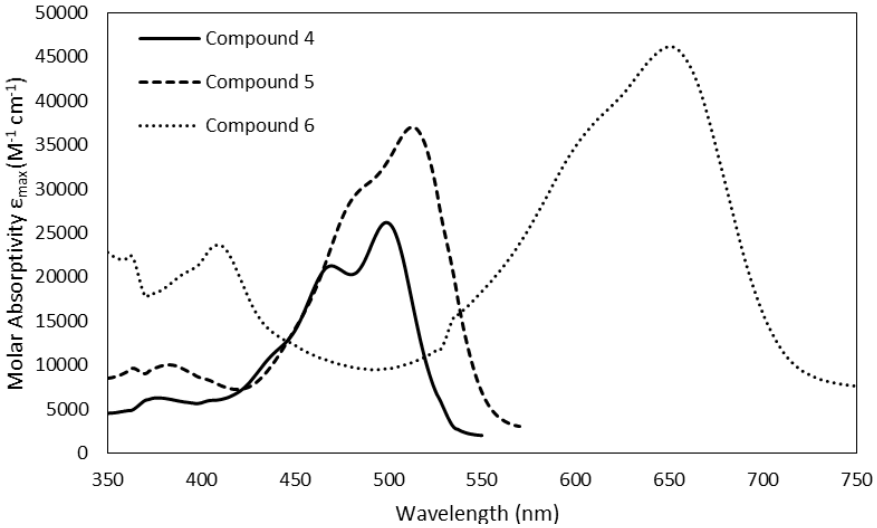

Figure 4.9: The UV-vis absorption spectra, plotted as molar absorptivity (M^{-1} cm^{-1}) versus wavelength (nm) of compounds **4**-**6** in in DMF

Table 4-2. Photophysical data of compounds **4**-**6** and **4**a-**6**a in $CHCl_3$

Compound	**λ_{max}(nm)/ε_{max} (M^{-1} cm^{-1})**	**λ_{ems}(nm)**	**Φ_F/λ_{exc}(nm)**	**Stokes shift (nm)**	**E_s(kcal mol^{-1})**	***f***	**τ_0 (ns)**	**E_g (eV)**
4	504(34100) 474(27500)	541	-	37	56.75	0.24	16.23	2.46
4a	526(57000) 491(40500)	552	0.006/460	26	54.37	0.33	12.80	2.23
5	518(38700) 485(30000)	562	-	44	55.21	0.50	8.117	2.39
5a	548(53400) 512(35800)	586	0.133/460	38	52.19	0.34	13.30	2.13
6	653(41500) 610(32000)	692	-	39	43.80	0.47	13.59	1.90
6a	704(32500) 436(14842)	727	0.007/460	23	40.63	0.19	39.60	1.64

Figure 4.8 and Figure 4.9 shows the UV-vis absorption spectra, plotted as molar absorptivity (M^{-1} cm^{-1}) versus wavelength (nm) of compounds **4-6** in $CHCl_3$ and DMF, respectively. Both compounds 5 and 6 have relatively high molar absorbtivities, indicating the high photon absorbing abilities of these compounds in visible region. It is clear that compound **6** has wider absorption band and highest molar absorbtivity at the absorption maxima, as compare to that of compound **4** and **5**. Photophysical data is summarized in Tables 4-2 and 4-3.

Table 4-3. Photophysical data of compounds 4-6 and 4a-6a in DMF

Compound	**λ_{max}(nm)/ε_{max} (M^{-1} cm^{-1})**	**λ_{ems}(nm)**	**Φ_F/λ_{exc}(nm)**	**Stokes shift (nm)**	**E_s(kcal mol^{-1})**	***f***	**τ_0 (ns)**	**E_g (eV)**
4	499(23800) 470(19400)	535	0.027	36	57.31	0.14	26.1	2.48
4a	523(38800) 488(27900)	546	-	23	54.68	0.22	19.10	2.24
5	513(37200) 480(29000)	559	0.040	46	55.75	0.48	8.23	2.42
5a	541(35100) 508(24700)	573	-	32	52.87	0.18	24.10	2.15
6	650(40800) 605(30700)	692	0.001	42	44.00	0.49	12.9	1.91
6a	704(27100) 433(12800)	732	-	28	40.63	0.17	45.00	1.61

Antisymmetric PMI compounds 4-6, where the synthesis and characterizations are presented here, are also compared with their symmetric bisimide compounds that was prepared recently in our laboratory, as a part of a related project. Structures of antisymmetric and symmetric perylene compounds that are relevant to this work, are shown in the

Figure 4.10. Bisimide and mono-imide compounds shows almost the same absorption pattern but bisimide peaks are further red-shifted than monoimides as shown in Figure 4.11 to Figure 4.16.

It is noteworthy that among the perylene tetracarboxylic derivatives, tetraesters are the weakest in terms of electron withdrawing ability, because of their weak perylene-core ester-carbonyls orbital interactions. Orbital interaction that enhances delocalization of electrons are stronger in bisimide derivatives and strongest in bisanhydride derivatives which are in accordance with the electron withdrawing ability of ester < imide < anhydride groups. Accordingly, same trend in the absorption (and emission) wavelength maxima of the compounds (1-6, as well as 4a-6a) were observed, where perylene tetraesters have shortest absorption (and emission) wavelength, and bisimides have the longest.

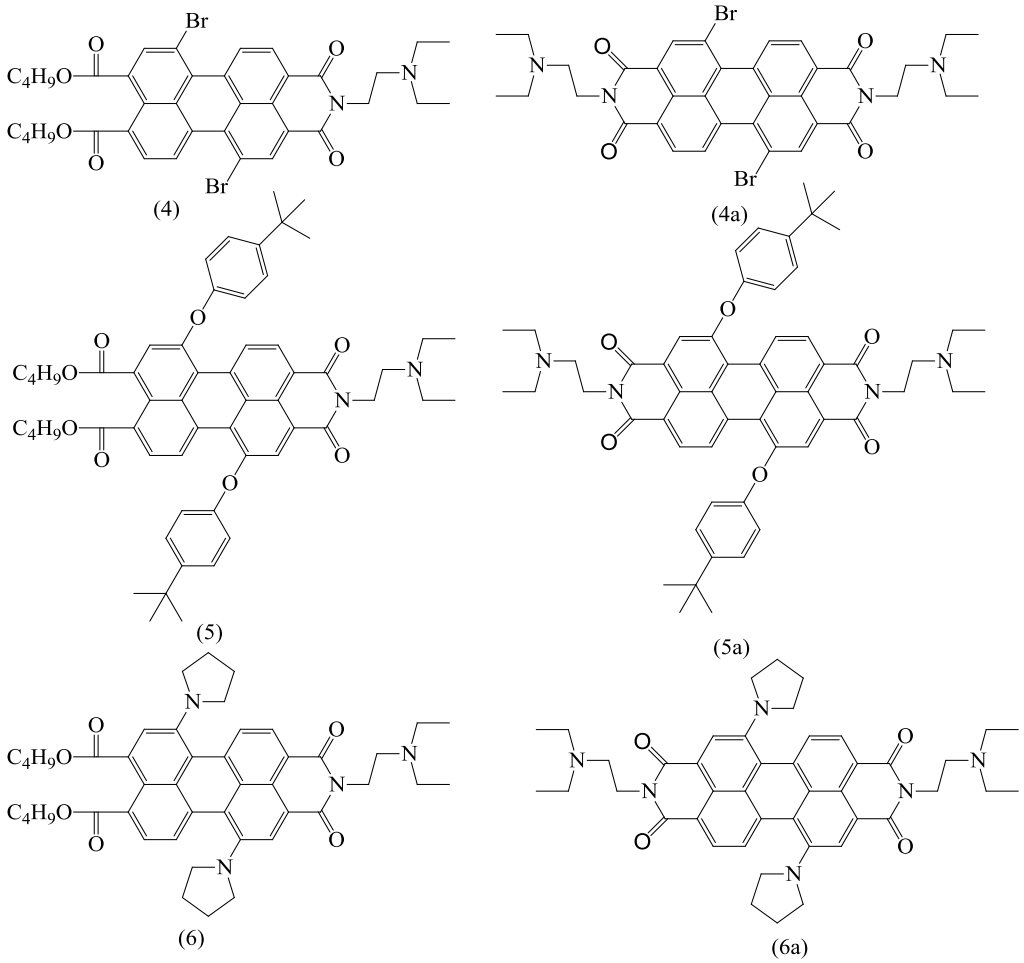

Figure 4.10: Symmetric and Asymmetric Perylene compounds

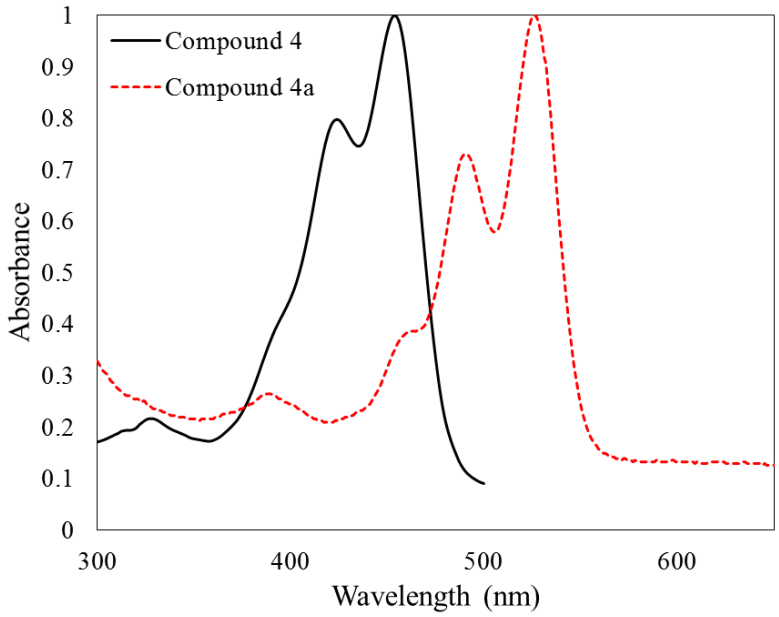

Figure 4.11: Comparison of Antisymmetric mono imide perylene (**4**) compound with symmetric bisimide (**4a**) in $CHCl_3$

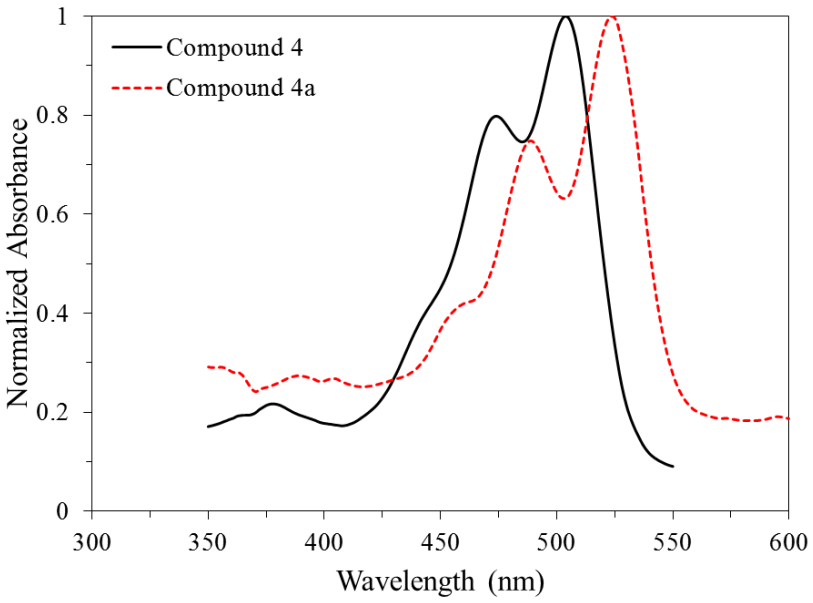

Figure 4.12: Comparison of Antisymmetric mono imide perylene (**4**) compound with symmetric bisimide (**4a**) in DMF

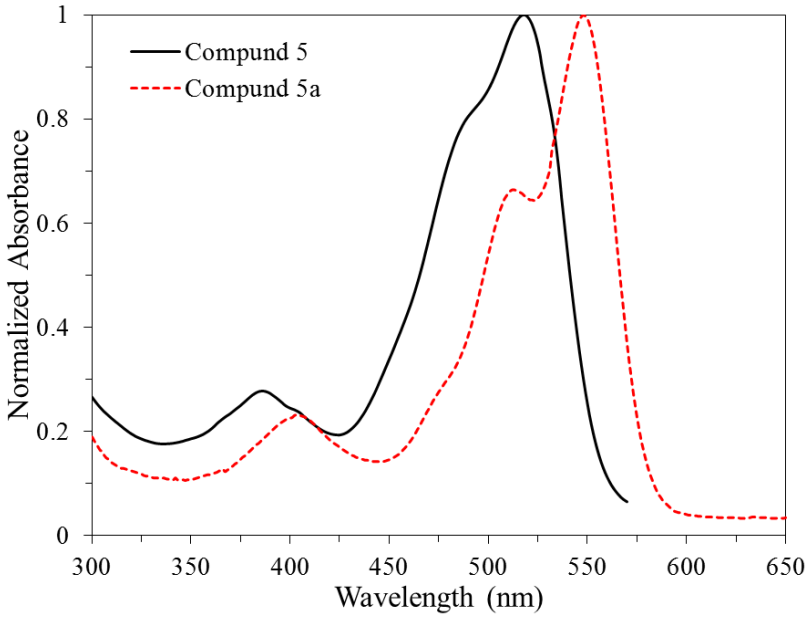

Figure 4.13: Comparison of Antisymmetric mono imide perylene (**5**) compound with symmetric bisimide (**5a**) in $CHCl_3$

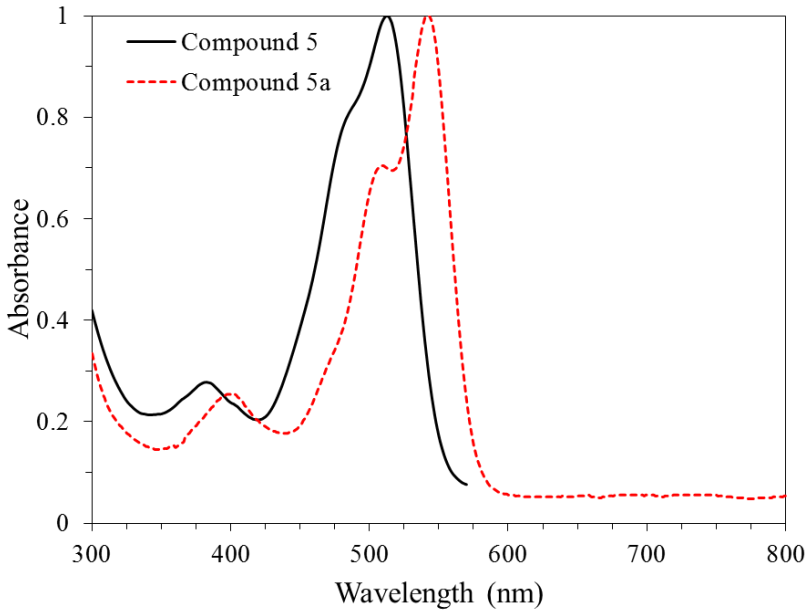

Figure 4.14: Comparison of Antisymmetric mono imide perylene (**5**) compound with symmetric bisimide (**5a**) in DMF

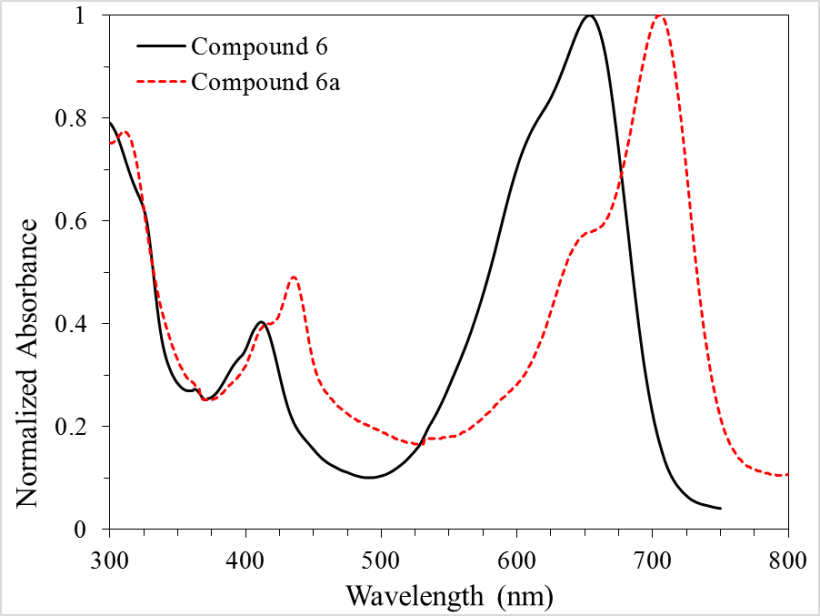

Figure 4.15: Comparison of Antisymmetric mono imide perylene (**6**) compound with symmetric bisimide (**6a**) in $CHCl_3$

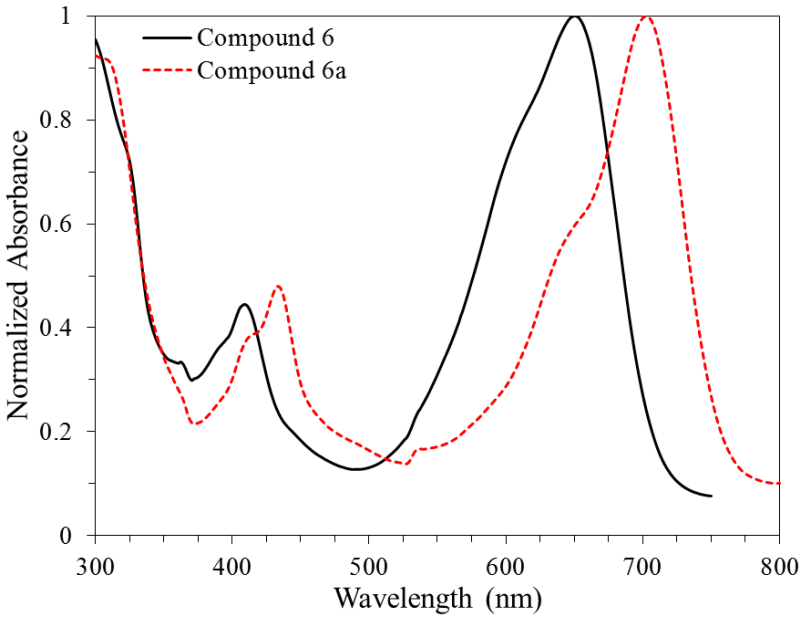

Figure 4.16: Comparison of Antisymmetric mono imide perylene (**6**) compound with symmetric bisimide (**6a**) in DMF

4.5 Steady-State Fluorescence

The Fluorescence spectra of all the compounds are recorded in $CHCl_3$ and DMF as shown in Figure 4.17 and Figure 4.18. It is evident that fluorescence maxima of compound **5** and **6** are red shifted significantly as compared to that of compound **4**.

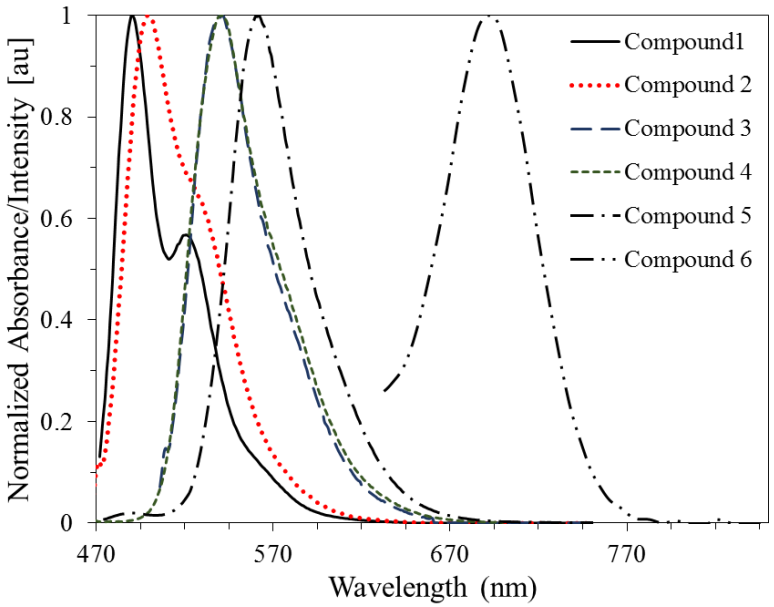

Figure 4.17: Normalized fluorescence spectra of compound **1** to **6** in $CHCl_3$

The emission spectrum of compound **6** is recorded with excitation at 460 nm in both $CHCl_3$ and in DMF. The emission band (λ_{ems} = 692 nm) shows 151 nm red shift in $CHCl_3$ and (λ_{ems} = 541 nm), and shows 157 nm red shift in DMF, compared to that of **4**. On the other hand, excitation of compound 5 at 460 nm both in $CHCl_3$ (λ_{ems} = 562 nm) and in DMF (λ_{ems} = 573 nm) lead to 27 nm and 38 nm red shifts in these solvents, respectively (compared to that of compound **4**).

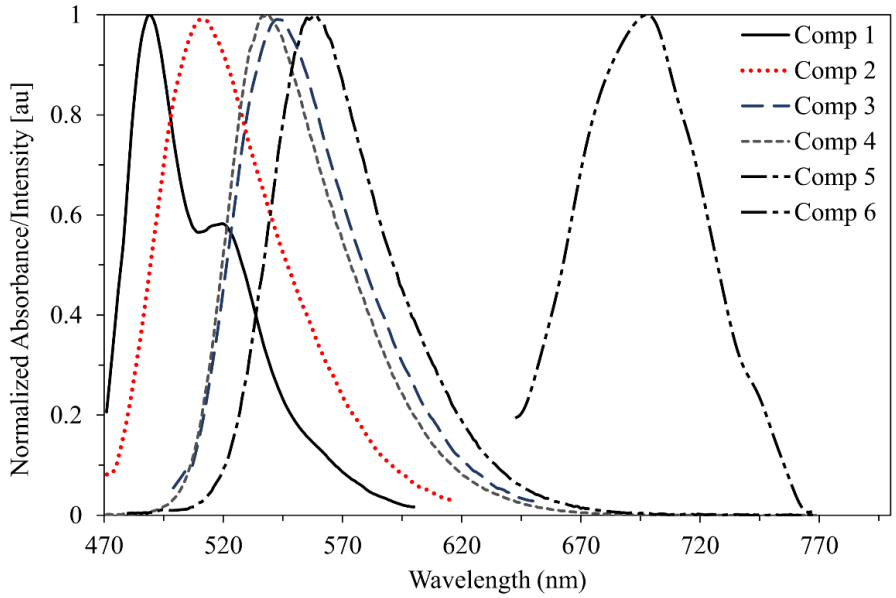

Figure 4.18: Normalized fluorescence spectra of compound **1** to **6** in DMF

Compounds 4-6 are weakly fluorescent. The quantum yields in DMF were determined relative to N,N'-bis(1,6-diisopropylphenyl)-perylene-3,4,9,10-tetracarboxdiimide, which has quantum yield equal to unity ($\Phi_F = 1.00$). To avoid self-quenching, dilute solution were employeed. The calculated quantum yields for compound **4**, **5**, **6** are 0.027, 0.040 and 0.001 respectively. The attached amino containing substituents at the imide positions, as well as electron donating groups at the bay region may be responsible of the observed low quantum yields. Photophysical data is summarized in Tables 4-2 and 4-3.

CHAPTER 5

CONCLUSION AND FUTURE WORK

In this research Novel 1,7-perylene-3,4,9,10-tetracarboxylic acid derivatives were successfully synthesized for understanding and comparison of their photophysical properties with that of symmetric perylene bisimides of the same family. To accomplish this task different electron donating groups, *i.e.* tertbutylyphenoxy and pyrrolidinyl groups, were successfully substituted at bay region of perylene unit. These compounds were sensitized, isolated, purified and characterized by NMR, HRMS, and FTIR-spectroscopy, as well as optical, and photophysical properties were studied by steady state UV-visible electronic absorption and fluorescence spectroscopy.

The molar absorptivity of N-[2-(diethylamino)ethyl]-1,7-dibromoperylene-3,4,9,10-tetracarboxy monoimide dibutylester (compound 4) are 34100 at 504 nm in $CHCl_3$ and 23800 at 499 nm in DMF. The molar absorptivity of N-[2-(diethylamino)ethyl]-1,7-di(4-tert-butylphenoxy)perylene-3,4,9,10-tetracarboxy monoimide dibutylester (compound **5**) are 38700 at 518 nm in $CHCl_3$ and 37200 at 513 nm in DMF. The molar absorptivity of N-[2-(diethylamino)ethyl]-1,7-di(pyrrolidinyl)perylene-3,4,9,10-tetracarboxy monoimide dibutylester. (compound **6**) are 41500 at 653 nm in $CHCl_3$ and 40800 at 650nm in DMF.

The measured molar absoprtivies are high and reflect the desired high photon absorbing ability. The UV-visible absorption spectrum of N-[2-(diethylamino)ethyl]-1,7-di(pyrrolidinyl)perylene-3,4,9,10-tetracarboxy monoimide dibutylester shows a broad absorption band extending to the red region of the spectrum. Absorption maxima of the lowest energy transition shifts to 650 in DMF and to 653 in $CHCl_3$.

The singlet excited energies of N-[2-(diethylamino)ethyl]-1,7-dibromoperylene-3,4,9,10-tetracarboxy monoimide dibutylester (compound **4**) are estimates as 56.75 kcal mol^{-1} in $CHCl_3$ and 57.31 kcal mol^{-1} in DMF with the optical band gap of 2.46 and 2.49 eV respectively. The

substitution of 4-(tert-butyl) phenol at bay region decreases the singlet excitation energies to 55.21 kcal mol^{-1} in $CHCl_3$ and 55.75 in DMF with optical band gap of 2.39 eV and 2.42 eV respectively for N-[2-(diethylamino)ethyl]-1,7-di(4-tert-butylphenoxy)perylene-3,4,9,10-tetracarboxy monoimide dibutylester (compound **5**). Substitution of pyrrolidine at bay region significantly decreases singlet excitation energy to 43.80 kcal mol^{-1} in $CHCl_3$ and 44 kcal mol^{-1} in DMF, with the estimated optical band gap of 1.90 and 1.91 eV respectively.

The N-[2-(diethylamino)ethyl]-1,7-di(4-tert-butylphenoxy)perylene-3,4,9,10-tetracarboxy monoimide dibutylester and N-[2-(diethylamino)ethyl]-1,7-di(pyrrolidinyl)perylene-3,4,9,10-tetracarboxy monoimide dibutylester display characteristics that are desired for a sensitizer component to be used in photovoltaic devices. The former results in a higher quantum yield while the later results in a broader absorption range (350-700 nm), which allows more photons to be captured. The substitution at bay region increases compound's solubility which helps to improve the processability of synthesized compounds.

Absorption and emission wavelength of perylene tetraester compounds have shorter wavelength compared to that of perylene monoimide diester compounds, where perylene tetracarboxylic bisimide compounds have the longest absorption and emission wavelengths. This trend is in the same line with the electron accepting properties of perylene tetraester (weakest electron acceptor), perylene monoimide diester and perylene bisimide compounds (strongest electron acceptor).

This work demonstrates that perylene tetracarboxylic ester unit is a versatile building block for the synthesis of variety of light harvesting systems. The resulting compounds are soluble in variety of organic solvents, and show broad absorption bands extending up to near infrared region.As a future work, it would be interesting to prepare monoimide monoanhydride analogues from perylene monoimide diester compounds synthesized and presented here. Research in this line is currently in progress at our laboratories.

BIBLIOGRAPHY

[1] "Future Global Energy Prosperity: The Terawatt Challenge," *MRS Bull.*, vol. 30, no. 06, pp. 412–417, Jun. 2005.

[2] C. W. Tan, K. H. Tan, Y. T. Ong, A. R. Mohamed, S. H. S. Zein, and S. H. Tan, "Carbon Nanotubes Applications: Solar and Fuel Cells, Hydrogen Storage, Lithium Batteries, Supercapacitors, Nanocomposites, Gas, Pathogens, Dyes, Heavy Metals and Pesticides," in *Environmental Chemistry for a Sustainable World*, E. Lichtfouse, J. Schwarzbauer, and D. Robert, Eds. Springer Netherlands, 2012, pp. 3–46.

[3] M. Khan, "A Study on the Optimization of Dye-Sensitized Solar Cells," 2013.

[4] D. Naylor and H. Ellis, "Characterization of dye-sensitized solar cells-Components for environmentally friendly photovoltaics.," Uppsala University, Sweden, 2014.

[5] M. Grätzel, "Solar energy conversion by dye-sensitized photovoltaic cells," *Inorg. Chem.*, vol. 44, no. 20, pp. 6841–6851, 2005.

[6] N. S. Lewis, "Toward Cost-Effective Solar Energy Use," *Science*, vol. 315, no. 5813, pp. 798–801, Feb. 2007.

[7] "First Solar, Inc. Announces Fourth Quarter and 2011 Financial Results (NASDAQ:FSLR)." [Online]. Available: http://investor.firstsolar.com/releasedetail.cfm?ReleaseID=652462. [Accessed: 29-Nov-2016].

[8] W. Shockley and H. J. Queisser, "Detailed Balance Limit of Efficiency of p-n Junction Solar Cells," *J. Appl. Phys.*, vol. 32, no. 3, pp. 510–519, Mar. 1961.

[9] "Photovoltaic Research | NREL." [Online]. Available: https://www.nrel.gov/pv/. [Accessed: 18-May-2017].

[10] H. Tributsch, "Reaction of Excited Chlorophyll Molecules at Electrodes and in Photosynthesis*," *Photochem. Photobiol.*, vol. 16, no. 4, pp. 261–269, Oct. 1972.

[11] N. Vlachopoulos, P. Liska, J. Augustynski, and M. Graetzel, "Very efficient visible light energy harvesting and conversion by spectral sensitization of high surface area polycrystalline titanium dioxide films," *J. Am. Chem. Soc.*, vol. 110, no. 4, pp. 1216–1220, Feb. 1988.

[12] B. O'regan and M. Grfitzeli, "A low-cost, high-efficiency solar cell based on dye-sensitized," *nature*, vol. 353, no. 6346, pp. 737–740, 1991.

[13] M. Grätzel, “The advent of mesoscopic injection solar cells,” *Prog. Photovolt. Res. Appl.*, vol. 14, no. 5, pp. 429–442, Aug. 2006.

[14] J. Barber and B. Andersson, “Revealing the blueprint of photosynthesis,” *Nature*, vol. 370, pp. 31–34, Jul. 1994.

[15] S. Ardo and G. J. Meyer, “Photodriven heterogeneous charge transfer with transition-metal compounds anchored to TiO_2 semiconductor surfaces,” *Chem Soc Rev*, vol. 38, no. 1, pp. 115–164, 2009.

[16] S. M. Feldt *et al.*, “Regeneration and recombination kinetics in cobalt polypyridine based dye-sensitized solar cells, explained using Marcus theory,” *Phys. Chem. Chem. Phys.*, vol. 15, no. 19, p. 7087, 2013.

[17] “Scopus.” [Online]. Available: https://www.scopus.com/. [Accessed: 18-May-2017].

[18] M. A. Marszalek, “Dye-sensitized Solar Cells: Detailed Studies Focused on the Molecular Engineering of D-[pi]-A Dyes and the Optimization of the Application of Ionic-liquid-based Electrolytes,” 2013.

[19] M. K. Nazeeruddin *et al.*, “Conversion of light to electricity by cis-X2bis(2,2’-bipyridyl-4,4’-dicarboxylate)ruthenium(II) charge-transfer sensitizers (X = Cl-, Br-, I-, CN-, and SCN-) on nanocrystalline titanium dioxide electrodes,” *J. Am. Chem. Soc.*, vol. 115, no. 14, pp. 6382–6390, Jul. 1993.

[20] A. B. F. Martinson, J. W. Elam, J. T. Hupp, and M. J. Pellin, “ZnO Nanotube Based Dye-Sensitized Solar Cells,” *Nano Lett.*, vol. 7, no. 8, pp. 2183–2187, Aug. 2007.

[21] H. Rensmo *et al.*, “High Light-to-Energy Conversion Efficiencies for Solar Cells Based on Nanostructured ZnO Electrodes,” *J. Phys. Chem. B*, vol. 101, no. 14, pp. 2598–2601, Apr. 1997.

[22] K. Hauffe, H. J. Danzmann, H. Pusch, J. Range, and H. Volz, “New Experiments on the Sensitization of Zinc Oxide by Means of the Electrochemical Cell Technique,” *J. Electrochem. Soc.*, vol. 117, no. 8, pp. 993–999, Aug. 1970.

[23] A. Hagfeldt, G. Boschloo, L. Sun, L. Kloo, and H. Pettersson, “Dye-Sensitized Solar Cells,” *Chem. Rev.*, vol. 110, no. 11, pp. 6595–6663, Nov. 2010.

[24] H. J. Snaith and C. Ducati, “SnO2-Based Dye-Sensitized Hybrid Solar Cells Exhibiting Near Unity Absorbed Photon-to-Electron Conversion Efficiency,” *Nano Lett.*, vol. 10, no. 4, pp. 1259–1265, Apr. 2010.

[25] R. Sharma, R. S. Mane, S.-K. Min, and S.-H. Han, “Optimization of growth of In2O3 nano-spheres thin films by electrodeposition for dye-sensitized solar cells,” *J. Alloys Compd.*, vol. 479, no. 1–2, pp. 840–843, Jun. 2009.

[26] A. Kay and M. Grätzel, “Dye-Sensitized Core−Shell Nanocrystals: Improved Efficiency of Mesoporous Tin Oxide Electrodes Coated with a Thin Layer of an Insulating Oxide,” *Chem. Mater.*, vol. 14, no. 7, pp. 2930–2935, Jul. 2002.

[27] A. Le Viet, R. Jose, M. V. Reddy, B. V. R. Chowdari, and S. Ramakrishna, “Nb2O5 Photoelectrodes for Dye-Sensitized Solar Cells: Choice of the Polymorph,” *J. Phys. Chem. C*, vol. 114, no. 49, pp. 21795–21800, Dec. 2010.

[28] P. L. Marek, “Biomimetic Dye Aggregate Solar Cells,” Ph.D. Thesis, Technische Universität, Darmstadt, 2012.

[29] X.-F. Wang *et al.*, “Dye-sensitized solar cells using a chlorophyll a derivative as the sensitizer and carotenoids having different conjugation lengths as redox spacers,” *Chem. Phys. Lett.*, vol. 408, no. 4–6, pp. 409–414, Jun. 2005.

[30] X.-F. Wang, O. Kitao, H. Zhou, H. Tamiaki, and S. Sasaki, “Extension of π-conjugation length along the Q y axis of a chlorophyll a derivative for efficient dye -sensitized solar cells,” *Chem. Commun.*, vol. 0, no. 12, pp. 1523–1525, 2009.

[31] G. Calogero, G. D. Marco, S. Caramori, S. Cazzanti, R. Argazzi, and C. Alberto Bignozzi, “Natural dye senstizers for photoelectrochemical cells,” *Energy Environ. Sci.*, vol. 2, no. 11, pp. 1162–1172, 2009.

[32] A. Olea, G. Ponce, and P. J. Sebastian, “Electron transfer via organic dyes for solar conversion,” *Sol. Energy Mater. Sol. Cells*, vol. 59, no. 1–2, pp. 137–143, Sep. 1999.

[33] G. Calogero *et al.*, “Efficient Dye-Sensitized Solar Cells Using Red Turnip and Purple Wild Sicilian Prickly Pear Fruits,” *Int. J. Mol. Sci.*, vol. 11, no. 1, pp. 254–267, Jan. 2010.

[34] Q. V. Anh, “Degradation of the solar cell dye sensitizer N719 Preliminary building of dye-sensitized solar cell,” Thesis. Denmark: Roskilde University, 2006.

[35] M. K. Nazeeruddin *et al.*, “Engineering of Efficient Panchromatic Sensitizers for Nanocrystalline TiO2-Based Solar Cells,” *J. Am. Chem. Soc.*, vol. 123, no. 8, pp. 1613–1624, Feb. 2001.

[36] C. Huang, “Perylene diimide-based materials for organic electronics and optical limiting applications,” Ph.D., Georgia Institute of Technology, United States -- Georgia, 2012.

[37] H. Langhals, “Cyclic carboxylic imide structures as structure elements of high stability. Novel developments in perylene dye chemistry,” *Heterocycles*, vol. 1, no. 40, pp. 477–500, 1995.

[38] P. J. Cameron and L. M. Peter, “Characterization of Titanium Dioxide Blocking Layers in Dye-Sensitized Nanocrystalline Solar Cells,” *J. Phys. Chem. B*, vol. 107, no. 51, pp. 14394–14400, Dec. 2003.

[39] A. D. Boehm, H. Arms, G. D. Henning, and P. Blaschka, “1,7-Diaroxy-oder -arylthiosubstituierte Perylen-3,4,9,10-tetracarbonsäuren, deren Dianhydride und Diimide 1,7-Diaroxy or -arylthiosubstituierte perylene-3,4,9,10-tetracarboxylic acids, their dianhydrides and diimides,” DE19547209 A1, 19-Jun-1997.

[40] J. Baggerman *et al.*, “Fluorescent Perylene Diimide Rotaxanes: Spectroscopic Signatures of Wheel–Chromophore Interactions,” *Chem. – Eur. J.*, vol. 13, no. 4, pp. 1291–1299, Jan. 2007.

[41] Z. Yuan, Y. Xiao, Z. Li, and X. Qian, “Efficient Synthesis of Regioisomerically Pure Bis(trifluoromethyl)-Substituted 3,4,9,10-Perylene Tetracarboxylic Bis(benzimidazole),” *Org. Lett.*, vol. 11, no. 13, pp. 2808–2811, Jul. 2009.

[42] S. Ferrere, A. Zaban, and B. A. Gregg, “Dye Sensitization of Nanocrystalline Tin Oxide by Perylene Derivatives,” *J. Phys. Chem. B*, vol. 101, no. 23, pp. 4490–4493, Jun. 1997.

[43] S. Wang *et al.*, “Dye sensitization of nanocrystalline TiO2 by perylene derivatives,” *Synth. Met.*, vol. 128, no. 3, pp. 299–304, May 2002.

[44] C. Zafer *et al.*, “New perylene derivative dyes for dye-sensitized solar cells,” *Sol. Energy Mater. Sol. Cells*, vol. 91, no. 5, pp. 427–431, Mar. 2007.

[45] J. Fortage, M. Séverac, C. Houarner-Rassin, Y. Pellegrin, E. Blart, and F. Odobel, “Synthesis of new perylene imide dyes and their photovoltaic performances in nanocrystalline TiO2 dye-sensitized solar cells,” *J. Photochem. Photobiol. Chem.*, vol. 197, no. 2–3, pp. 156–169, Jun. 2008.

[46] M. Planells, F. J. Céspedes-Guirao, L. Gonçalves, A. Sastre-Santos, F. Fernández-Lázaro, and E. Palomares, “Supramolecular interactions in dye-sensitised solar cells,” *J. Mater. Chem.*, vol. 19, no. 32, pp. 5818–5825, Aug. 2009.

[47] B. Liu, W. Zhu, W. Wu, K. M. Ri, and H. Tian, “Hybridized ruthenium(II) complexes with high molar extinction coefficient unit: Effect of energy band and adsorption on photovoltaic performances,” *J. Photochem. Photobiol. Chem.*, vol. 194, no. 2–3, pp. 268–274, Feb. 2008.

[48] Y. Jin, J. Hua, W. Wu, X. Ma, and F. Meng, “Synthesis, characterization and photovoltaic properties of two novel near-infrared absorbing perylene dyes containing benzo[e]indole for dye-sensitized solar cells,” *Synth. Met.*, vol. 158, no. 1–2, pp. 64–71, Jan. 2008.

[49] C. Li and H. Wonneberger, “Perylene Imides for Organic Photovoltaics: Yesterday, Today, and Tomorrow,” *Adv. Mater.*, vol. 24, no. 5, pp. 613–636, Feb. 2012.

[50] M. K. Nazeeruddin, R. Humphry-Baker, D. L. Officer, W. M. Campbell, A. K. Burrell, and M. Grätzel, “Application of metalloporphyrins in nanocrystalline dye-sensitized solar cells for conversion of sunlight into electricity,” *Langmuir*, vol. 20, no. 15, pp. 6514–6517, 2004.

[51] M. K. Nazeeruddin *et al.*, “Efficient near IR sensitization of nanocrystalline TiO 2 films by ruthenium phthalocyanines,” *Chem. Commun.*, vol. 0, no. 6, pp. 719–720, 1998.

[52] Q. Wang *et al.*, “Efficient Light Harvesting by Using Green Zn-Porphyrin-Sensitized Nanocrystalline TiO2 Films,” *J. Phys. Chem. B*, vol. 109, no. 32, pp. 15397–15409, Aug. 2005.

[53] D. Pugliese, “New insights in Dye-sensitized Solar Cells: novel nanostructured photoanodes, metal-free dye, quasi-solid electrolytes and physics-based modeling,” phd, Politecnico di Torino, 2014.

[54] S. Ferrere, A. Zaban, and B. A. Gregg, “Dye Sensitization of Nanocrystalline Tin Oxide by Perylene Derivatives,” *J. Phys. Chem. B*, vol. 101, no. 23, pp. 4490–4493, Jun. 1997.

[55] G. Oskam, B. V. Bergeron, G. J. Meyer, and P. C. Searson, “Pseudohalogens for Dye-Sensitized TiO2 Photoelectrochemical Cells,” *J. Phys. Chem. B*, vol. 105, no. 29, pp. 6867–6873, Jul. 2001.

[56] P. Wang, S. M. Zakeeruddin, J.-E. Moser, R. Humphry-Baker, and M. Grätzel, “A Solvent-Free, SeCN-/(SeCN)3- Based Ionic Liquid Electrolyte for High-Efficiency Dye-Sensitized Nanocrystalline Solar Cells,” *J. Am. Chem. Soc.*, vol. 126, no. 23, pp. 7164–7165, Jun. 2004.

[57] S. A. Sapp, C. M. Elliott, C. Contado, S. Caramori, and C. A. Bignozzi, “Substituted Polypyridine Complexes of Cobalt(II/III) as Efficient Electron-Transfer Mediators in Dye-Sensitized Solar Cells,” *J. Am. Chem. Soc.*, vol. 124, no. 37, pp. 11215–11222, Sep. 2002.

[58] S. Hattori, Y. Wada, S. Yanagida, and S. Fukuzumi, “Blue Copper Model Complexes with Distorted Tetragonal Geometry Acting as Effective Electron-Transfer Mediators in Dye-Sensitized Solar Cells,” *J. Am. Chem. Soc.*, vol. 127, no. 26, pp. 9648–9654, Jul. 2005.

[59] A. Yella *et al.*, “Porphyrin-Sensitized Solar Cells with Cobalt (II/III)–Based Redox Electrolyte Exceed 12 Percent Efficiency,” *Science*, vol. 334, no. 6056, pp. 629–634, Nov. 2011.

[60] F. Fabregat-Santiago *et al.*, "Correlation between Photovoltaic Performance and Impedance Spectroscopy of Dye-Sensitized Solar Cells Based on Ionic Liquids," *J. Phys. Chem. C*, vol. 111, no. 17, pp. 6550–6560, May 2007.

[61] N. Cai *et al.*, "An Organic D-π-A Dye for Record Efficiency Solid-State Sensitized Heterojunction Solar Cells," *Nano Lett.*, vol. 11, no. 4, pp. 1452–1456, Apr. 2011.

[62] P. R. Somani and S. Radhakrishnan, "Solid state electrochemical reaction in photocells made using conducting polyaniline and sensitized with methylene blue," *J. Solid State Electrochem.*, vol. 7, no. 3, pp. 166–170, Mar. 2003.

[63] K. Murakoshi, R. Kogure, Y. Wada, and S. Yanagida, "Solid State Dye-Sensitized TiO2 Solar Cell with Polypyrrole as Hole Transport Layer.," *Chem. Lett.*, no. 5, pp. 471–472, 1997.

[64] Y. Saito, T. Kitamura, Y. Wada, and S. Yanagida, "Poly(3,4-ethylenedioxythiophene) as a hole conductor in solid state dye sensitized solar cells," *Synth. Met.*, vol. 131, no. 1–3, pp. 185–187, Nov. 2002.

[65] P. Ravirajan *et al.*, "Hybrid Polymer/Zinc Oxide Photovoltaic Devices with Vertically Oriented ZnO Nanorods and an Amphiphilic Molecular Interface Layer," *J. Phys. Chem. B*, vol. 110, no. 15, pp. 7635–7639, Apr. 2006.

[66] A. Hauch and A. Georg, "Diffusion in the electrolyte and charge-transfer reaction at the platinum electrode in dye-sensitized solar cells," *Electrochimica Acta*, vol. 46, no. 22, pp. 3457–3466, Aug. 2001.

[67] A. Hagfeldt and M. Graetzel, "Light-Induced Redox Reactions in Nanocrystalline Systems," *Chem. Rev.*, vol. 95, no. 1, pp. 49–68, Jan. 1995.

[68] G. Smestad, C. Bignozzi, and R. Argazzi, "Testing of dye sensitized TiO2 solar cells I: Experimental photocurrent output and conversion efficiencies," *Sol. Energy Mater. Sol. Cells*, vol. 32, no. 3, pp. 259–272, Mar. 1994.

[69] S. Lee, Y. Jun, K.-J. Kim, and D. Kim, "Modification of electrodes in nanocrystalline dye-sensitized TiO2 solar cells," *Sol. Energy Mater. Sol. Cells*, vol. 65, no. 1–4, pp. 193–200, Jan. 2001.

[70] E. Olsen, G. Hagen, and S. Eric Lindquist, "Dissolution of platinum in methoxy propionitrile containing LiI/I2," *Sol. Energy Mater. Sol. Cells*, vol. 63, no. 3, pp. 267–273, Jul. 2000.

[71] A. Kay and M. Grätzel, "Low cost photovoltaic modules based on dye sensitized nanocrystalline titanium dioxide and carbon powder," *Sol. Energy Mater. Sol. Cells*, vol. 44, no. 1, pp. 99–117, Oct. 1996.

[72] M. K. Nazeeruddin *et al.*, "Conversion of light to electricity by cis-X2bis (2, 2'-bipyridyl-4, 4'-dicarboxylate) ruthenium (II) charge-transfer sensitizers (X= Cl-, Br-, I-, CN-, and SCN-) on nanocrystalline titanium dioxide electrodes," *J. Am. Chem. Soc.*, vol. 115, no. 14, pp. 6382–6390, 1993.

[73] W. L. F. Armarego and C. L. L. Chai, *Purification of laboratory chemicals*, 7th ed. Amsterdam : London: Elsevier/Butterworth-Heinemann, 2013.

[74] H. J. Yvon and others, "A guide to recording Fluorescence Quantum Yields," *HORIBA Jobin Yvon Ltd Stanmore Middx. UK*, 2012.

[75] A. T. Rhys Williams, S. A. Winfield, and J. N. Miller, "Relative fluorescence quantum yields using a computer-controlled luminescence spectrometer," *Analyst*, vol. 108, no. 1290, pp. 1067–1071, 1983.

[76] S. Sengupta *et al.*, "Synthesis of regioisomerically pure 1, 7-dibromoperylene-3, 4, 9, 10-tetracarboxylic acid derivatives," *J. Org. Chem.*, vol. 79, no. 14, pp. 6655–6662, 2014.

[77] R. K. Dubey, M. Niemi, K. Kaunisto, A. Efimov, N. V. Tkachenko, and H. Lemmetyinen, "Direct Evidence of Significantly Different Chemical Behavior and Excited-State Dynamics of 1,7- and 1,6-Regioisomers of Pyrrolidinyl-Substituted Perylene Diimide," *Chem. – Eur. J.*, vol. 19, no. 21, pp. 6791–6806, May 2013.

APPENDIX

^{1}H NMR, ^{13}C NMR, HRMS, UV-vis and fluorescence emission spectra for synthesized compounds 1-6.

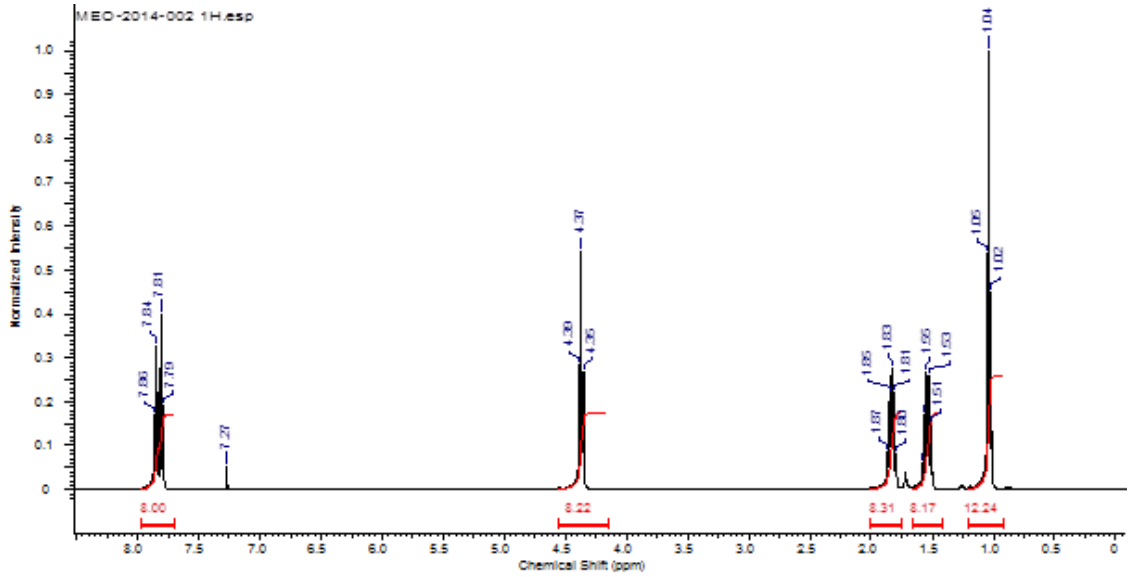

Figure A.1: ^{1}H NMR Spectrum of compound **1**

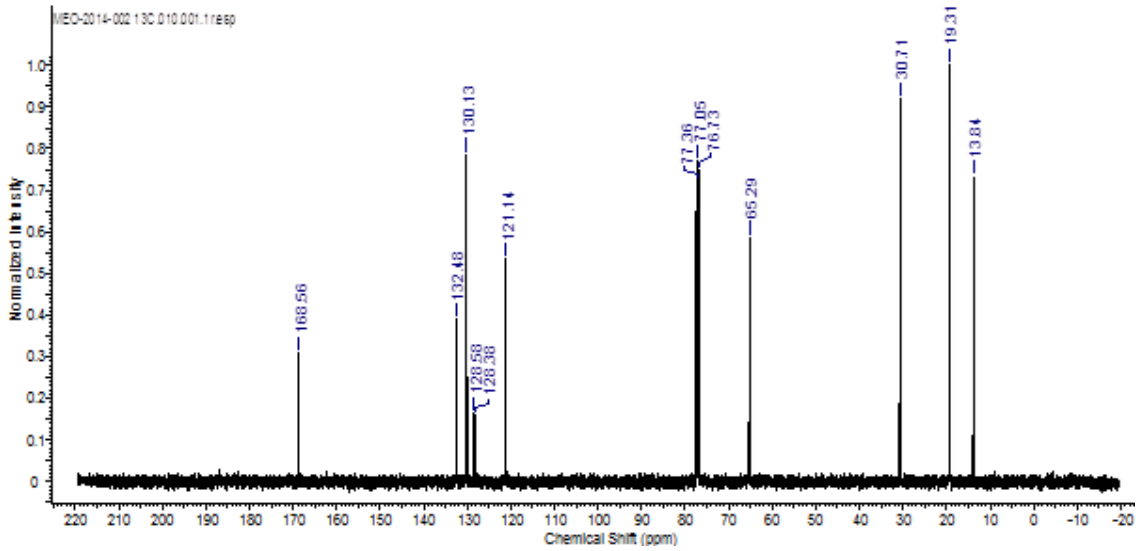

Figure A.2: ^{13}C NMR Spectrum of compound **1**

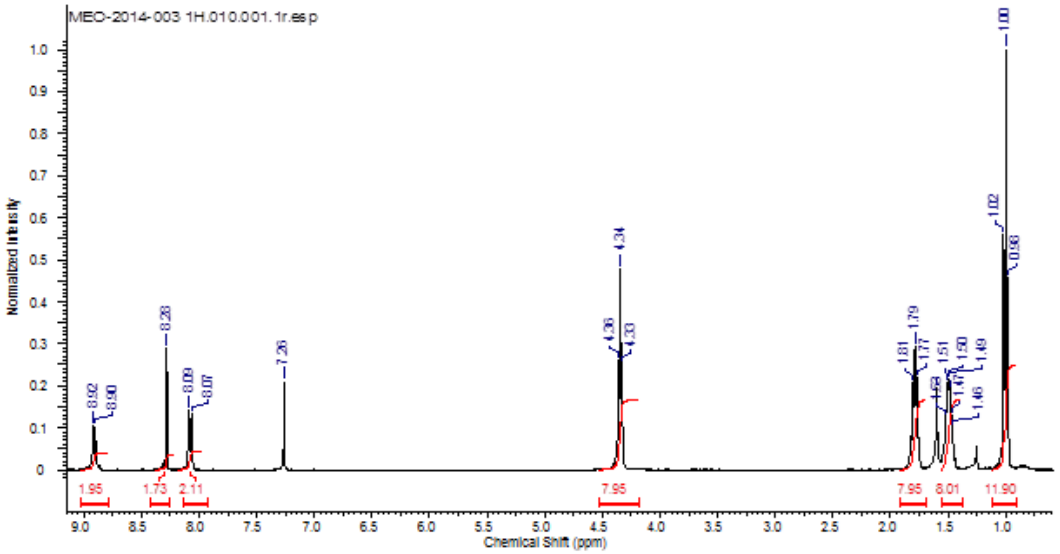

Figure A.3: ^{1}H NMR Spectrum of compound **2**

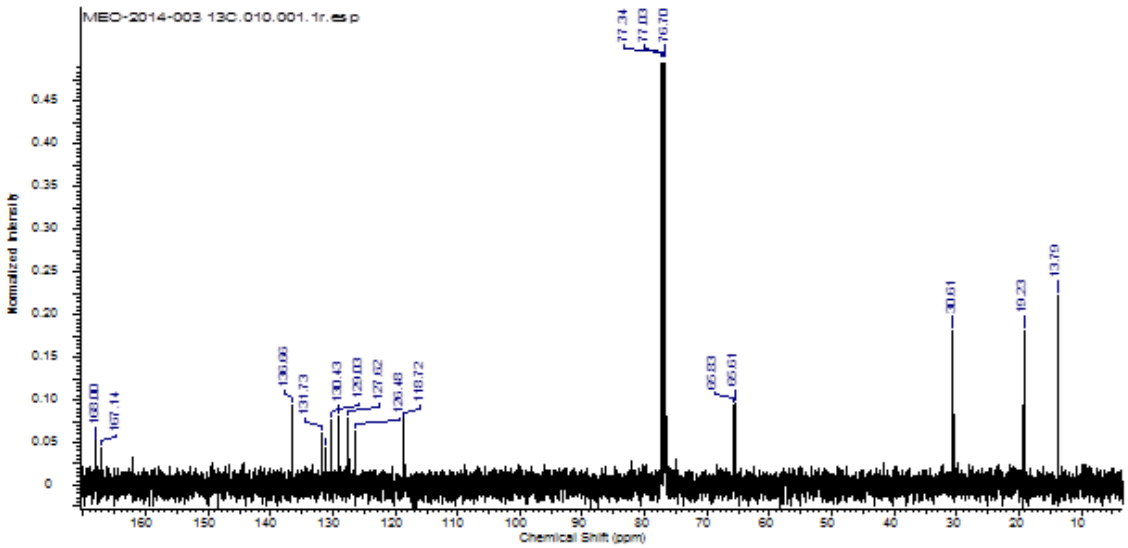

Figure A.4: ^{13}C NMR Spectrum of compound **2**

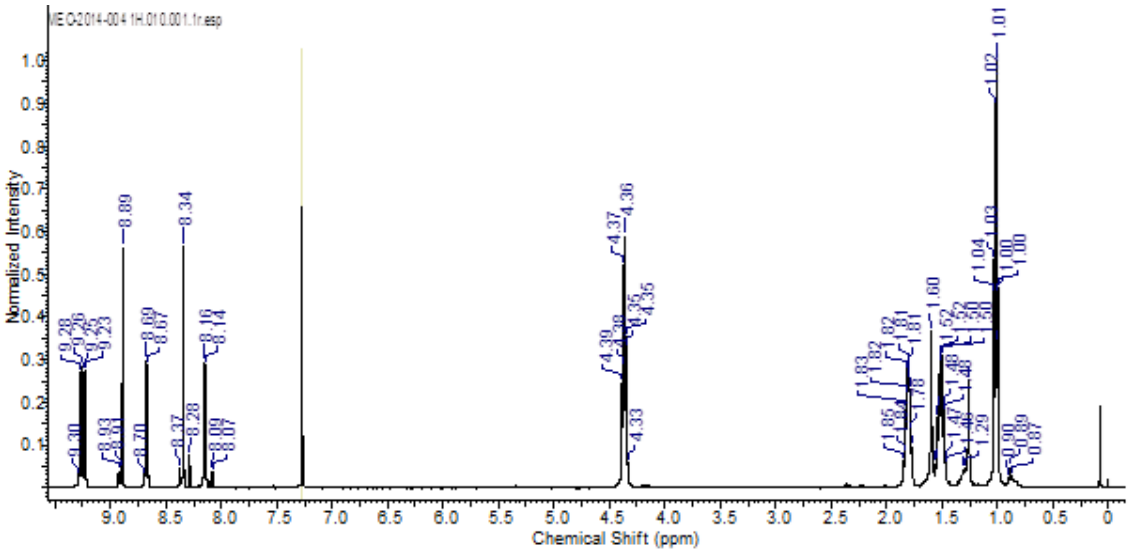

Figure A.5: ^{1}H NMR Spectrum of compound **3** in deuterated chloroform ($CDCl_3$)

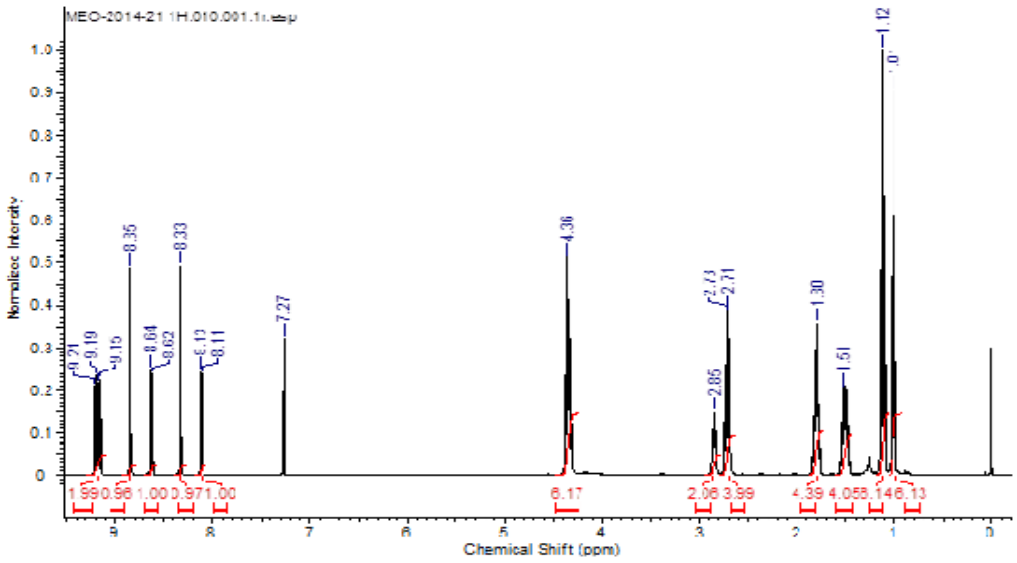

Figure A.6: ^{1}H NMR spectrum of compound **4**

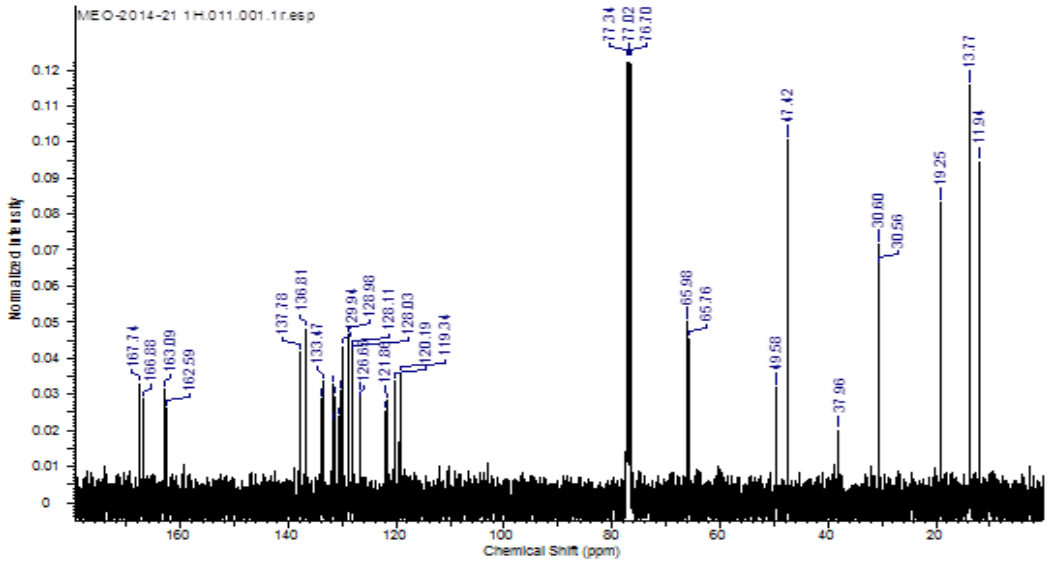

Figure A.7: ^{13}C NMR spectrum of compound **4**

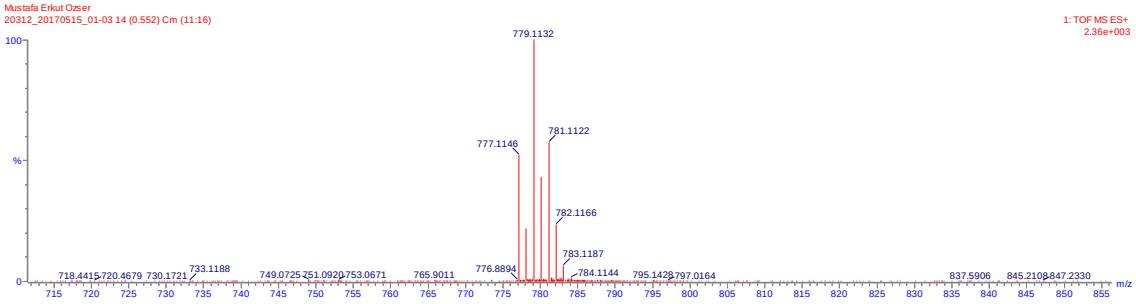

Figure A.8: HRMS of compound **4**

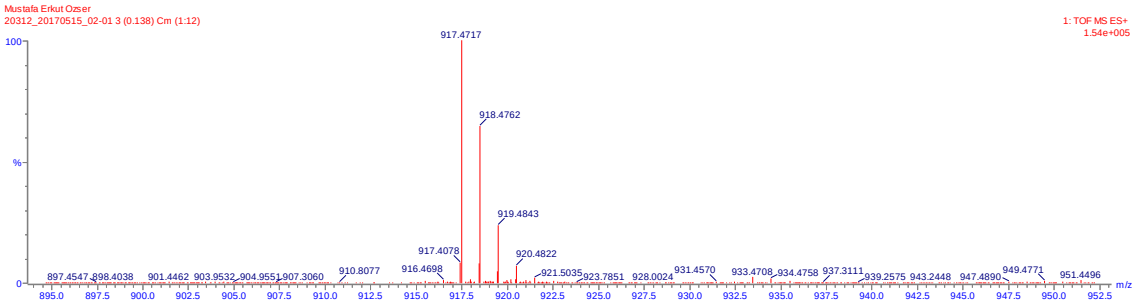

Figure A.9:HRMS of compound **5**

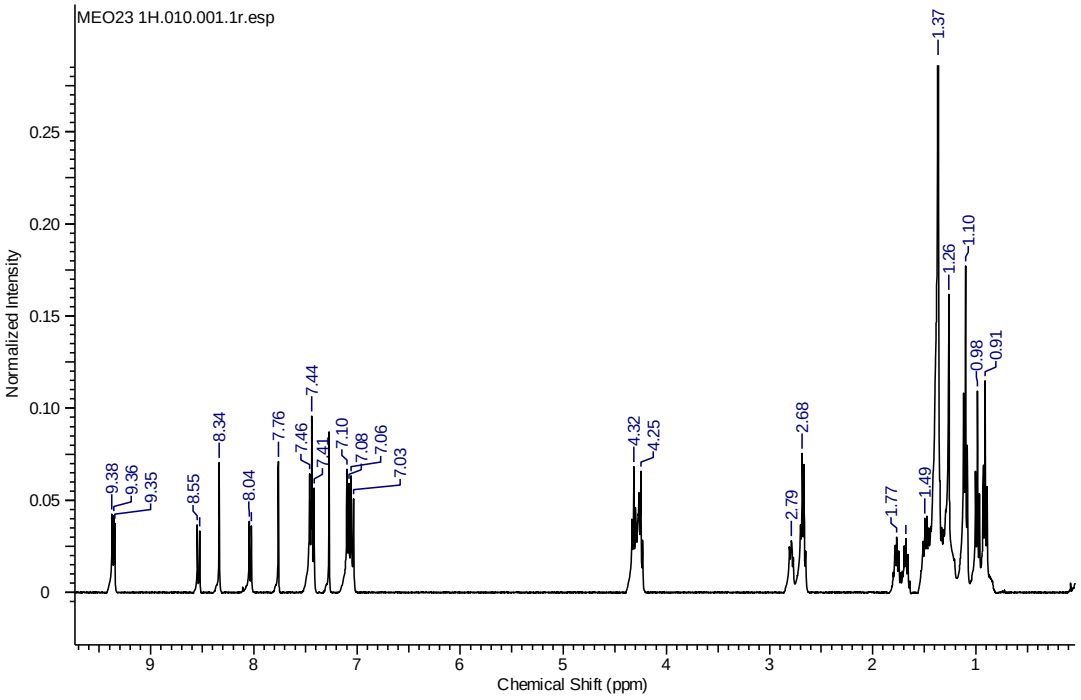

Figure A.10: ^{1}H NMR of compound **5**

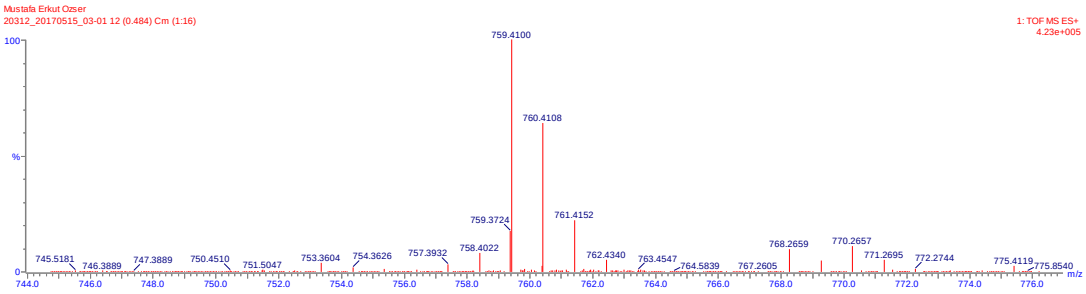

Figure A.11: HRMS of compound **6**

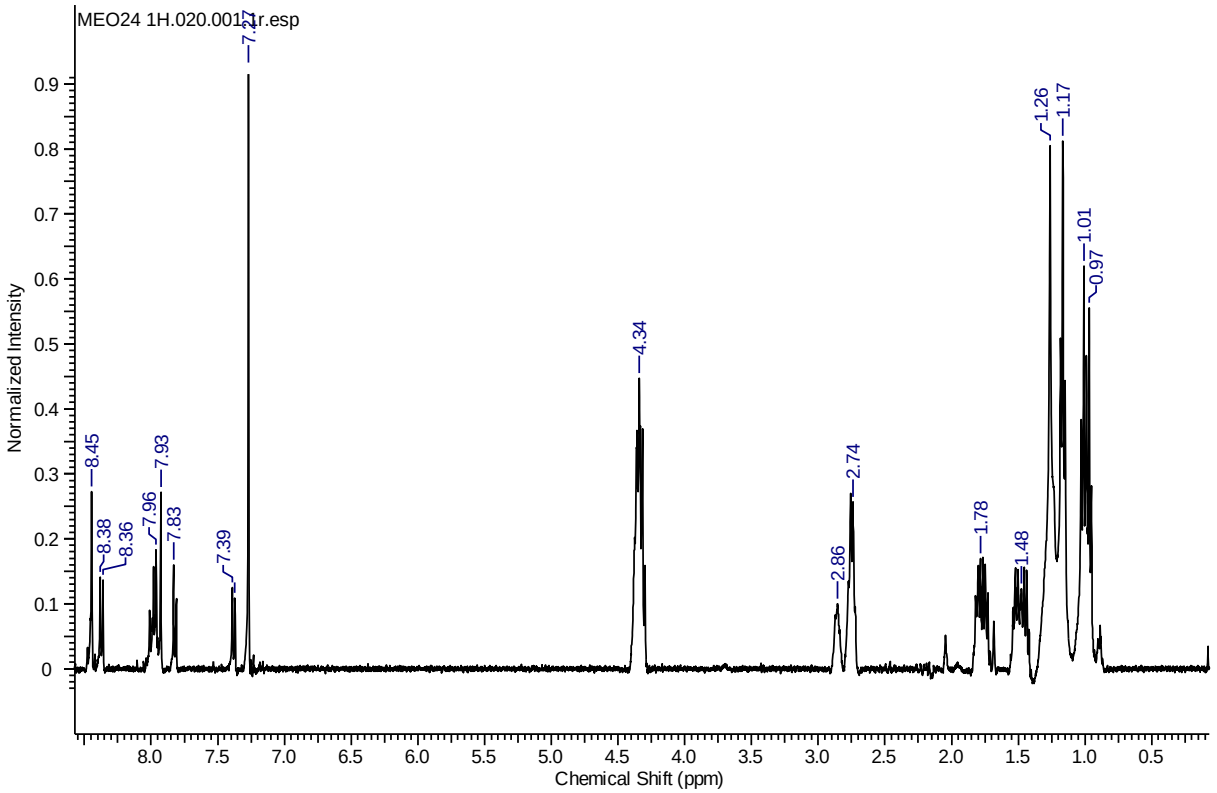

Figure A.12: ^{1}H NMR of compound **6**

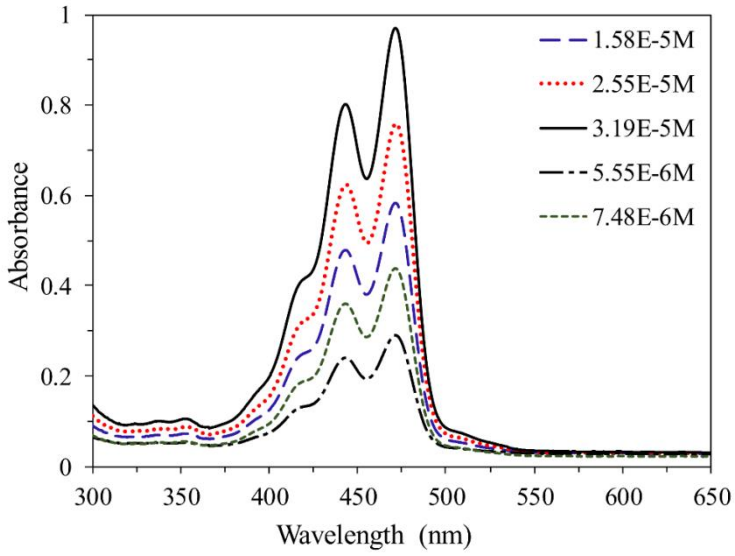

Figure A.13: Absorbance of compound **1** in Chloroform ($CHCl_3$)

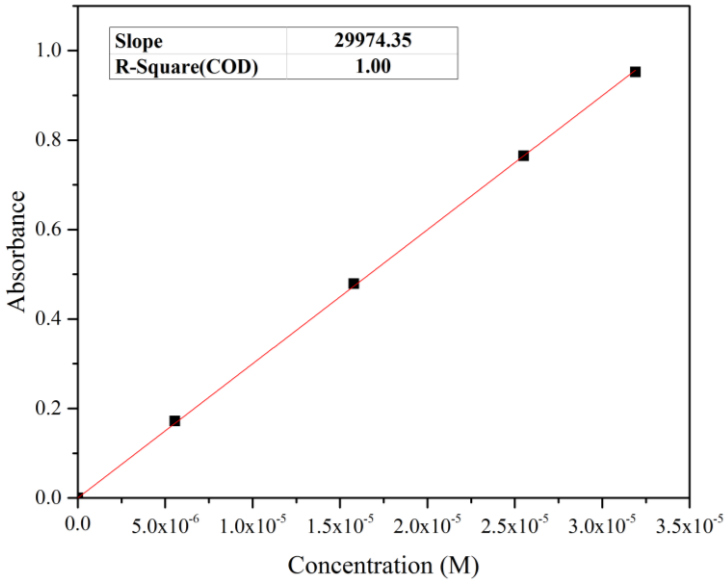

Figure A.14: Absorbance versus concentration plot of compound **1** at 472 nm in $CHCl_3$

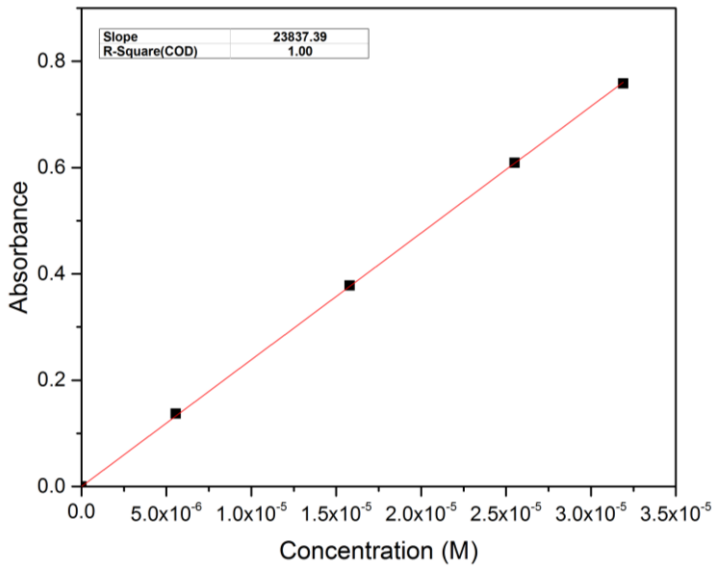

Figure A.15: Absorbance versus concentration plot of compound **1** at 443 nm in $CHCl_3$

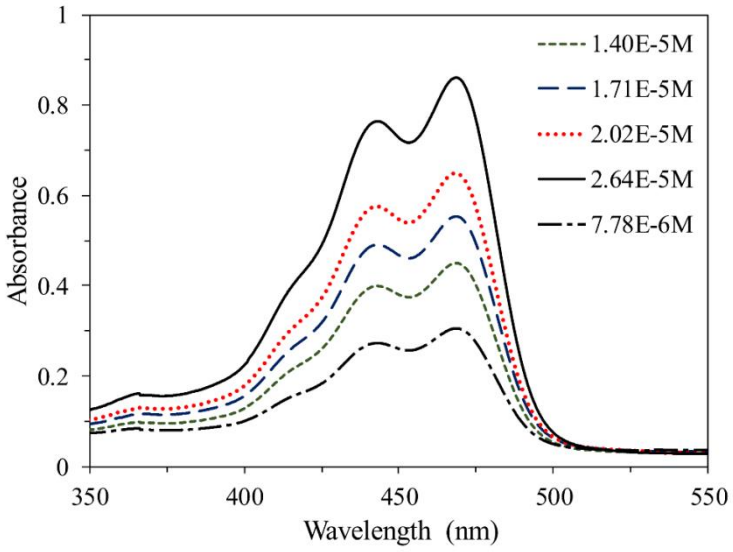

Figure A.16: Absorbance of compound **2** in Chloroform ($CHCl_3$)

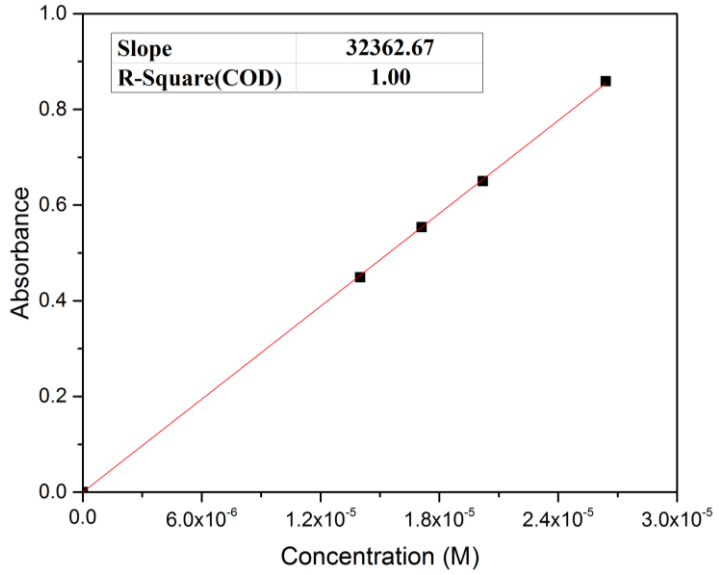

Figure A.17: Absorbance versus concentration plot of compound **2** at 468 nm in $CHCl_3$

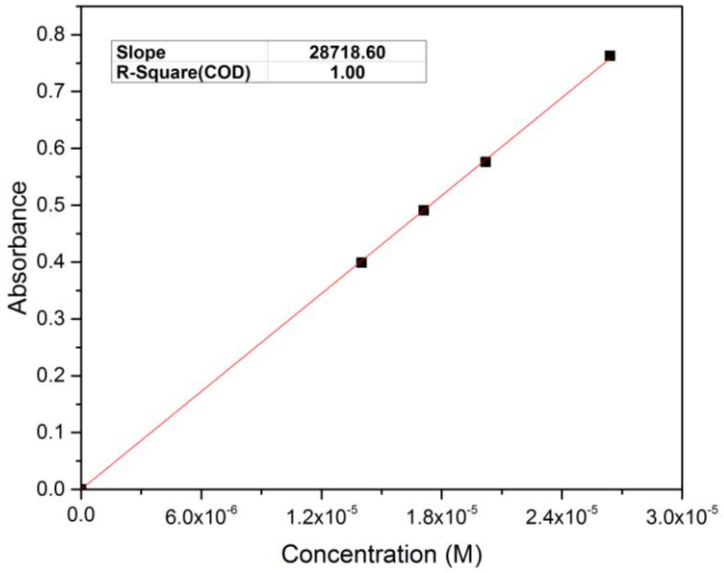

Figure A.18: Absorbance versus concentration plot of compound **2** at 443 nm in $CHCl_3$

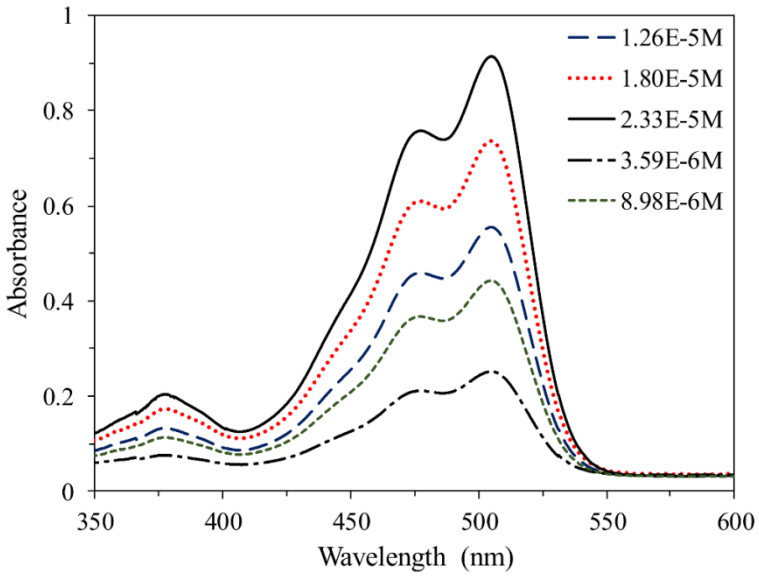

Figure A.19: Absorbance of compound **3** in chloroform ($CHCl_3$)

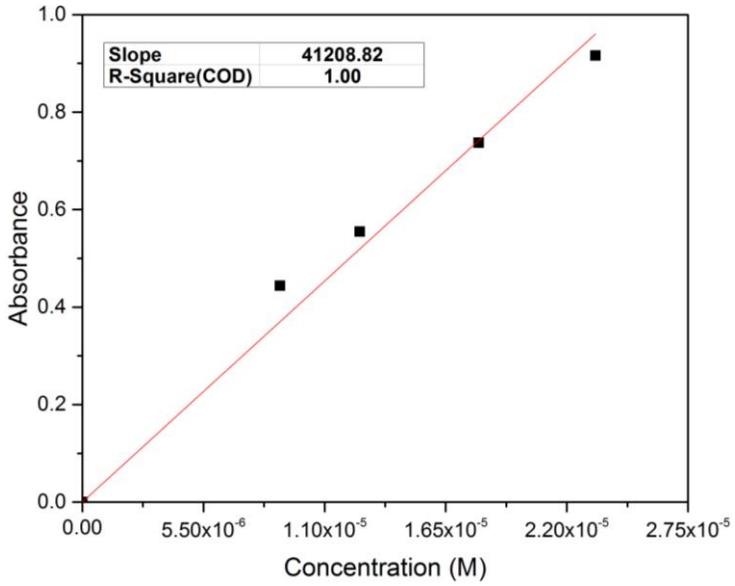

Figure A.20: Absorbance versus concentration plot of compound **3** at 505 nm in $CHCl_3$

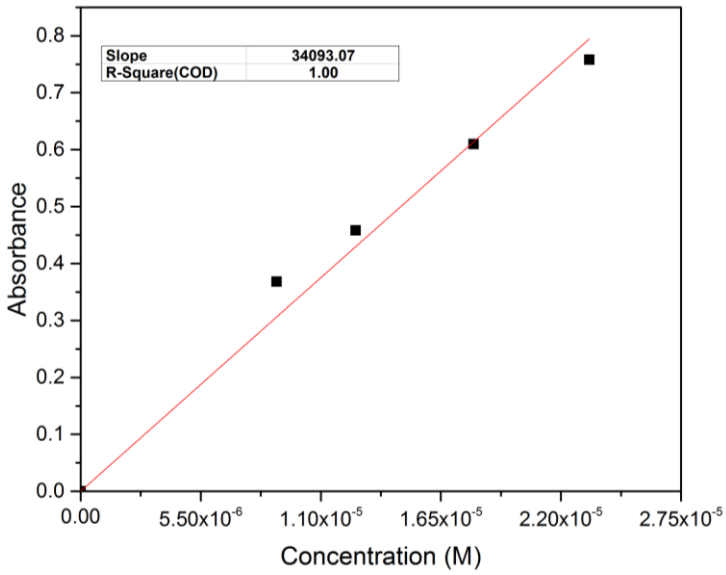

Figure A.21: Absorbance versus concentration plot of compound **3** at 484 nm in $CHCl_3$

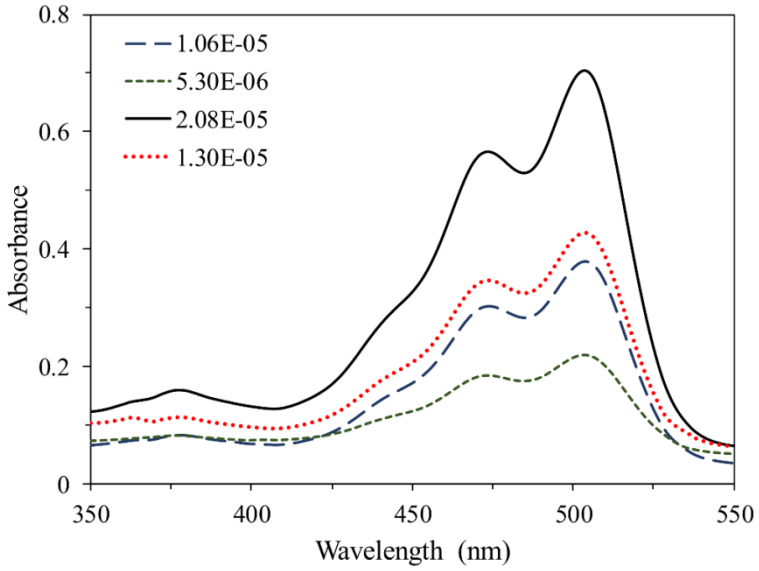

Figure A.22: Absorbance of compound **4** in chloroform ($CHCl_3$)

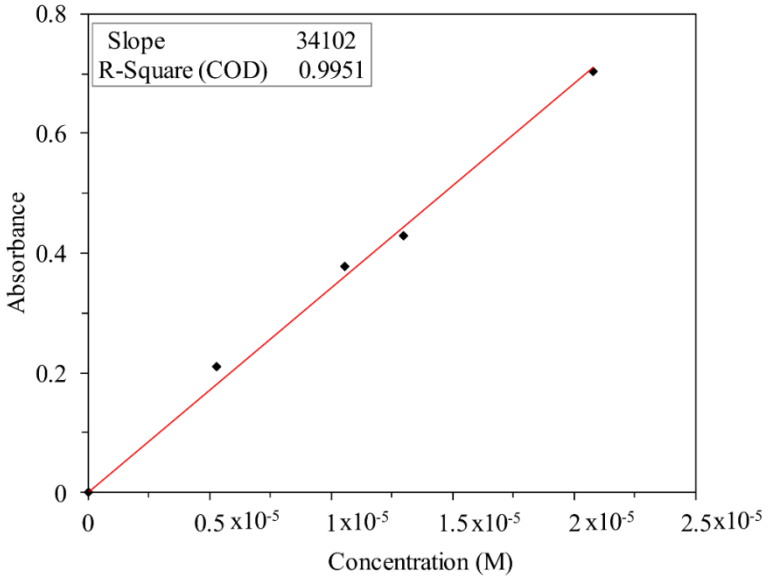

Figure A.23: Absorbance versus concentration plot of compound **4** at 504 nm in $CHCl_3$

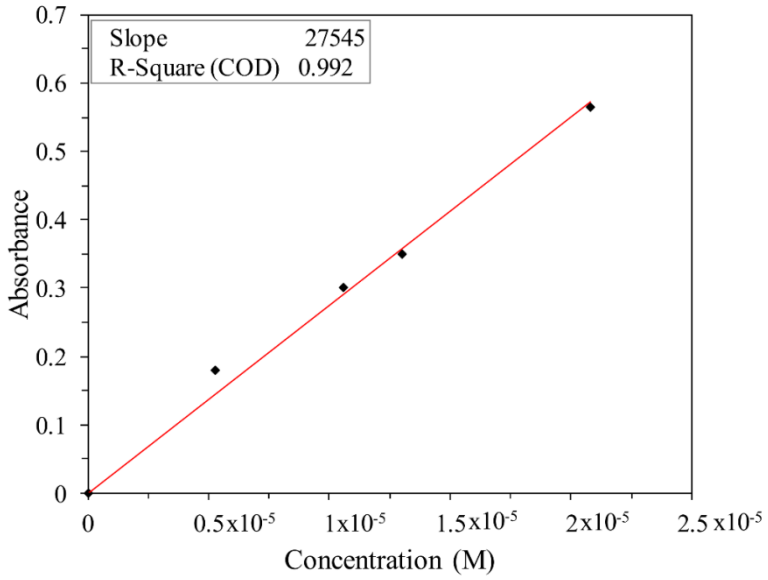

Figure A.24: Absorbance versus concentration plot of compound **4** at 474 nm in $CHCl_3$

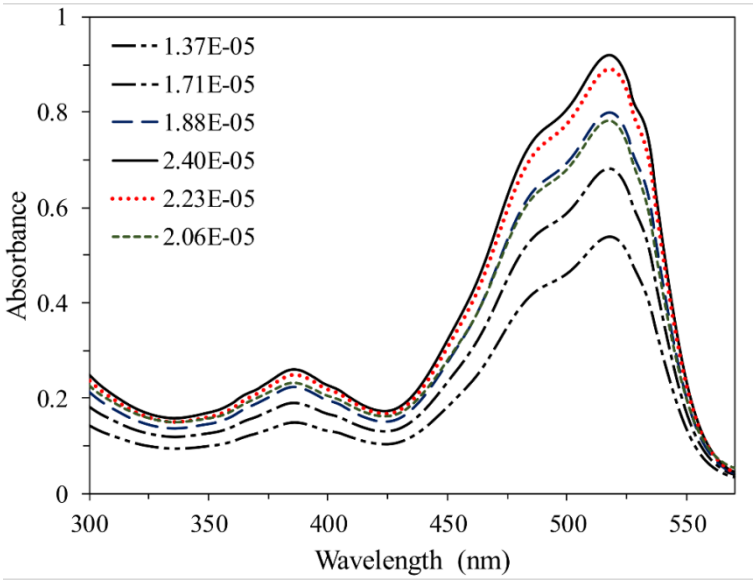

Figure A.25: Absorbance of compound **5** in Chloroform ($CHCl_3$)

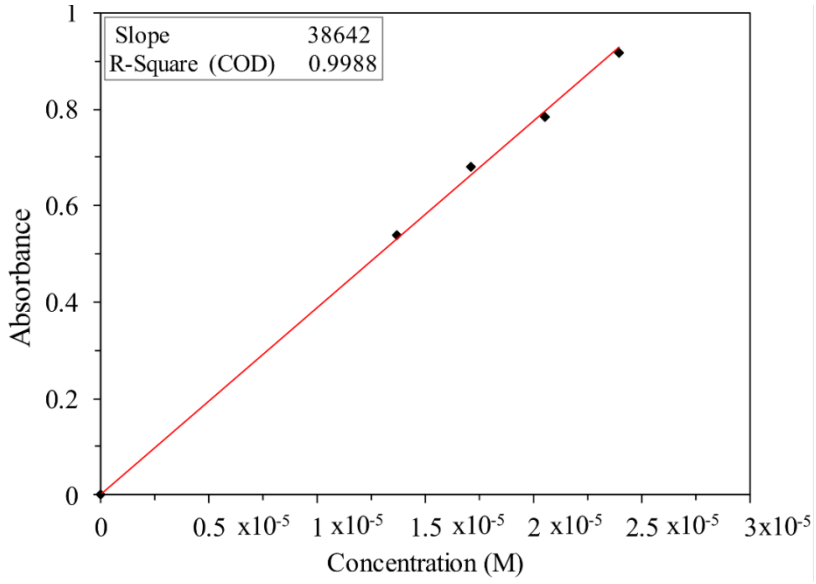

Figure A.26: Absorbance versus concentration plot of compound **5** at 518 nm in $CHCl_3$

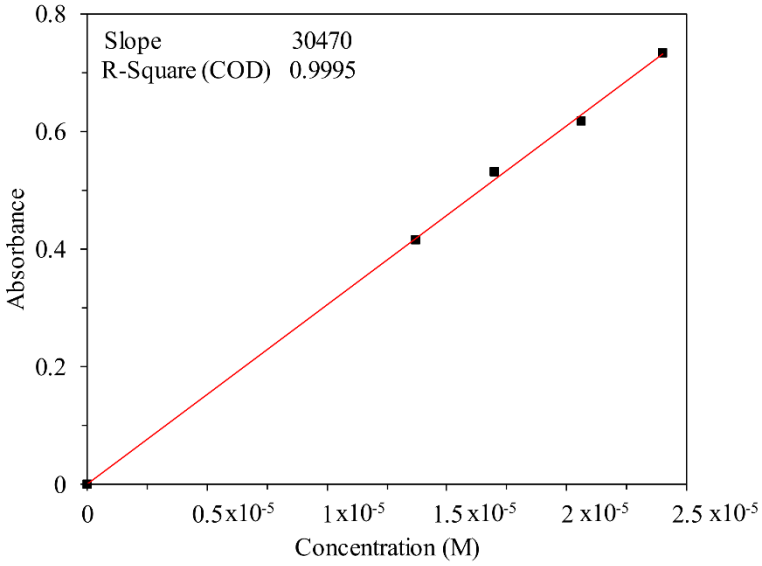

Figure A.27: Absorbance versus concentration plot of compound **5** at 485 nm in $CHCl_3$

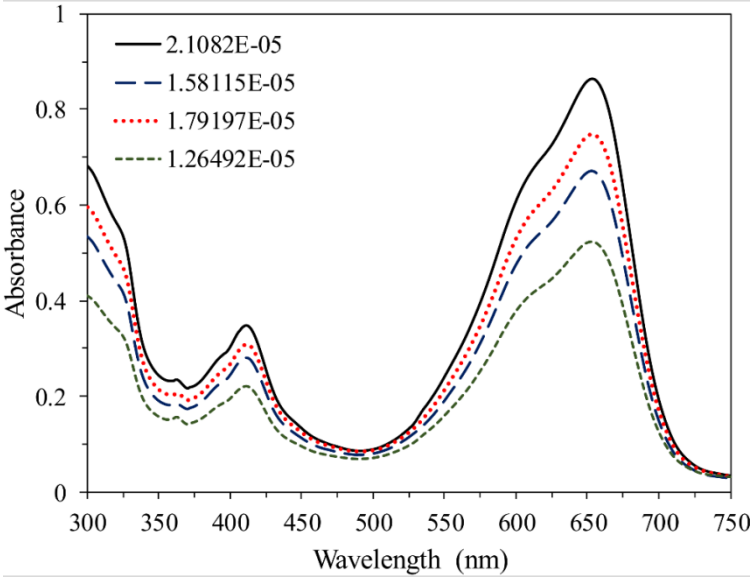

Figure A.28: Absorbance of compound **6** in chloroform ($CHCl_3$)

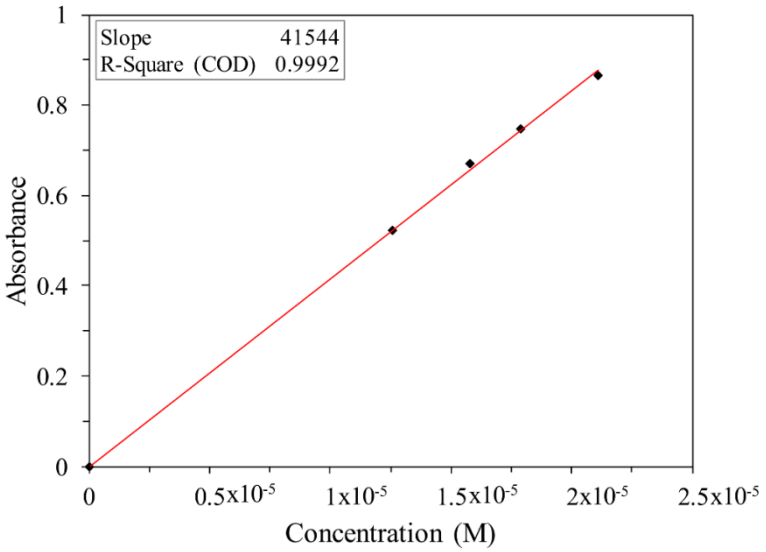

Figure A.29 Absorbance versus concentration plot of compound **6** at 653 nm in $CHCl_3$

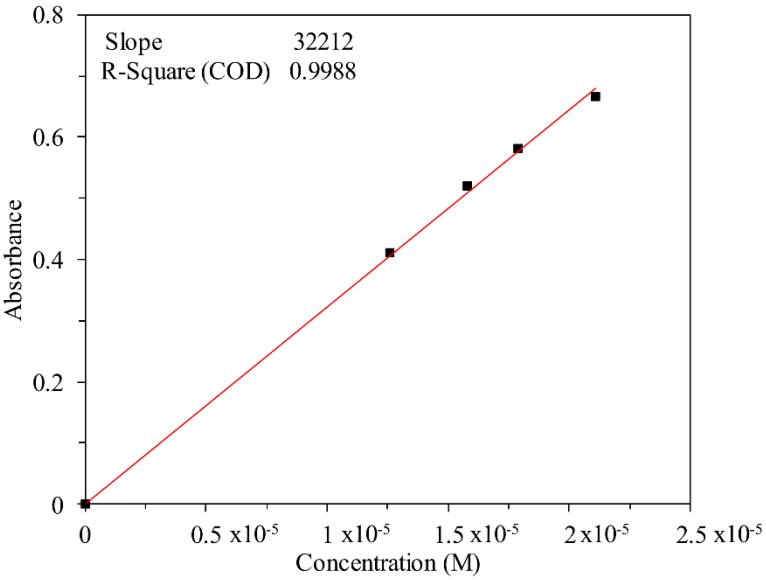

Figure A.30: Absorbance versus concentration plot of compound **6** at 610 nm in $CHCl_3$

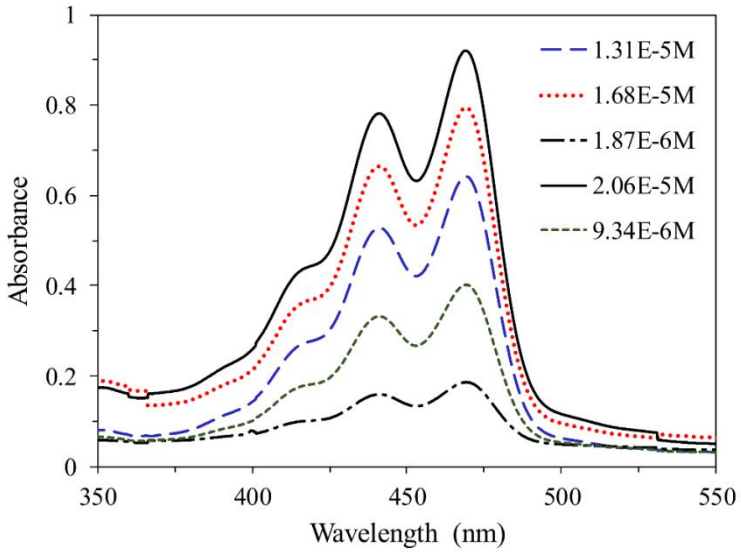

Figure A.31: Absorbance of compound **1** in Dimethylformamide (DMF)

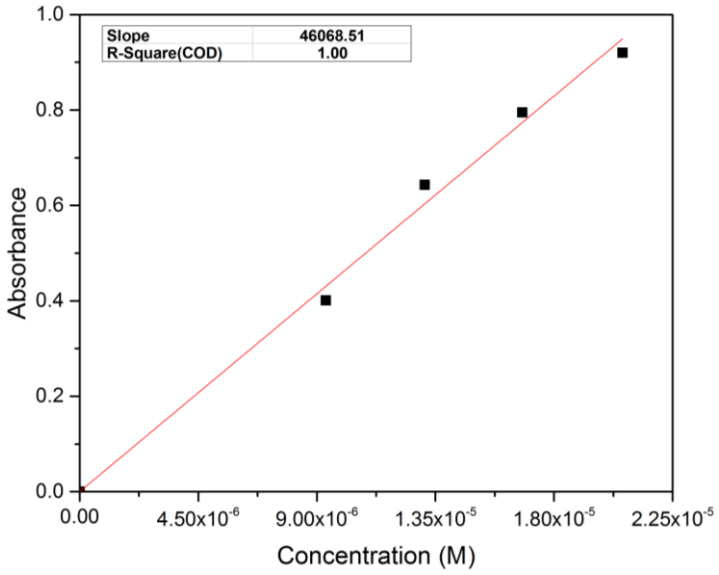

Figure A.32: Absorbance versus concentration plot of compound **1** at 469 nm in DMF

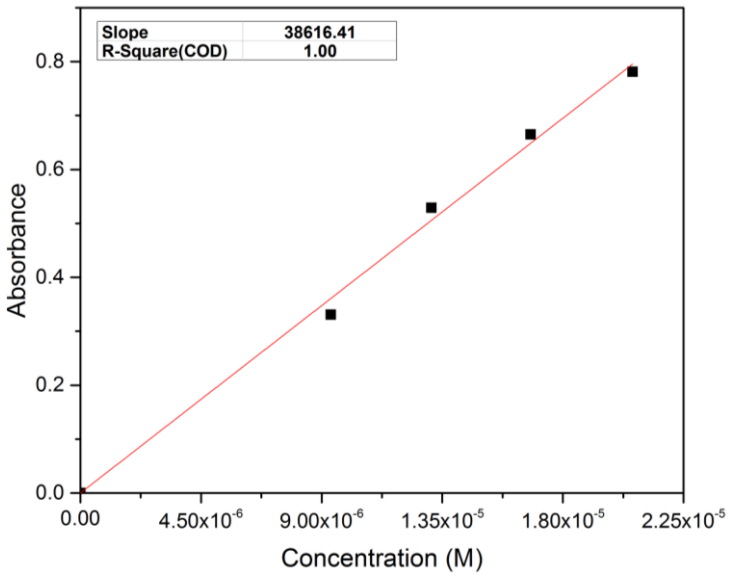

Figure A.33: Absorbance versus concentration plot of compound **1** at 441 nm in DMF

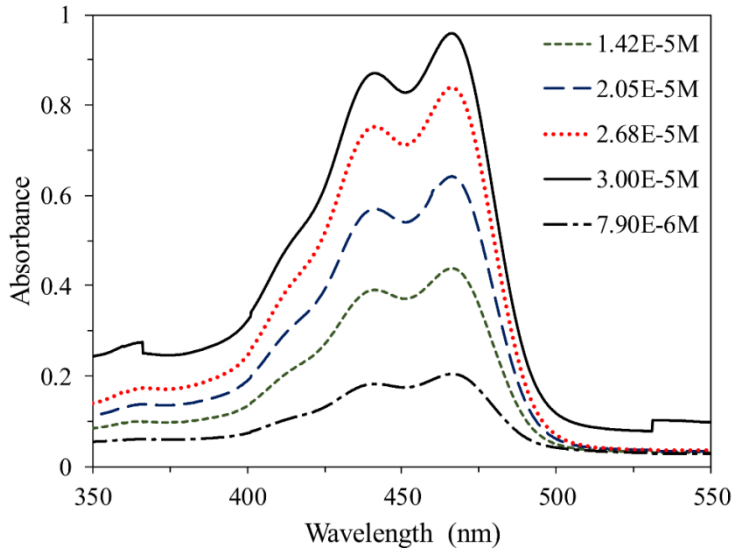

Figure A.34: Absorbance of compound **2** in Dimethylformamide (DMF)

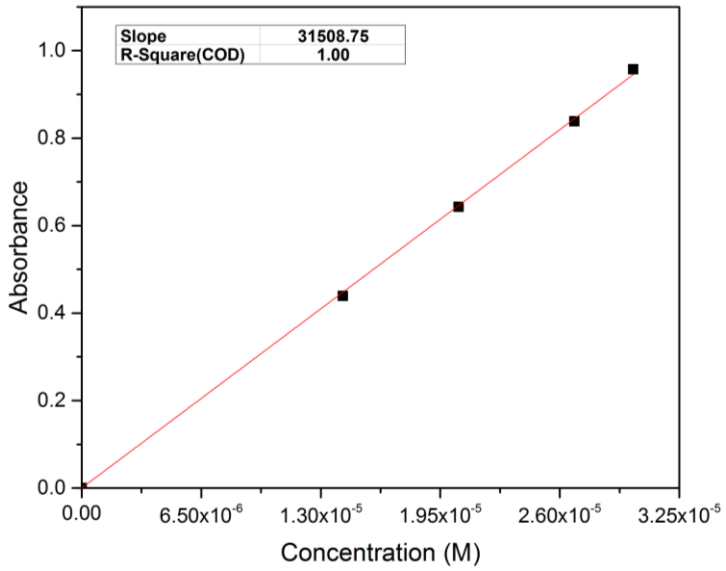

Figure A.35: Absorbance versus concentration plot of compound **2** at 466 nm in DMF

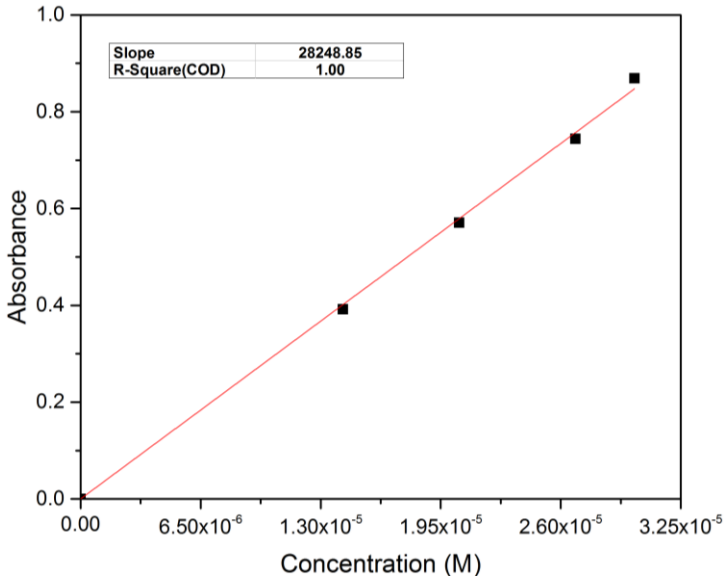

Figure A.36: Absorbance versus concentration plot of compound **2** at 441 nm in DMF

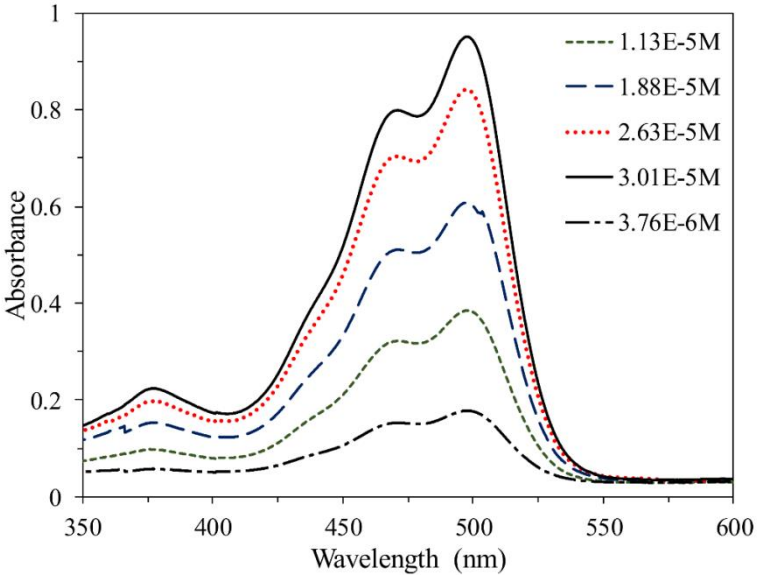

Figure A.37: Absorbance of compound **3** in Dimethylformamide (DMF)

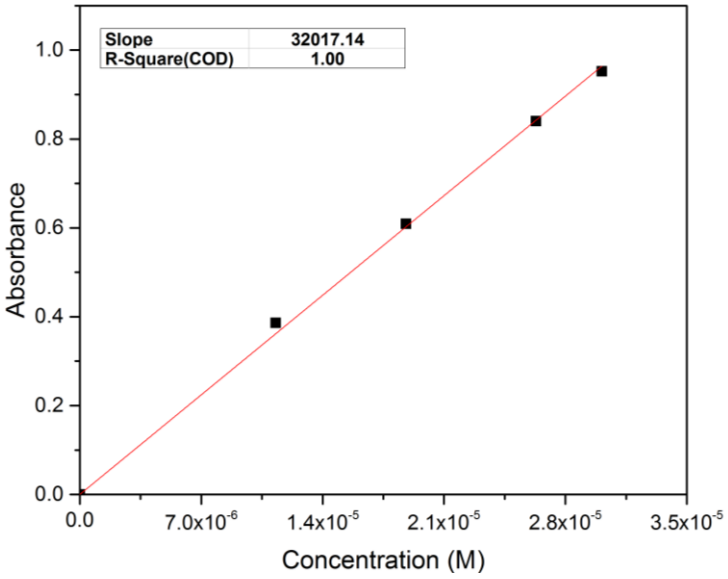

Figure A.38: Absorbance versus concentration plot of compound **3** at 497 nm in DMF

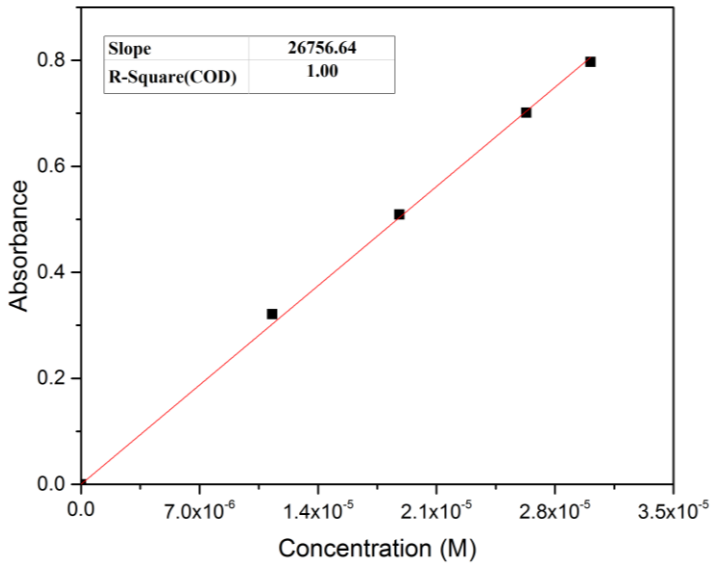

Figure A.39: Absorbance versus concentration plot of compound **3** at 469 nm in DMF

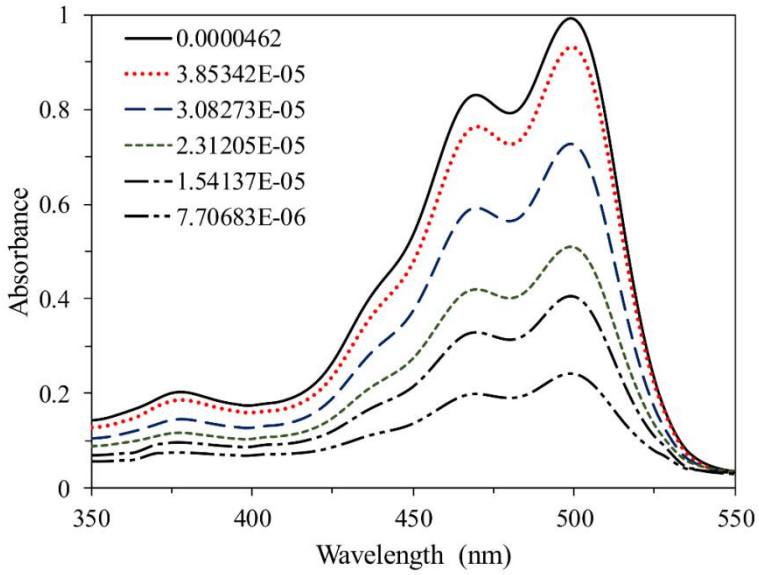

Figure A.40: Absorbance of compound **4** in Dimethylformamide (DMF)

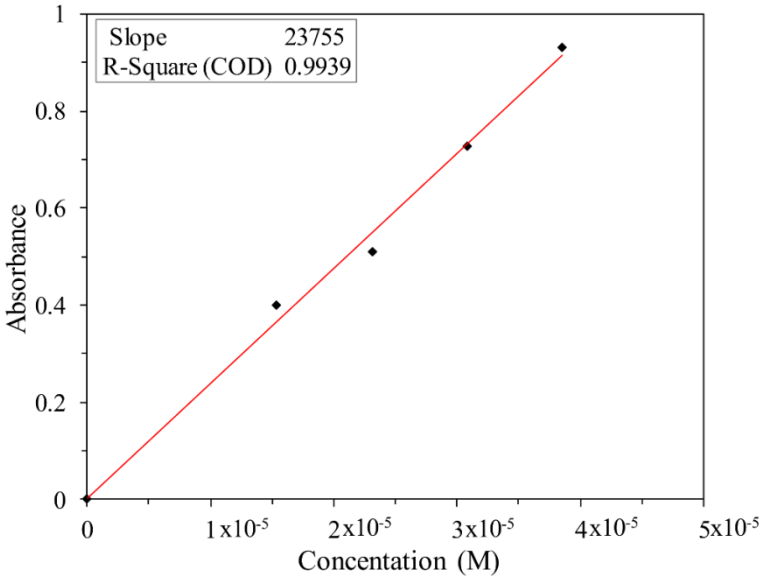

Figure A.41: Absorbance versus concentration plot of compound **4** at 499 nm in DMF

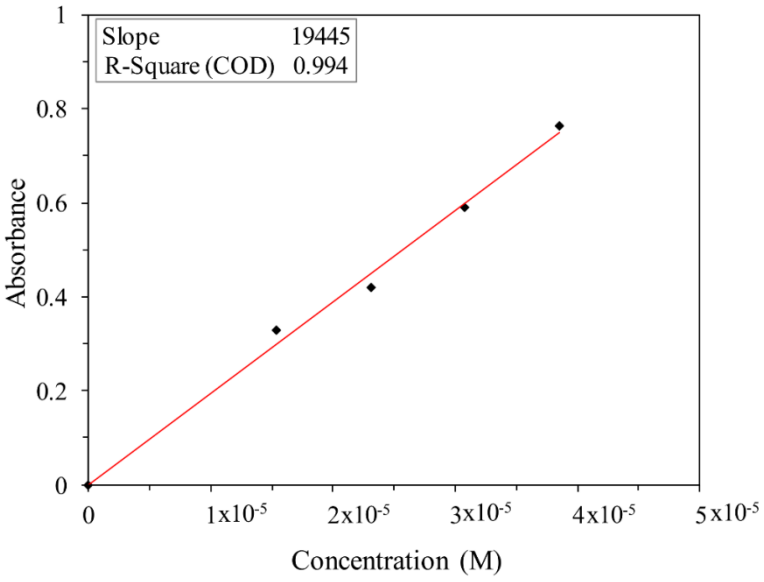

Figure A.42: Absorbance versus concentration plot of compound **4** at 470 nm in DMF

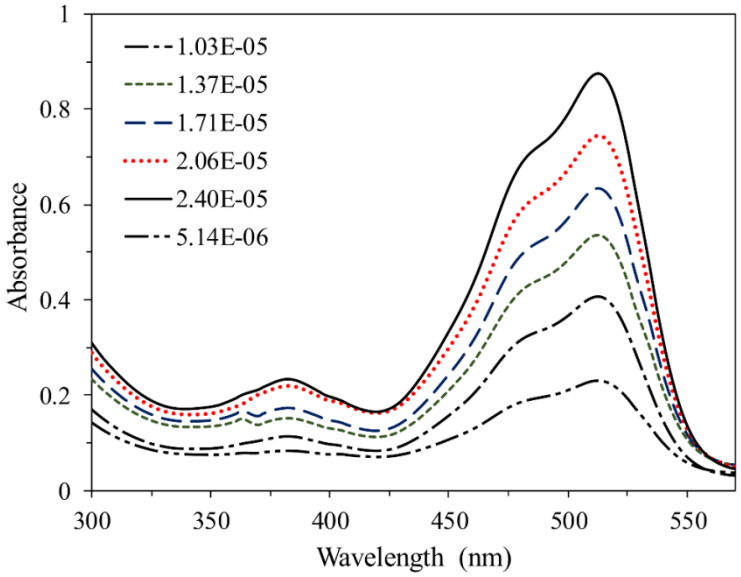

Figure A.43: Absorbance of compound **5** in Dimethylformamide (DMF)

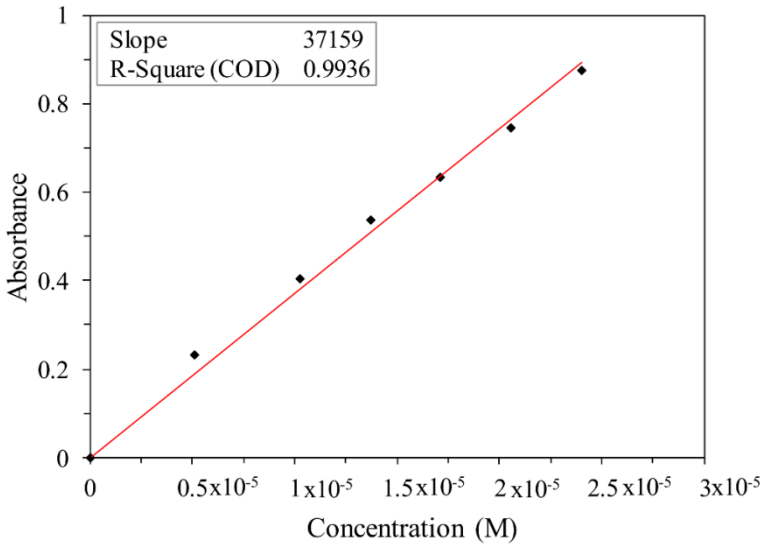

Figure A.44: Absorbance versus concentration plot of compound **5** at 513 nm in DMF

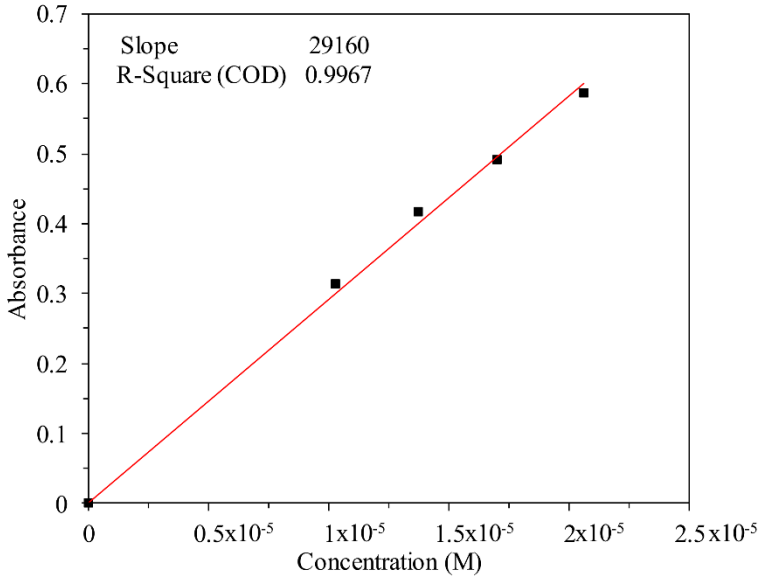

Figure A.45: Absorbance versus concentration plot of compound **5** at 480 nm in DMF

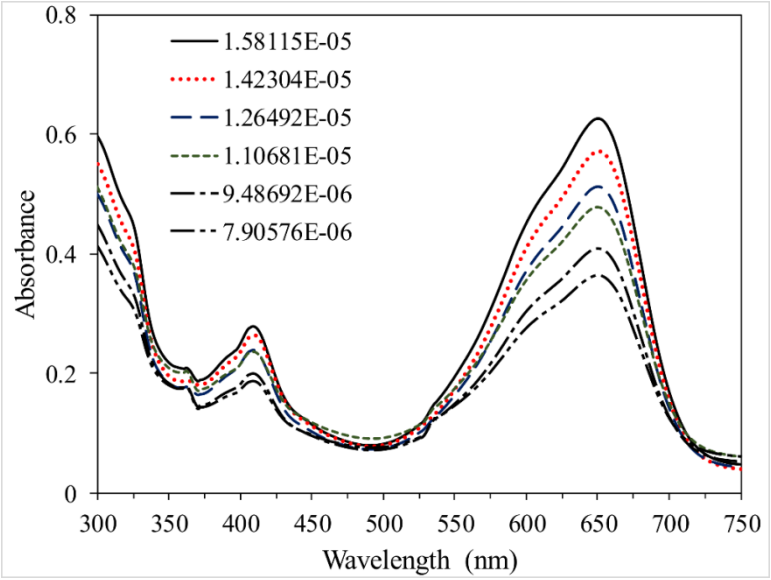

Figure A.46: Absorbance of compound **6** in Dimethylformamide (DMF)

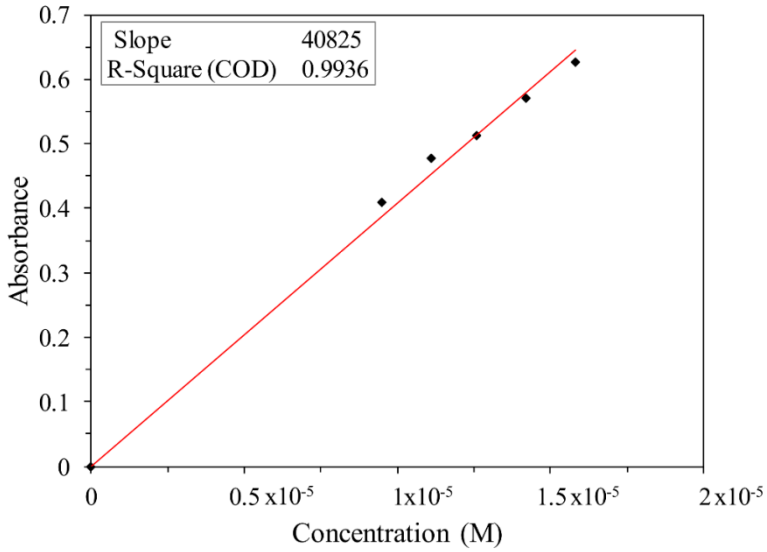

Figure A.47: Absorbance versus concentration plot of compound **6** at 650 nm in DMF

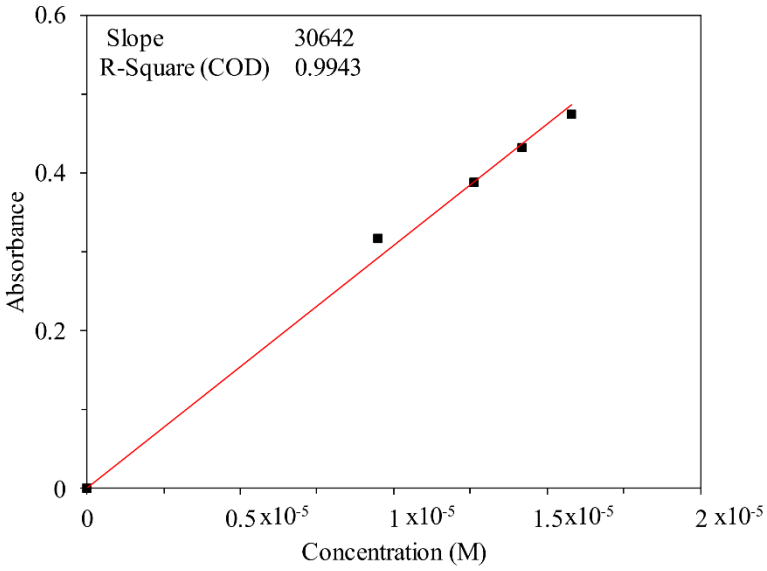

Figure A.48: Absorbance versus concentration plot of compound **6** at 605 nm in DMF

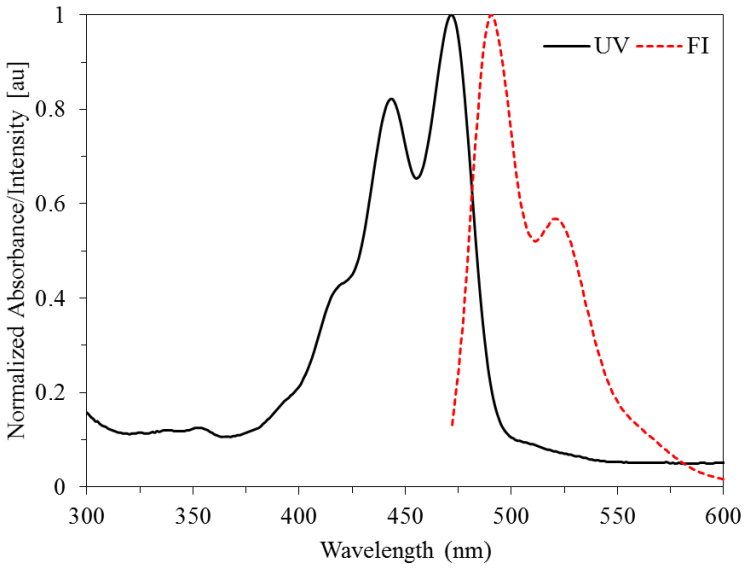

Figure A.49: Normalized absorption and emission of compound **1** in $CHCl_3$

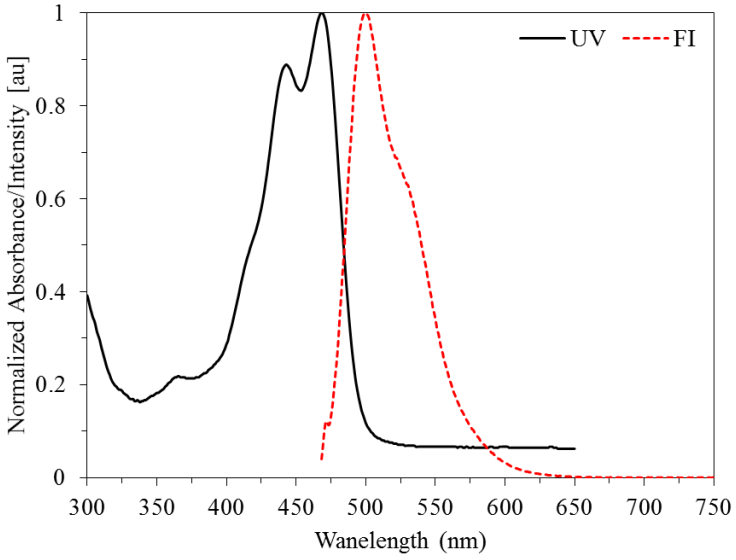

Figure A.50: Normalized absorption and emission of compound **2** in $CHCl_3$

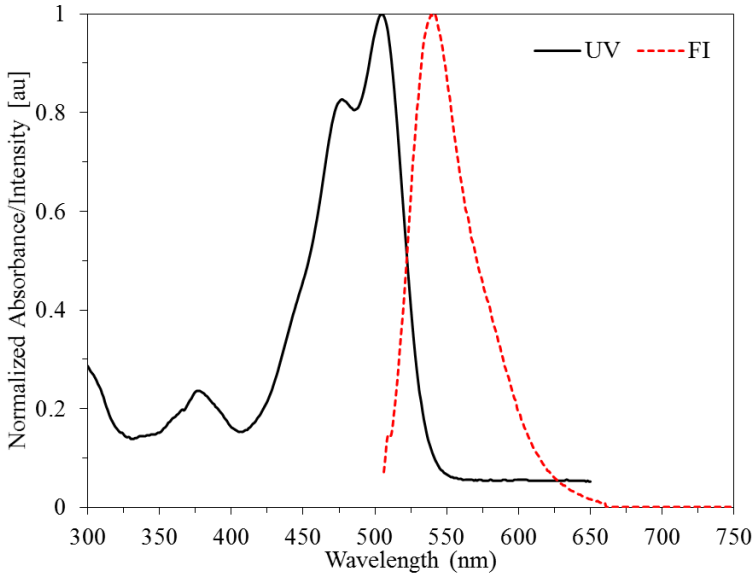

Figure A.51: Normalized absorption and emission of compound **3** in $CHCl_3$

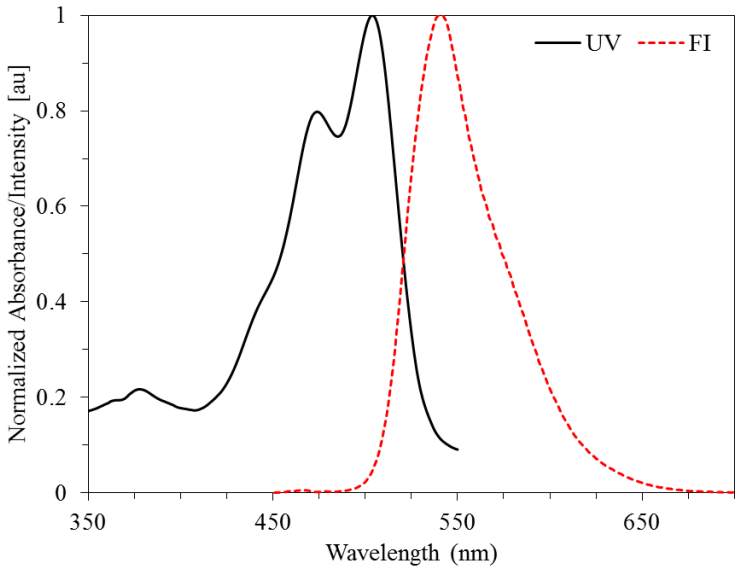

Figure A.52: Normalized absorption and emission of compound **4** in $CHCl_3$

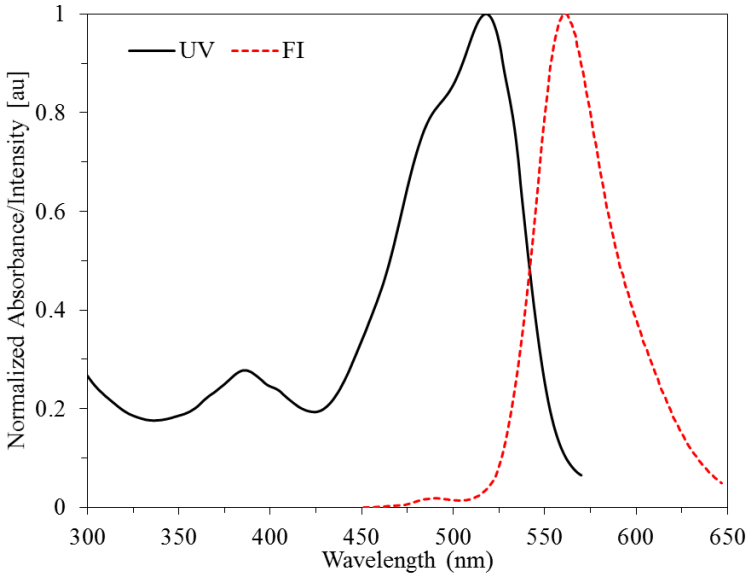

Figure A.53: Normalized absorption and emission of compound **5** in $CHCl_3$

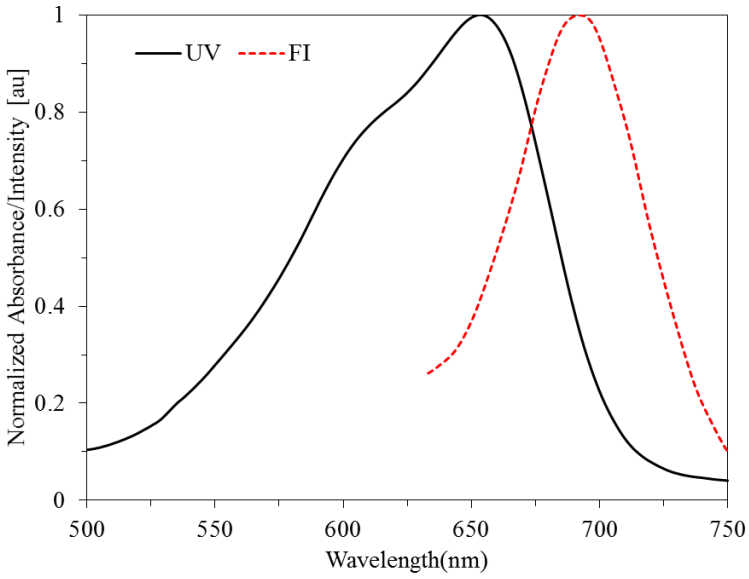

Figure A.54: Normalized absorption and emission of compound **6** in $CHCl_3$

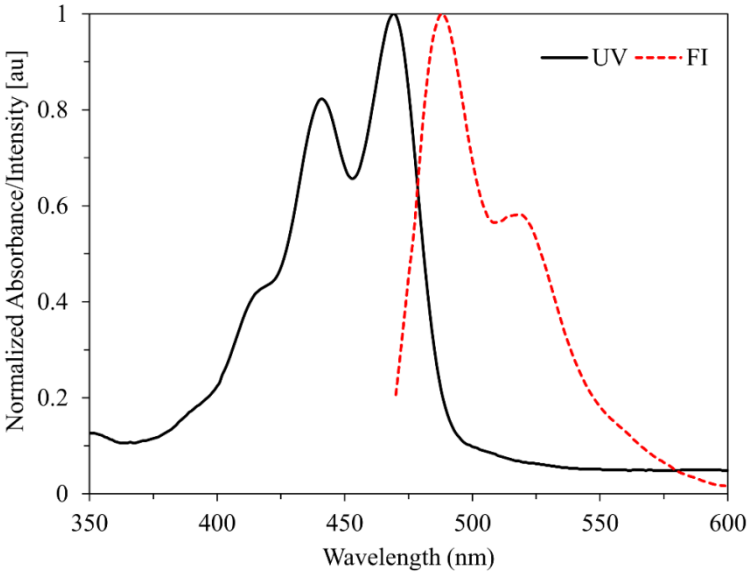

Figure A.55: Normalized absorption and emission of compound **1** in DMF

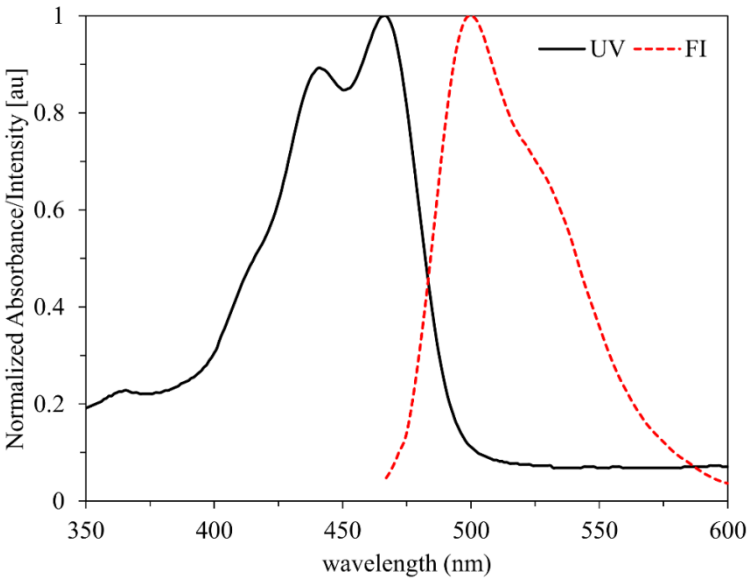

Figure A.56: Normalized absorption and emission of compound **2** in DMF

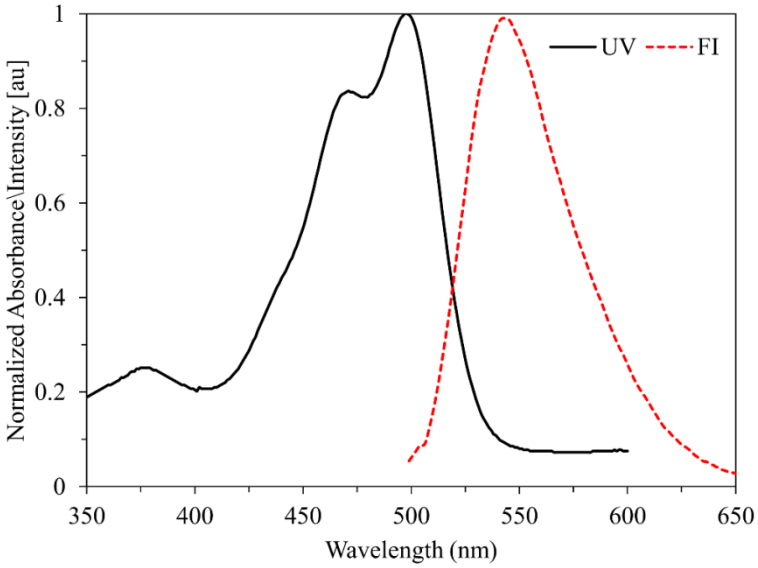

Figure A.57: Normalized absorption and emission of compound **3** in DMF

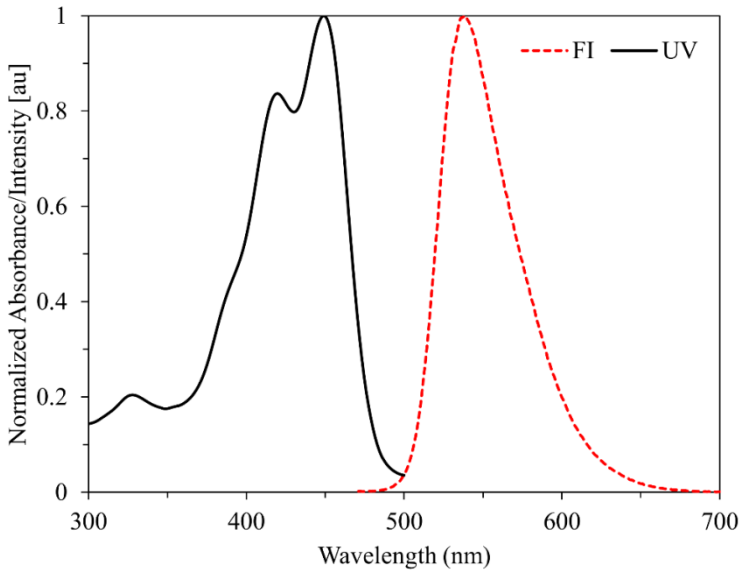

Figure A.58: Normalized absorption and emission of compound **4** in DMF

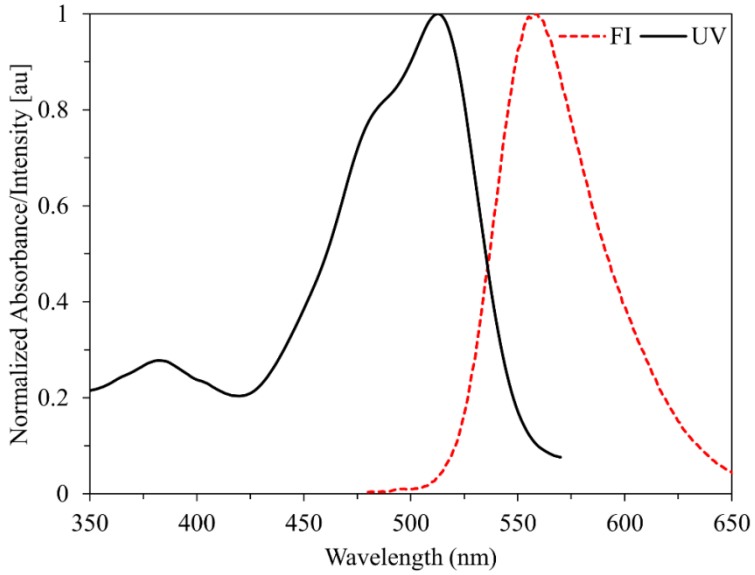

Figure A.59: Normalized absorption and emission of compound **5** in DMF

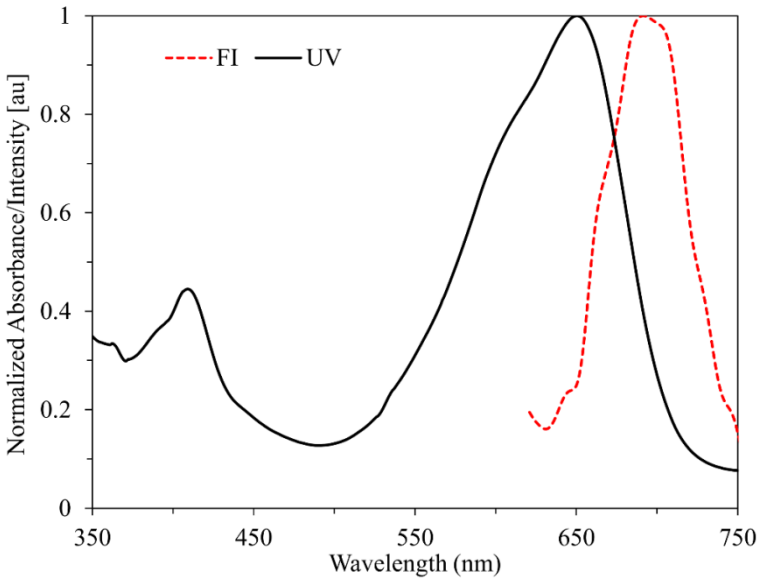

Figure A.60: Normalized absorption and emission of compound **6** in DMF